DISSERTATION

SIGNALING BY K63-LINKED POLYUBIQUITIN IN

AUTOPHAGY-RELATED VESICULAR TRAFFICKING

Submitted by

Francesco Scavone

Department of Biochemistry and Molecular Biology

In partial fulfillment of the requirements

For the Degree of Doctor of Philosophy

Colorado State University

Fort Collins, Colorado

Fall 2019

Doctoral Committee:

　　Advisor: Robert Cohen
　　Co-Advisor: Tingting Yao

　　Santiago Di Pietro
　　Diane Ordway

ABSTRACT

SIGNALING BY K63-LINKED POLYUBIQUITIN IN

AUTOPHAGY-RELATED VESICULAR TRAFFICKING

In eukaryotic cells, endocytosis and autophagy represent fundamental pathways that contribute to cell homeostasis. Intersection of the endocytic and autophagosomal trafficking routes has been previously recognized, as both systems share specific compartments contributing to cargo degradation via the lysosome, and both use an identical subset effectors involved in vesicular trafficking and membrane fusion. By helping to target proteins to the lysosome, ubiquitin (Ub) also acts as a common factor in both pathways. The relative contributions of endocytic and autophagy pathways to degradation of ubiquitinated cargo are mostly unknown. A critical unanswered question is how ubiquitinated cargo is targeted to a particular degradative pathway. Ub can be conjugated to other proteins as a single Ub or chains of multiple Ub (polyUb). Many types of polyUb, distinguished by different Ub–Ub linkages, are present in cells, where they are thought to be recognized by decoders (i.e., receptors or adaptors) to signal various biological processes. K63-polyUb has been implicated in endocytosis of cell surface receptors, budding of viral proteins, and autophagy of damaged organelles and invading pathogens. However, the extent and details of the relationship between K63-polyUb and lysosomal targeting via either endocytosis or autophagy are poorly understood. These deficiencies are due in part to the lack of tools to study Ub-dependent signaling. We have previously developed a genetically-encoded specific K63-polyUb sensor, "Vx3," to facilitate identification, localization, and functional characterization of signaling by K63-polyUb *in vivo* [Sims *et al., Nat. Methods* (2012)]. When Vx3 is expressed in cells, it localizes to cytoplasmic foci that colocalize with the autophagic transmembrane protein

ATG9A, the autophagic cargo receptor p62 (SQSTM1), which preferentially bind K63-polyUb, and late endosomal/lysosomal markers. Proteins identified by mass spectrometry and likely modified by K63-polyUb appear to be transmembrane proteins known to recycle between endosomes and plasma membrane, such as transferrin receptor (TfR) and major histocompatibility complex I (MHC-I). Here, we show that K63-polyUb modifies endocytic transmembrane proteins to signal their delivery to the lysosomes. Fluorescence and electron microscopy data revealed that Vx3 accumulates K63-polyUb-decorated vesicles into cytoplasmic foci at an intermediate stage of the transmembrane protein degradation pathway; these foci include components of both endocytic and autophagy membranes. We observed that K63-polyUb-decorated vesicles co-clustering with ATG9A are found juxtaposed to endolysosomes, consistent with the idea of fusion block imposed by Vx3. By using a system to inducibly disable Vx3 inhibition, we tracked delivery of K63-polyubiquitinated cargo to the highly acidic and degradative lysosomal compartments. We also report that ESCRT dysfunction leads to accumulation Vx3 foci, indicating an augmentation of K63-polyubiquinated cargo destined to lysosomal degradation via the multivesicular late endosomes. Despite the established role for endocytosis in cargo sorting and recycling, there is evidence that autophagy may also play a role in regulating these events. By using Vx3 to inhibit autophagy-related membrane trafficking, our study also reveal a functional crosstalk between the Ub-dependent sorting of endocytic cargo into multivesicular late endosomes and the retromer-mediated retrieval of transmembrane proteins from maturing endosomes.

TABLE OF CONTENTS

LIST OF TABLES

LIST OF FIGURES

Chapter 3

Chapter 4

Chapter 1: Introduction

1.1: The ubiquitin system

The conjugation of ubiquitin (Ub) to other cellular proteins – a process referred to as ubiquitination – controls a wide repertoire of degradative and non-degradative events in eukaryotic cells. Ubiquitination usually results in the formation of an isopeptide bond between the C-terminal glycine of Ub and the side chain of an acceptor lysine residue [1]. Similar to protein phosphorylation, ubiquitination is highly dynamic and readily reversible: Ub-protein ligases (E3s), in concert with Ub-activating enzyme (E1) and Ub-conjugating enzyme (E2s), mediate the conjugation of Ub to specific substrates, whereas deubiquitinating enzymes (DUBs) catalyze the opposing deconjugation reaction [1,2]. Different types of Ub modifications have been detected in cells. In addition to the conjugation of a single Ub (monoUb), substrates are commonly modified with extended chain(s) of polyubiquitin (polyUb) in which Ub moieties are linked to each other via a Ub Lys residue or the Ub amino terminus. Because all of Ub's seven lysine residues and Met1 have been found in Ub–Ub linkages *in vivo* [3,4], at least eight structurally distinct polyUb chains linked via Lys6, Lys11, Lys27, Lys29, Lys37, Lys48, Lys63, or Met1 can be assembled on target substrate (**Fig 1.0**). Furthermore, chains containing branches or a mixture of different linkages also exist [5].

Generally, substrate specificity is conferred by several hundred distinct E3 Ub ligases (~600 in the human genome) that, in concert with accessory factors and adaptors, recognize target substrates and mediate transfer of ubiquitin from Ub–E2 thioester complexes. E3s can be divided into the *R*eally *I*nteresting *N*ew *G*ene (RING) and the *H*omologous to the *E*6-AP *C*arboxyl *T*erminus E6-associated protein (HECT) families. Although both types of E3s bridge E2s and substrates, they differ in that HECT-family proteins relay Ub from E2 to substrate by forming an intermediate Ub-

E3 thioester linkage with the ubiquitin C-terminus, whereas RING E3s transfer ubiquitin directly from an E2[6]. E2s have the capacity to determine polyUb linkage-type and chain topology[7]. For example, the E2 enzyme UBE2N (also known as Ubc13) heterodimerizes with UBE2V1 and assemble K63-linked polyUb [2]. In another example, a hybrid E2/E3 enzyme, which displays both activities, has been documented; UBE2O (also called E2-230K) has been reported to conjugate either monoUb [8] or K63-polyUb onto target substrates [9]. DUBs are less numerous (99 currently identified in the human genome) than E3s, and each is dedicated to remove Ub or polyUb from a subset of substrates. There are seven families of DUBs: USP, UCH, OTU, MJD, MINDY, ZUP1 (all classified as cysteine proteases), and JAMM (zinc-dependent metalloproteinases) [10].

The many different forms of polyUb modifications are thought to direct the different fates of ubiquitinated proteins [11]. For example, whereas polyUb assembled through Ub Lys48 (K48-polyUb) targets proteins for proteasomal degradation, polyUb linked via Ub Lys63 (K63-polyUb) has been associated with signaling functions in DNA repair, inflammatory responses, endocytosis and autophagy. The prevailing model for a code determined by polyUb linkage-type maintains that each unique type of polyUb might elicit a subset of functionally distinct cellular outcomes via selective recognition by effector proteins that carry at least one Ub-Binding Domain (UBD) [12]. Many UBDs (~20 different families) and their distinct modes of noncovalent interaction with Ub have been described [12]. However, their ability to discriminate among different polyUb linkage-types has been rarely assessed comprehensively [13], and limited mechanistic insight is available to date.

1.1.1: Pathways of Ub-dependent proteolysis

Degradation of intracellular material is essential for cell homeostasis and also for response to environmental change, stress, and programs of growth or differentiation. In general, proteins are degraded in response to a specific biological signal (e.g., ligand binding to a receptor); alternatively, faulty or damaged proteins are recognized and rapidly degraded within cells, thereby eliminating the risk of toxicity from aberrant or aggregated proteins. Loss of proteostasis leads to the accumulation of damaged proteins and is a hallmark neurodegenerative disorders like Parkinson's and Alzheimer's diseases [14]. In eukaryotic cells, the major protein degradative pathways are the ubiquitin-proteasome system and the lysosome, with the latter being at the convergence of two separate membrane-mediated proteolytic processes, endocytosis and autophagy [15,16] (**Fig 1.1**). A fundamental question is how a particular substrate is targeted for a particular degradative pathway. Ub acts as a common denominator in the targeting of intracellular substrates to either the 26S Proteasome or the lysosome, although the decision to use a particular route may be influenced by the cellular localization of E3s, the polyUb linkage type, and/or the polyUb chain length [16]. For degradation of K63-polyUb modified proteins, a clear bias for the endosomal and autophagosomal pathways has emerged from studies in both yeast and mammals that have focused on Ub signaling in cellular trafficking. In the following paragraphs, I will highlight some examples of Ub-dependent regulation of endocytosis and autophagy, and describe previous evidence for K63-polyUb signaling during transmembrane protein trafficking and lysosomal turnover.

1.2: Ub as a signal for endocytosis of cell surface transmembrane proteins

Ubiquitination of cell surface transmembrane proteins serves as a signal for internalization and endosomal sorting into intralumenal vesicles of multivesicular late endosomes. Most of our

understanding of ubiquitin-dependent internalization and endocytic sorting of cell surface proteins comes from studies on ligand-activated receptor tyrosine kinases (RTKs), with the epidermal growth factor receptor (EGFR) being the best characterized example of such a pathway. Early studies based on the chimeric EGFR fusion with a mutant ubiquitin bearing lysine-to-arginine substitutions showed that monoUb was sufficient to promote internalization [17]. However, other studies also showed that EGFR ubiquitination is not required for internalization, as a nonubiquitinatable form of EGFR presented no internalization defects [18,19]. At the cell surface, Epsin and Eps15 are candidates for endocytic adaptor proteins as they contain a class of UBDs called Ubiquitin Interacting Motifs (UIMs) that can recognize ubiquitinated cargo and recruit them into clathrin-coated pits [20]. Following internalization either by clathrin-dependent or independent endocytosis, transmembrane proteins are routed to early endosomes, where they can recycle back to the plasma membrane or undergo a series of sorting steps that culminate with lysosomal degradation and thereby termination of receptor signaling. Evidence suggests that K63 is the primary polyUb linkage-type involved in endosomal sorting by the ESCRT machinery. Endocytic cargo is typically marked with K63-polyUb, and yeast mutants incapable of assembling Ub chains linked via K63 have major defects in multivesicular body (MVB) sorting [21]. More recently, analysis by quantitative mass-spectrometry has revealed that the ligand-activated EGFR is modified by tetra to hexa-Ub chains linked via K63 [22,23]. In human cells, K63-polyUb has also been proposed to regulate endosomal sorting rather than plasma membrane internalization [24,25]. Concordantly, studies of the MHC class I (MHC-I) protein revealed that attachment of K63-polyUb directs that receptor to the lysosome [26].

Several E3 ubiquitin ligases play key roles in regulating transport through the endocytic pathway, including ubiquitin ligases of the Cbl (for Cas-Br-M ecotropic retroviral transforming sequence)

and Nedd4 (neural precursor-cell-expressed, developmentally down-regulated 4) families. The RING-type E3s of the Cbl family modify cell surface proteins with Ub sorting signals that facilitate cargo internalization and subsequent targeting to the lysosome [27]. In the case of ligand-stimulated EGFR, c-Cbl E3 Ub ligase can be recruited to the cell surface either by direct interaction with the phosphorylated receptor or through adaptor proteins [28]. The family of HECT-domain Nedd4 E3 Ub ligases also regulates endocytosis of cell surface receptors by directly ubiquitinating them, or through modification of multiple components of the endocytic machinery [29-31]. While Rsp5, the sole yeast orthologue of the conserved mammalian Nedd4 E3s, is responsible for the ubiquitination of the vast majority of proteins that are targeted to the vacuole [32], human cells encode nine different Nedd4 E3 Ub ligases, including Nedd4, Nedd4L and HECW1, which modify transmembrane proteins for their endosomal transport from either the plasma membrane or Golgi to the lysosome. These enzymes catalyze conjugation of K63-polyUb on a large variety of protein substrates through regulation by calcium signaling, lipid binding, autoinhibitory conformations, or protein-protein interaction with adaptor molecules [31,33,34].

The selection of plasma membrane proteins for Ub conjugation can either occur as a response to a biological signal such as binding of a cognate ligand (as described for EGFR activation), thereby facilitating receptor down-regulation, or as a quality control (QC) mechanism to eliminate faulty proteins from the cell surface. The best understood systems of cellular protein quality control (QC) are those of cytoplasmic, soluble proteins. However, accumulating evidence indicates that transmembrane proteins exported through the biosynthetic pathway are subjected to peripheral QC along the endocytic pathway, as well as at the plasma membrane, where accumulation of aggregation-prone proteins could cause cell surface damage and loss of cell integrity.

In yeast, damaged membrane proteins that escape ER QC through the ER-associated degradation (ERAD) pathway are largely targeted for Ub conjugation by Rsp5, the Nedd4-family ligase that also downregulates native cell-surface proteins. Some examples of faulty proteins that are ubiquitinated by Rsp5 for endocytic transport to lysosomes include: mutated versions of the Pma1 ATPase, the cell wall sensor Wsc1, and the arginine permease Can1 [35-37]. In mammals, the Cystic Fibrosis Transmembrane conductance Regulator (CFTR) with a ΔF508 mutation is the paradigm for a misfolded transmembrane protein. Although most ΔF508-CFTR is efficiently degraded via ERAD, a small fraction escapes the ER QC and reaches the plasma membrane where the CHIP (C-terminus of Hsp70-interacting protein) E3 Ub ligase selectively recognizes and ubiquitinates it through the interaction with the co-chaperones Hsc70/Hsp90 [38-40]. Once poly-ubiquitinated, ΔF508-CFTR undergoes rapid clathrin-mediated endocytosis by the adaptor protein AP2 and is sorted for lysosomal degradation via the MVB pathway [40]. However, loss of CHIP only partially inhibited turnover of protein from the cell surface, indicating the involvement of additional layers of regulation that rely on Ub conjugation machineries. Other E3 enzymes shown to ligate K63-polyUb onto ΔF508-CFTR as a peripheral QC response include RFFL, which ubiquitinates unfolded CFTR via a chaperone-independent mechanism[41], and Nedd4L, which ubiquitinates CFTR regardless of its folding state [42].

1.2.1: Ub as a signal for cargo sorting into MVBs

Sorting of endosomal proteins and their subsequent targeting into MVBs is mediated by the endosomal sorting complexes required for transport (ESCRT). In the early endosomes, nonubiquitinated transmembrane proteins are recycled back to the plasma membrane, while ubiquitinated transmembrane proteins are recognized by components of the ESCRT machinery

and incorporated into intralumenal vesicles to generate MVBs. The ESCRT machinery consists of four subcomplexes (0, I, II and III) and several accessory factors whose order of recruitment and function has been extensively characterized [43] (**Fig 1.2**). ESCRT-0, ESCRT-I and ESCRT-II act early in the sorting process and all three complexes contain a plethora of UBDs, giving them the potential to cooperatively recognize and coordinate sorting of ubiquitinated cargo [28]. ESCRT-0, which consists of Hrs (Vps27 in yeast) and STAM1/2, is recruited to endosomal membranes via binding to phosphatidylinositol 3-phosphate (PI3P) [44-46]. ESCRT-0 contains several UBDs (approximately five in yeast), which can either facilitate simultaneous interaction with several cargo proteins or, alternatively, confer high-affinity binding to cargo through an avidity-based mechanism. Hrs contains a double-sided UIM that can bind two Ub moieties; the yeast counterpart, Vps27, instead, has two single-sided UIMs. STAM1/2 contain both a UIM and a VHS domain for binding Ub. Loss of the UIM in mammalian Hrs or of the UIMs in the yeast Vps27 causes defects in endocytic cargo sorting [47]. Hrs also recruits clathrin at the sites of intralumenal vesicle formation [48] where it functions to increase the concentration of ESCRT-0 in restricted clathrin coats on endosomal subdomains. It has been suggested that Hrs/clathrin coat serves to concentrate ubiquitinated cargo before its incorporation into endosomal invaginations [49]. ESCRT-0 recruits ESCRT-I through interaction between Hrs and TSG101 (a subunit of the ESCRT-I) [50]. Interaction between ESCRT-I and ESCRT-II facilitates formation of a supercomplex that promotes bud formation and cargo sorting. ESCRT-II, ALIX, and charged multivesicular body protein (CHMP) 7 have been reported to act as upstream factors for ESCRT-III recruitment and assembly. Finally, ESCRT-III proteins (CHMP6, CHMP4A, CHMP3 and CHMP2) in concert with the AAA-type ATPase VPS4A/B mediate membrane scission and intralumenal vesicle formation [47]. In a model for ESCRT function during cargo sorting and MVB biogenesis, ESCRT-0 selects and captures

ubiquitinated cargo, ESCRT-I and ESCRT-II supercomplex induces formation of membrane buds that invaginate into the lumen of endosomes, and ESCRT-III forms polymers around the neck of the invagination, thereby facilitating membrane constriction and scission to generate intralumenal vesicles [28].

Ubiquitinated cargo was originally thought to be sorted sequentially from ESCRT-0 to ESCRT-I and subsequently to ESCRT-II. However, recent studies suggest that ESCRT-0 initially clusters ubiquitinated cargo within endosomal subdomains to facilitate the downstream cooperative binding of additional UBDs [28]. K63-polyUb has been suggested to play a major role in mediating sorting of endocytic cargo into MVBs [24]. Thus, it is tempting to speculate that multiple UBDs from the ESCRT complex are optimally arrayed to facilitate an avid interaction with polyUb chains harboring K63-linkages. Before cargo incorporation into the intralumenal vesicles of the MVBs, ubiquitin is removed from the transmembrane proteins by DUBs to recycle Ub. The non-selective DUB USP8 and the K63-polyUb specific DUB AMSH have been linked to ESCRT function, as suggested by the attenuated degradation of cargo via MVBs observed upon their loss. A key role for USP8 has been attributed to its ability to deubiquitinate and stabilize ESCRT-0 [51,52], thus preventing its proteasomal degradation. Moreover, USP8 also controls the ubiquitination state of the ESCRT-III components and may promote their assembly [53].

1.2.2: Endosomal recycling of membrane proteins by the retromer complex

Recycling of transmembrane cargo is critical for the regulation of several cellular processes such as nutrient uptake, cell–cell adhesion, and cell migration [54]. For example, recycling of EGFR to the plasma membrane is considered to be important for the maintenance of its signaling activity. The ubiquitination status of activated receptor complexes determines their sorting between

8

recycling and degradation and thereby dictates receptor fate. Ligand-stimulated EGFRs that cannot recruit the E3 Ub ligase Cbl, and thus cannot be ubiquitinated, are not degraded by the lysosome but are instead rapidly recycled [55]. Furthermore, studies following the prototypical recycling cargo TfR that was engineering as a chimeric fusion with Ub showed that ubiquitination diverts the receptor into the MVB pathway, away from recycling [49].

Endosomal sorting involves the partitioning of transmembrane cargo into tubules that originate from the endosome and subsequently pinch off to form discrete transport vesicles. Based on a previous observation that TfR was recycled in the absence of its entire cytosolic tail, thereby precluding adaptors binding or ubiquitination, it was originally concluded that endocytic cargo undergoes recycling in the absence of any sorting signal, through a "default" pathway that occurs by bulk membrane flow [56]. However, a critical re-evaluation of endosomal recycling of TfR and other cargo during the past two decades has established the existence of sorting sequences and identified machineries that control cargo sorting and induce tubulation; this machinery includes adaptor proteins (APs), sorting nexins (SNXs), and the coat complex retromer [56].

The retromer is a highly conserved heterotrimeric protein complex that localizes on the limiting membrane of early and late endosomes and plays a major role in diverting cargo from the degradative pathway by directing it to either the plasma membrane or the *trans*-Golgi network (TGN) (**Fig 1.3**). Its deficiency results in perturbation of general recycling and missorting of transmembrane proteins to the lysosome for degradation [56,57]. The retromer assembles from a high-affinity heterotrimeric core complex composed of VPS35, VPS29, and one of two VPS26 subunits, VPS6A or VPS26B [58], in association with membrane-bound SNX–BAR (Bin–Amphiphysin–Rvs) proteins, which tether the retromer on the limiting membrane of the endosomes [59-61], and several other accessory proteins such as Rab7a, a Rab involved in endosome maturation and lysosomal

fusion, and TBC1D5, a GAP (GTPase-activating protein) for Rab7a [59,60]. Recruitment of the retromer to the endosome occurs either by interaction with the PI3P-binding protein SNX3 [61], or through binding to the activated form of Rab7a [59,60] (**Fig 1.3**). TBC1D5 has been proposed to act as a negative regulator of the retromer, modulating the GTP-bound state of Rab7a on the endosomes [62]. In addition to TBC1D5, the retromer complex also interacts with the WASH machinery, a macromolecular complex that was identified by affinity purification of one of its components: Wiskott-Aldrich syndrome homologue 1 (WASH1), an actin nucleation promoting factor [63]. WASH complex recruitment to the endosomes occurs through direct interaction between FAM21, a subunit of the WASH complex, with the cargo recognition domain subunit VPS35 [64,65]. Its function is to stimulate actin filament nucleation by the Arp2/3 complex [66], thereby promoting formation of localized actin patches that serve to segregate and concentrate membrane proteins into subdomains of the endosome before tubule formation, membrane fission, and transport to either the plasma membrane or TGN [67]. By acting in concert with the retromer and various retromer-associated SNXs, the WASH complex has been implicated as a master regulator of endocytic cargo transport, such as the plasma membrane recycling of α5β1 integrin [68], Wntless receptor [69,70] and TfR [71], or the retrieval of the CI-M6PR to the Golgi [9,65]. Importantly, the retromer–WASH complexes have also been shown to regulate trafficking of transmembrane proteins into specialized organelles during various forms of autophagy [72,73].

1.3: Autophagy signaling and molecular machineries

Macroautophagy (hereafter referred as autophagy) is an intracellular process in which damaged organelles, misfolded proteins, or invading microbes are enveloped by double-membrane vesicles, called autophagosomes, and then released into lysosomes for their breakdown [74]. Defects in

autophagy are linked to the pathogenesis of several human disorders that include neurodegeneration and cancer [14]. Initially viewed as a bulk degradative system to recycle nutrients in response to starvation, autophagy is now known to be a highly regulated process used constitutively and also to respond to various stress and developmental signals [75,76]. One potent inducer of autophagy is amino acid starvation. In amino acid-rich conditions, the mechanistic target of rapamycin complex 1 (mTORC1) inhibits autophagy by phosphorylating and inactivating ULK1 (Atg1 in yeast), whereas on sensing a decrease in amino acid levels, mTORC1 relieves the inhibition of ULK1, thereby strongly activating autophagy [77,78].

Autophagy comprises distinct membrane-mediated steps (**Fig 1.4**). First, cytoplasmic cargo is enveloped by newly formed cup-shaped double-membrane structures, termed phagophores, to form autophagosomes. Different cellular compartments, including ER, Golgi complex, mitochondria, or recycling endosomes, have been described as potential sources for the membrane origin of the phagophore [79].

More than 30 autophagy-related proteins (ATGs) are sequentially recruited and used during autophagosome biogenesis. The ULK1 complex initiates phagophore nucleation by regulating localization and activation of the phosphatidylinositol 3-kinase (PI3K) class III complex [80], which includes Beclin1 and the kinase VPS34. Synthesis of PI3P generates a platform for recruitment of WIPI1-4 proteins (WD-repeat PI3P effectors) and the ATG12-ATG5-ATG16L1 complex, which are required to conjugate LC3 (Atg8 in yeast) to the lipids of the autophagosomal membrane during phagophore elongation and closure [81-85] (**Fig 1.4**). The lipidated form of the protein LC3 is a major constituent of the autophagy-related organelle membranes (i.e., phagophore, autophagosomes, and autolysosomes) [86] (**Fig 1.4**).

The early stages of autophagosome formation also depend on ATG9A and VMP1, two transmembrane proteins implicated in autophagy. Vesicles containing ATG9A, the only transmembrane core ATG protein, are thought to supply lipids to autophagosomes [79]. Depletion of ATG9A inhibits starvation-induced autophagy, consistent with an essential role in initiating autophagosome biogenesis [87]; ATG9A function is also required for selective autophagy (see below) of *Salmonella typhimurium* [88]. ATG9A's trafficking route involves multiple organelles and is regulated by large number of protein machineries that control ATG9A sorting and transport (see **Fig 3.0** in Chapter 3). Upregulation of autophagy results in a redistribution of ATG9A from the juxtanuclear region of the recycling endosomes and Golgi, where it normally resides, to the peripheral LC3-positive structures, which correspond to the sites of autophagosome formation [89,90]. Several autophagy components, including the ULK1 kinase complex in mammalian cells and Atg2 and Atg18 (the human orthologue of WIPI2) in yeast, have been also implicated in modulating ATG9A localization at the phagophore assembly site [90-92].

VMP1 is a multispanning ER-resident protein that plays an essential role in autophagosome formation by directly recruiting Beclin1, thereby promoting PI3P synthesis by the PI3K complex [93]. More recently, it has been suggested that VMP1 has a role in regulating contact sites between the ER and various organelles [94]. Specifically, VMP1 has been reported to recruit the PI3K at the ER–plasma membrane contact site to facilitate mobilization of membrane to the site of autophagosome formation [95]. Moreover, another report suggested that VMP1 controls ER–phagophore contact site through the SERCA pump to facilitate autophagosome formation [96].

After the phagophore seals its edges, a fully formed autophagosome undergoes maturation and lysosomal targeting. The maturation steps comprises a series of events in which all ATG proteins are disassembled from the organelle surface following removal of PI3P by phosphoinositide

phosphatases (e.g., family of Myotubularin-related, MTMR, proteins) and cytoplasmic-side LC3 by members of the ATG4 protease family [97]. Next, the fusion of autophagosomes with lysosomes delivers cargo for degradation; this can occur either directly via maturation into "autolysosomes", or indirectly via the formation of hybrid compartments ("amphisomes") that originate from autophagosome fusion with endosomes. A group of soluble N-ethylmaleimide-sensitive factor activating protein receptors (SNAREs) has been implicated in membrane fusion of autophagosomes and late endosomes or lysosomes; these include Syntaxin 17 (STX17), SNAP29, and VAMP7 or VAMP8 [98] (**Fig 1.4**). Autophagosomes also acquire Rab7, which in turn interacts with the homotypic fusion and protein sorting (HOPS) tethering complex to mediate fusion with lysosomes (**Fig 1.4**). Importantly, STX17 also directly interacts with the HOPS complex [98,99].

1.3.1: Ub as a signal for selective autophagy

Accumulation of Ub inclusions has been detected in brain tissues of knock-out mice lacking ATG5 or ATG7 [100,101], essential autophagic proteins that lipidate LC3 on the autophagosomal membrane. Ub might serve as a regulatory signal for selective autophagy [102-104]. The best characterized function of Ub in selective autophagy initially came from the identification of the autophagic cargo receptor p62 (also known as SQSTM1) to mediate degradation of ubiquitinated substrates (cargo) via the simultaneous interaction with Ub and a nascent autophagosome[104]. Whereas starvation-induced autophagy is a non-selective process that degrades randomly engulfed cytosolic components in order to fuel the cell in the absence of nutrients, during selective autophagy specific substrates are marked with Ub and recognized by autophagic cargo receptors for their packaging into autophagosomes. Besides p62, other known autophagic cargo receptors include neighbor of BRCA1 (NBR1), nuclear dot protein 52 (NDP52), optineurin (OPTN), and Tax1 Binding Protein

1 (TAX1BP1). All of these adaptors contain both LC3-interacting region (LIR) motifs and several UBDs in their protein sequences, which allows them to simultaneously bind to Ub and LC3 to bridge ubiquitinated cargo and autophagosomal membranes [103]. So far, three different UBDs have been identified during selective autophagy: ubiquitin-associated (UBA), ubiquitin binding in A20-binding inhibitor of NF-kappa-B (ABIN) and NF-kappa-B essential modulator (UBAN), and ubiquitin-binding zinc finger (UBZ) domains. UBA domains are found in p62 and NBR1, while UBAN and UBZ domains are found in OPTN, NDP52 and TAX1BP1 [105,106].

Several types of selective autophagy are classified based on their substrates: e.g., aggrephagy (removal of aggregated proteins), mitophagy (degradation of damaged mitochondria), pexophagy (removal of peroxisomes), ER-phagy (degradation of ER membrane), and xenophagy (clearance of bacteria or viruses). Autophagy of Salmonella *typhimurium* (*Salmonella*) is one of the most studied types of selective autophagy to date; here, the interplay between Ub and autophagic cargo receptors have been extensively described. Upon infection, *Salmonella* resides within a modified phagosomal compartment called the *Salmonella*-containing vacuole (SCV). Cytosolic *Salmonella* that escape the SCVs are rapidly marked with ubiquitin and targeted for autophagy by p62, NDP52 and OPTN. Depletion experiments indicated that all three autophagic adaptors act in the same pathway to cooperatively drive efficient autophagic removal of bacteria [103]. In the case of p62, binding of Ub-decorated *Salmonella* occurs via the C-terminal UBA domain [104], which was suggested to recognize K63-polyUb *in vitro* [107,108]. Similarly, OPTN recruitment to invading *Salmonella* required a functional UBAN domain, which is known to specifically interact with linear polyUb [109]. In addition, *Salmonella* residing in damaged SCVs can also be targeted by autophagy [102,110]. In this latter case, modified carbohydrate structures on the SCV recruit galectins

and Ub to initiate autophagosome formation through recruitment of NDP52 [110], which has been suggested to have a preference for K63-polyUb [109].

1.3.2: The connection between endocytosis and autophagy

Several studies have shed light onto how endocytosis and autophagy pathways are intertwined. The endocytic and autophagic systems serve as cellular degradative pathways that converge at the same endpoint. An example of interconnection between autophagy and endocytosis has been reported for the degradation of endocytosed Connexin-43, a gap junction protein [111]. In response to certain stresses, endocytosis is responsible for removing the gap junctions from the plasma membrane to reduce cellular adhesion between neighboring cells [112]. Subsequently, vesicles containing Connexin-43 are degraded by autophagy [113,114]; this indicates that both systems cooperate to complete lysosomal turnover of gap junctions. These studies also show that degradation of internalized gap junction proteins via the autophagosomal route depends on the autophagic cargo receptor p62 [115]. Interestingly, Connexin-43 was also reported to undergo K63-polyubiquitination to regulate gap junction internalization [116].

The contribution of the endocytic pathway to autophagy has been mostly documented for the delivery of lysosomal hydrolases and the machinery to acidify vesicles during the late stages of autophagosome maturation: i.e., autophagosome fusion with late endosomes or lysosomes. After digestion, the degradation products need to leave the autolysosomes with the aid of specialized transporters, which are also provided by the endocytic system [117]. However, more recent evidence for the contribution of endocytosis to the early stages of autophagy is also starting to emerge, and mainly comes from the discovery that recycling endosomes marked with Rab11a were found to participate in autophagosome biogenesis by delivery of membranes to the growing phagophore [118-

[120]. The early autophagy regulators ATG9A and ATG16L1 are internalized from the plasma membrane via distinct clathrin-coated pits and reach the Rab11a-positive recycling endosomes where they fuse in a process requiring the activity of the SNARE protein VAMP3 [119]. In addition, the PI3P-binding WIPI2, which in turn recruits ATG16L1, has been reported to interact with Rab11a. Both ULK1 and ATG9A are present on recycling endosomes, but on different subdomains [118]; the ULK1 kinase complex phosphorylates ATG9A and facilitates its vesicular trafficking in response to autophagy [90]. Trafficking of ATG9A during autophagy is also mediated by the endosomal retromer–WASH machinery [72] (see Chapter 3).

Both endocytosis and autophagy are known to utilize a set of identical effector proteins. For example, Beclin1, a subunit of the PI3K complex, is also found on early endosomes, where it can promote generation of PI3P on the Rab11a-positive domains [120]. Another connection between endocytosis and autophagy concerns the requirement of membrane fission reactions of the ESCRT complex. Although ESCRTs have been implicated in generating endosomal invaginations during sorting and degradation of ubiquitinated cargo (see paragraph 1.2.1), there is increasing evidence of their role in autophagy [43,121]. Depletion of individual ESCRT complexes in mammalian cells results in accumulation of autophagosomes, most likely due to inhibited fusion with the endolysosomal system [122-124]. Previous studies showed that the endocytic and autophagic pathways intersect when autophagosomes fuse with MVBs to form a hybrid compartment called amphisome [125,126]. Thus, one possibility is that ESCRT deficiency impairs intralumenal vesicle formation and MVB biogenesis and, indirectly, autophagosome maturation. More recent work has suggested a direct involvement of the ESCRT machinery in other types of autophagy. One example is endosomal microautophagy, which is a noncanonical form of autophagy where autophagic cargo is directly invaginated into lysosomes through the coordinated function of VPS4A/B, TSG101,

Alix and the chaperone molecule Hsc70 [127]. Interestingly, ESCRT-mediated intralumenal vesicles formation during MVB biogenesis has been also implicated in secretory pathways involving exosome biogenesis and secretory autophagy [128]. Work in human cells showed that autophagy and ESCRT components cooperate in regulating unconventional secretion of ΔF508-CFTR as a mechanism of QC[129]. Similarly, recent studies in yeast suggested the requirement for ESCRT-III in the unconventional export of misfolded proteins through CUPS (ER-derived vesicles and tubules surrounded by a cup-shaped membranes), which also colocalize with autophagic components [130].
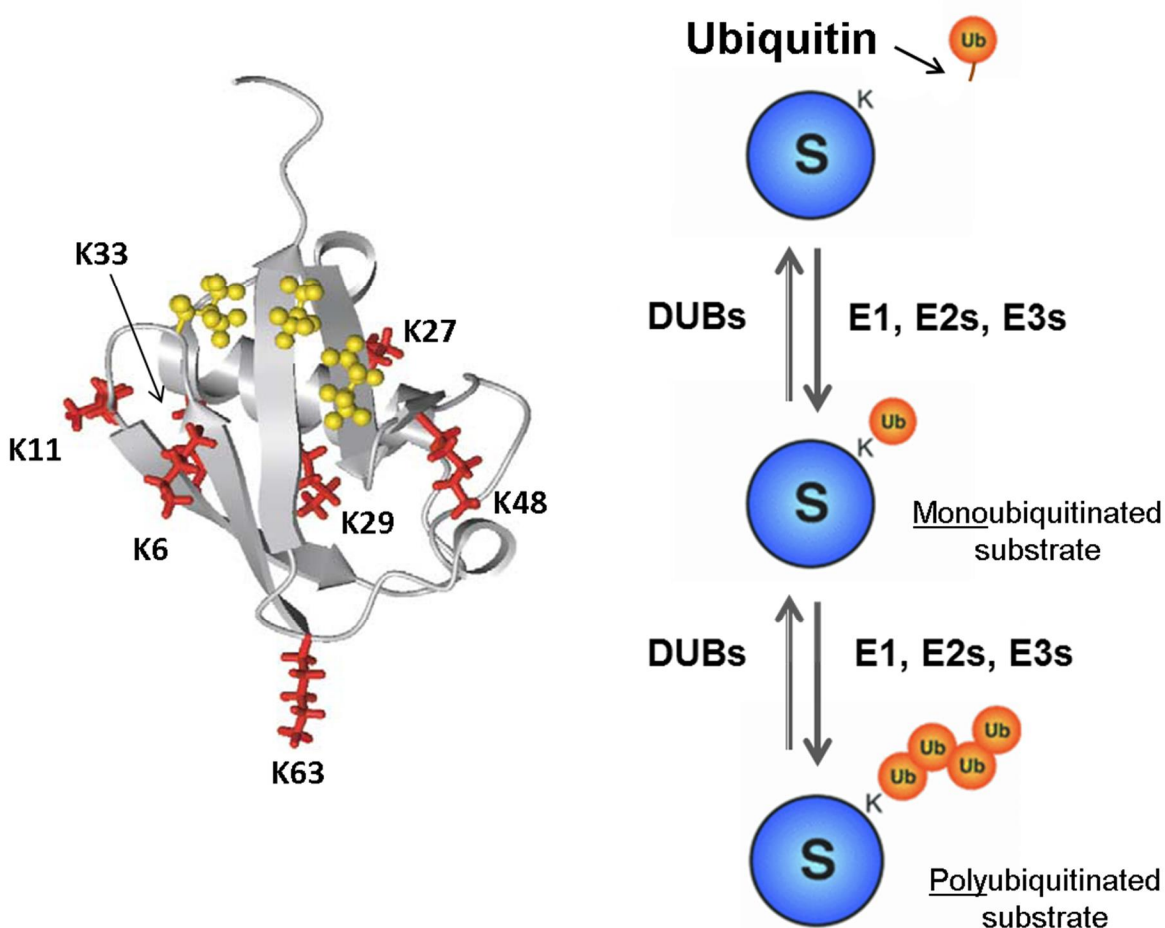
Figure 1.0: Ub conjugation and deconjugation of a substrate. Ribbon diagram of the main features of the Ub molecule. The seven lysine residues are shown in red and labeled, while the L8–I44–V70 hydrophobic patch is shown in gold ball-and-stick (right panel). Schematic diagram showing Ub conjugation onto a substrate (S) through a cascade of three enzymatic reactions mediated by the Ub enzymes E1, E2s and E3s. Ubiquitination is reversible and it can be deconjugated by the enzymatic activity of DUBs. Substrates can be either modified with a single Ub molecule or a chain of polyUb. Ub has seven lysine residues (K6, K11, K27, K29, K33, K48 and K63), and together with the Nα amino group of the methionine residue (Met1) can assemble eight potential homotypic polyUb signals. Adapted from Pickart CM., Fushman D., *Curr Opin Chem Biol*. 2004; Dec;8(6):610-6 and Komander D., *Biochem Soc Trans*. 2009. Oct;37(Pt 5):937-53. doi: 10.1042/BST0370937.
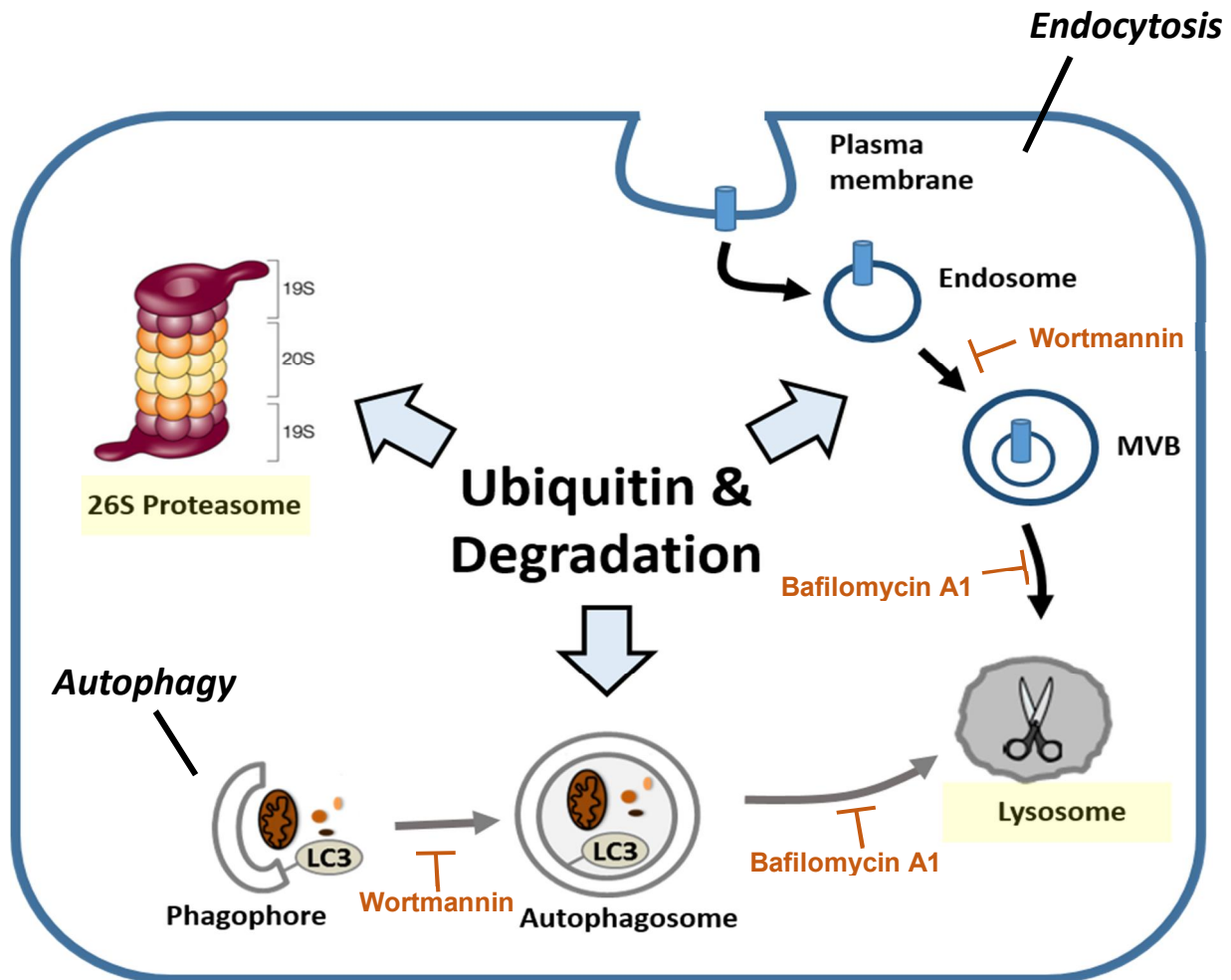
Figure 1.1: Ub regulates different degradation pathways. Overview of three major cellular proteolytic systems where Ub plays a fundamental role: 26S Proteasome system, endocytosis and autophagy. Specific protein effectors associate with ubiquitinated protein substrates to determine their proteolytic fate. The endocytic and autophagic pathways merge at the lysosomes and share a requirement for several machineries including *v*-ATPases (inhibited by Bafilomycin A1), phosphoinositide 3-kinase activity (inhibited by wortmannin) and ESCRTs (see main text for further details). Adapted from Clague, MJ., Urbe S., *Cell*. 2010; Nov 24;143(5):682-5. doi: 10.1016/j.cell.2010.11.012.
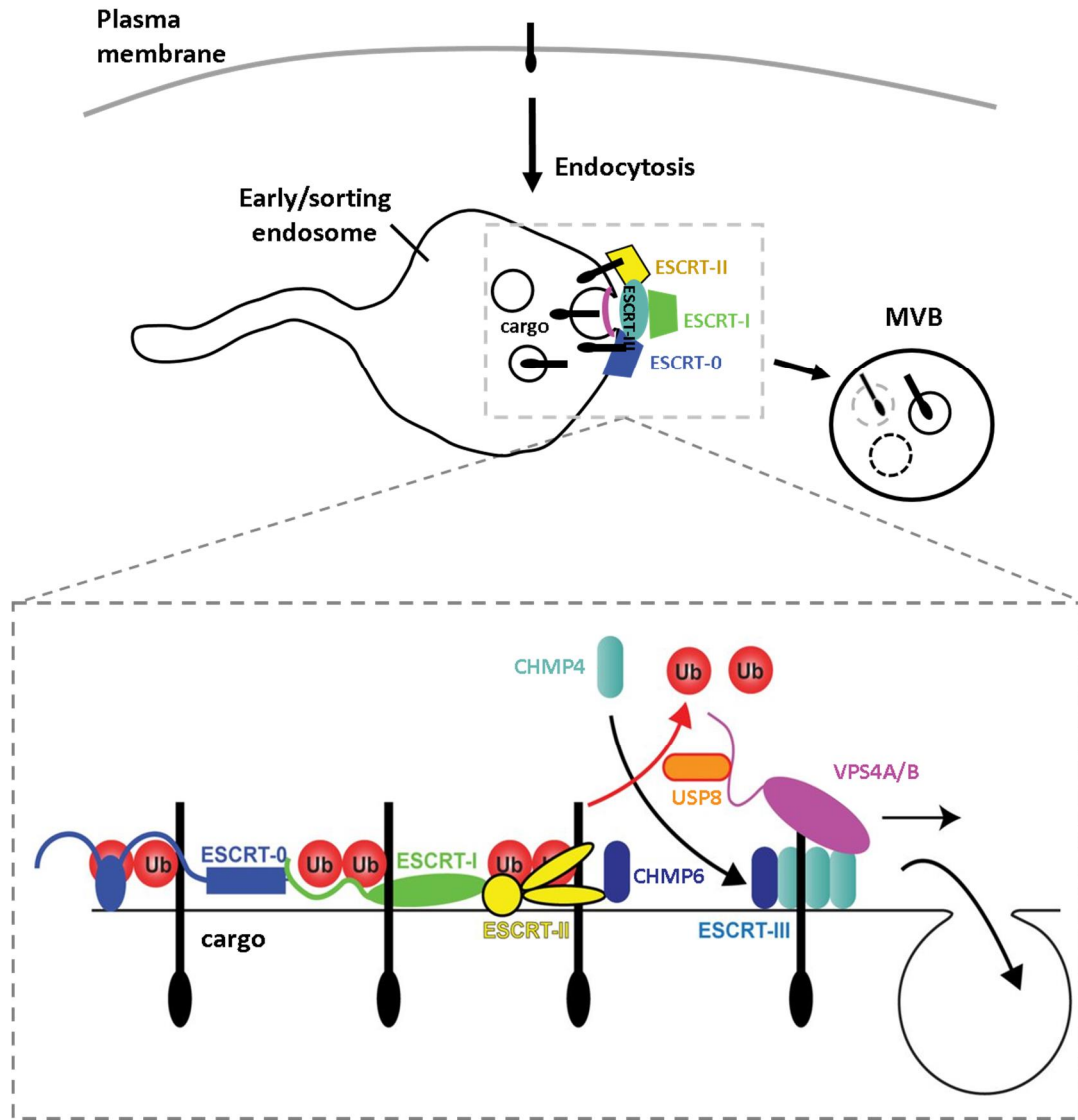
Figure 1.2: ESCRT-mediated sorting of ubiquitinated transmembrane protein cargo into MVBs. Internalized ubiquitinated transmembrane proteins at the early/sorting endosome are recognized by the ESCRTs for their sorting into intralumenal vesicles of MVBs (top panel). The ESCRTs act in sequence: the class ESCRT-0 (*blue*) is targeted to PI3P-containing endosomal membranes via its FYVE domain and binds ubiquitinated cargo (*black*) via UIM motifs. Subsequently it recruits/activates ESCRT-I (*green*) and ESCRT-II (*yellow*) on endosomes, which also bind ubiquitinated cargo. The action of a number of VPS4A/B (*magenta*) and CHMP proteins (*indigo* and *cyan*) assemble the ESCRT-III complex to initiate membrane deformation and biogenesis of intraluminal vesicles. Recruitment of USP8 (*orange*), the deubiquitinating enzyme to remove Ub from cargo before its entry into the buds, is necessary to recycle Ub (*red*). The concerted action of different ESCRT components and several UBDs results in the sorting of cargo into the MVB pathway (bottom panel). Adapted from Tabernero L., Woodman P., 2018. Biochem Soc Trans. 2018;46:1037–46.
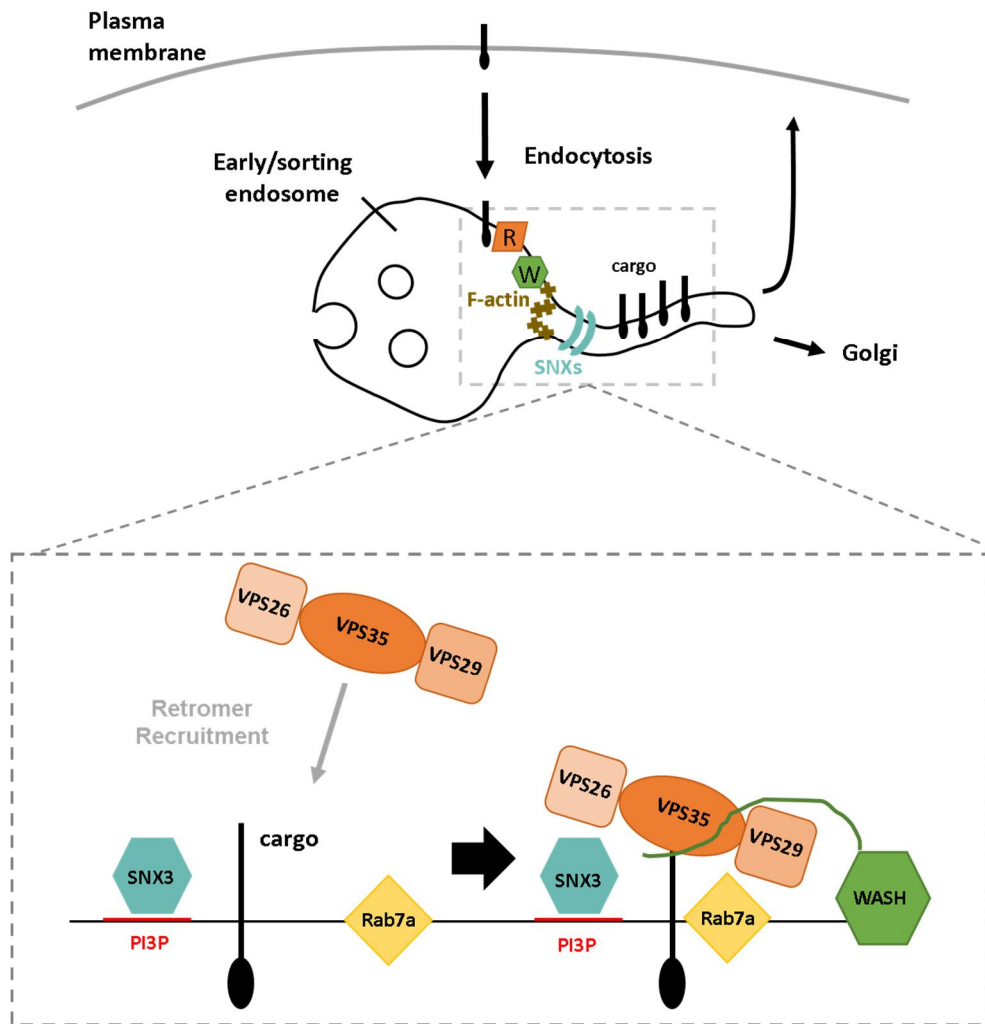
Figure 1.3: Retromer-dependent recycling of transmembrane proteins. Upon internalization, endocytosed transmembrane proteins can be retrieved to the Golgi or recycled back to the plasma membrane via the concerted action of the retromer complex (R, *orange*), the WASH complex (W, green) and a series of SNXs proteins (*cyan*). SNXs (*cyan*) promote membrane curvature through their BAR domain. Cargo (*black*) is recognized by the cargo-selective subcomplex of the retromer (R, *orange*) for their sorting into endosomal tubules and their subsequent delivery to Golgi or plasma membrane. The WASH complex (W, *green*) activates Arp2/3-mediated actin (*brown*) nucleation required for membrane tubule scission (top panel). Recruitment of the cargo-selective retromer heterotrimeric complex (Vps35–Vps29–Vps26, *light* and *dark orange*) is mediated by Rab7a (*yellow*) and the PI3P(*red*)-interacting Snx3 (*cyan*). The VPS35 core subunit of the retromer interacts with the C-terminal tail of FAM21, a subunit of the WASH (*green*) complex, to promote cargo sorting and transport (bottom panel). Adapted from Seaman MJ., 2012. J. of Cell Sci. 125: 4693-4702; doi: 10.1242/jcs.103440.
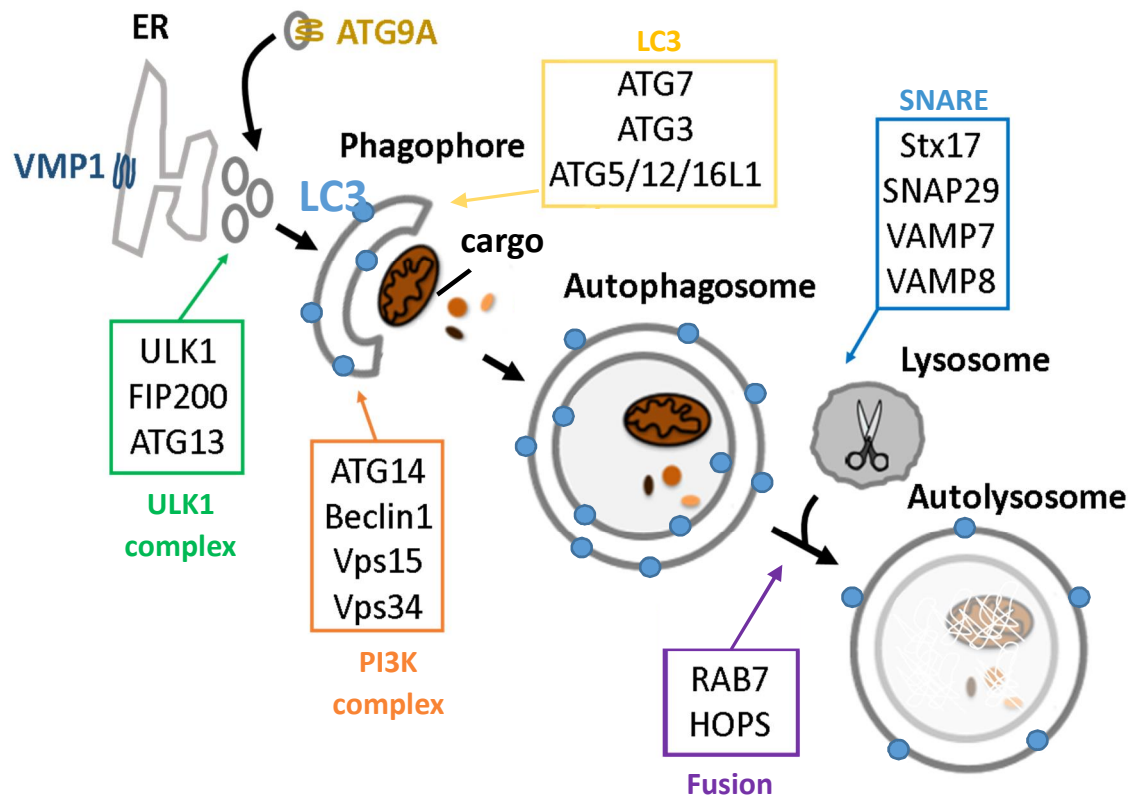
Figure 1.4: The autophagy pathway and autophagy regulators. Autophagy is a membrane-mediated, stepwise process in which double-membrane structures ("phagophores") envelope cytoplasmic material ("cargo") to form autophagosomes. The fusion of autophagosomes with lysosomes delivers cargo for degradation. Autophagy regulators are grouped based on their function. ATG9A (*gold*) and VMP1 (*blue*) are the two sole transmembrane proteins involved in this process. LC3 (*light blue*) is conjugated to phosphatidylethanolamine and marks all the autophagosomal compartments. See text for details.

Chapter 2: K63-polyUb-dependent traffic of transmembrane proteins into lysosomes

Introduction:

Ub can be conjugated to other proteins either as single Ub or as a polyUb chain. Many types of polyUb, distinguished by different Ub–Ub linkages, are present in cells [3,4]; one example is K63-polyUb, which serves as a signal for endosomal trafficking to the lysosomes [131]. Previous studies suggest that K63-polyUb is involved in the plasma membrane internalization and the sorting into multivesicular body (MVB) of transmembrane proteins such as the epidermal growth factor receptor (EGFR) [26,28,47]. Canonical endolysosomal degradation requires maturation from early endosome to MVB, followed by fusion with highly acidic, degradative lysosomes. The endosomal sorting complexes required for transport (ESCRT) recognizes ubiquitinated cargo in endosomes and sort them into intraluminal vesicles of MVBs before their degradation. Ub attachment to transmembrane proteins strongly correlates with their lysosomal turnover [28]. Although the endocytic delivery of ubiquitinated cargoes to lysosomes constitutes the main pathway for plasma membrane protein degradation, recent studies also support the involvement of autophagy in the turnover of endocytosed cargo [113,120].

In autophagy, "to-be-degraded" cytosolic components, such as vesicles containing membrane proteins, protein aggregates, or whole damaged organelles, are sequestered by double-membrane vesicles, called autophagosomes, and then released into lysosomes for their breakdown [132]. Initially viewed as a bulk degradative system to recycle nutrients in response to starvation, autophagy is now known to be a highly regulated process used constitutively and also to respond to diverse stresses. More than 30 autophagy-related proteins (ATGs) are sequentially recruited and used during the stages of autophagy [14,79]. The lipidated form of the protein LC3 is a major constituent of the autophagosomal membrane [86]. Different cellular compartments, including ER, Golgi,

mitochondria, endosomes, or plasma membrane have been described as potential sources for the membrane origin of the autophagosome [79]. The transmembrane protein ATG9A acts at an early stage of autophagosome biogenesis, possibly by delivering lipids from the plasma membrane to the forming autophagosome.

K63-polyUb chains have been shown to be required in selective forms of autophagy. The evidence for the interplay between Ub and autophagy is based largely on the ability of several autophagic cargo receptors (e.g., p62/SQSTM1) to mediate degradation of ubiquitinated substrates by simultaneous interaction with Ub and LC3 [104]. After cargo engulfment, autophagosomes fuse with lysosomal compartments to form degradative autolysosomes.

The extent and details of the relationship between Ub and autophagy are poorly understood. Importantly, the relative contribution of endocytosis and autophagy pathways to transmembrane protein proteolysis, as well as the reasons for the redundancy of degradative systems in lysosomal turnover of ubiquitinated cargo are, for the most part, unknown. Specifically, *what type(s) of Ub modification is involved in autophagy, how Ub signals recognition of cargo for lysosomal targeting, and whether Ub plays a role in determining the decision between proteolysis by endolysosomes or autophagy* are not well understood; these deficiencies are due in part to the lack of tools to study Ub-dependent signaling. We have previously described a K63-polyUb specific sensor, "Vx3," that can be used to detect and also to inhibit K63-polyUb-dependent signaling [133]. Vx3 contains three UBDs connected by two structured linkers designed to promote avid interaction with three adjacent Ub moieties in K63-linked polyUb (**Fig 2.0**). Expressing Vx3 in living cells allowed us to visualize and identify cellular compartments enriched in K63-polyUb. Here we report that K63-polyUb modifies a variety of transmembrane proteins of the post-Golgi endosomal system to signal their delivery to the lysosomes. Vx3 sequesters ATG9-positive vesicles that co-

localize with ubiquitinated transmembrane proteins at the ER:endosome interface. By tightly binding to K63-polyUb, Vx3 inhibits receptor(s) or DUB(s) whose functions may play important roles in fusion of ubiquitinated cargo-containing vesicles with endolysosomes. Our work supports a role for endogenous K63-polyUb in regulating lysosomal targeting of transmembrane proteins via autophagy-related vesicular trafficking.

Results:

2.1 Vx3 is a sensor and an inhibitor of selective autophagy

Expression of Vx3-EGFP in HeLa cells generates cytoplasmic foci that stain for K63-polyUb (**Fig 2.1A**). In contrast, a non-binding control protein, Vx3NB-EGFP, remains diffuse (**Fig 2.1B**), indicating that Vx3 foci depend on Ub binding. In the cytosol, polyUb inclusions have been previously described as sites of autophagic clearance wherein polyUb is used to recruit autophagy cargo receptors to protein aggregates [100,104]. We examined localization of Vx3-EGFP with several autophagic and endocytic markers (see colocalization analysis reported in **Table 1**). We found that ~55% of Vx3 foci overlapped with endogenous LC3 upon transient transfection, whereas only ~20% of LC3-positive signals overlapped with Vx3 (**Fig 2.2A**; **Table 1**). Surprisingly, in HeLa cells stably expressing Vx3-EGFP under the control of a Doxycycline (Dox)-inducible promoter (hereafter called HeLa-Vx3), Vx3 did not colocalize with LC3 in the absence of autophagy stimuli (**Fig 2.2B**; **Table 1**). However, treatment with Lipofectamine 2000 (without DNA) induced Vx3 and LC3 colocalization around liposomes as early as 4 h after addition (**Fig 2.2B**). These foci also stained for galectin-3 (**Fig 2.2C**), a marker of damaged membranes, which suggests that the generation of K63-polyUb may have been a consequence of endosome rupture that signals autophagy initiation [102]. A similar observation was made when HeLa-Vx3 was infected with

Salmonella enterica serovar Typhimurium, which activates selective autophagy [134]. At 1 h post-infection, Vx3 was seen surrounding a subpopulation of intracellular *Salmonella* that associated with LC3 (**Fig 2.2B**) and galectin-3 (**Fig 2.2C**).

Vx3 displays higher affinity and specificity for K63-polyUb than any of the known naturally-occurring polyUb-receptors; by its expression, it can be used to disrupt K63-polyUb-dependent interactions within living cells [133]. We hypothesized that, by binding to K63-polyUb with high affinity, Vx3 would interfere with selective autophagy signaling *in vivo*. To test this, we infected Dox-inducible HEK293-Vx3 or Vx3NB cells with *Salmonella* and measured intracellular bacterial growth over time. Intracellular proliferation of *Salmonella* was significantly higher in the presence of Vx3 (**Fig 2.3A**), indicating that Vx3 expression blocks selective autophagy of *Salmonella*. Further evidence that Vx3 interferes with selective autophagy was obtained using the dual-fluorescent reporter EGFP-mRFP-LC3 [135]. The reporter in autophagosomes shows both EGFP (*green*) and mRFP (*magenta*) signals (colocalization: *white*), but because EGFP fluorescence is quenched by the acidic pH in lysosomes, EGFP-mRFP-LC3 in autolysosomes emit only mRFP fluorescence (*magenta*). We found that the white/magenta ratio of LC3 foci was higher in HeLa cells transiently transfected with Vx3 compared to Vx3NB (**Fig 2.3B**), suggesting that Vx3 blocks autophagosome maturation or fusion with lysosomes.

We next looked to see if K63-polyUb is involved in non-selective autophagy where cytoplasmic material is engulfed by autophagosomes in response to nutrient starvation. Nutrient starvation does not trigger Vx3 and LC3 colocalization (**Fig 2.4A**). Furthermore, neither the starvation-induced increase in LC3 puncta (**Fig 2.4B**) nor LC3-II turnover (**Fig 2.4C**) was affected by Vx3 expression. Thus, K63-polyUb is not required for bulk, non-selective autophagy, and Vx3-EGFP can be used to identify and inhibit signaling by K63-polyUb in selective autophagy.

2.2 Vx3 colocalizes with ATG9A and K63-polyubiquitinated transmembrane proteins

Without selective autophagy induction, HeLa-Vx3 foci localized to cytoplasmic structures that did not contain LC3 (**Fig 2.2A**). One possibility is that Vx3 inhibits an early stage of autophagosome formation that precedes LC3 conjugation. Alternatively, K63-polyubiquitinated proteins may be associated with membranes in trafficking pathways unrelated to autophagy. The transmembrane protein ATG9 acts early in autophagosome biogenesis together with the ULK1 kinase complex [14]. Strikingly, we observed that Vx3 foci are always marked by endogenous ATG9A (**Fig 2.5A**; **Table1**), but not by components of the ULK1-kinase complex (e.g., ULK1, FIP200) or many downstream autophagy regulators (e.g., Beclin1, ATG16L1, WIPI2b) (**Fig 2.5B**). Vx3 foci also contain p62/SQSTM1, an autophagy adaptor and a common component of protein aggregates (**Fig 2.5C**; **Table 1**).

2.2.1 Ectopically expressed VMP1-iRFP is K63-polyubiquitinated

Like ATG9A, the ER-resident multi-spanning membrane protein VMP1 is also known to regulate autophagy-related vesicular trafficking [79,93]. We found that stable co-expression of VMP1-iRFP and Vx3-EGFP showed nearly complete colocalization (**Table 1**). These Vx3 and VMP1-containing foci also colocalized with ATG9A (**Fig 2.6A**). Overexpression of VMP1-iRFP alone induces K63-polyubiquitination (**Fig 2.6B**), although co-expression of Vx3 promotes larger VMP1-positive structures when compared to control cells expressing Vx3NB (**Fig 2.6C**). Our results show that Vx3-EGFP co-immunoprecipitated VMP1-iRFP but not endogenous VMP1 (**Fig 2.6D**). Endogenous VMP1 does not form the punctate structures but colocalizes with markers of the ER [96]. However, fusion of fluorescent tags (in particular mRFP and its derivatives) to a

transmembrane protein of interest tend to induce formation of aggregates [136]. That overexpression of VMP1-iRFP induces cytoplasmic foci positive for K63-polyUb suggests that such structures represent protein aggregates. Nevertheless, HeLa-Vx3 cells stably expressing VMP1-iRFP becomes a useful model system due to increased number and size of Vx3 foci (compare **Figs 2.5A** and **2.6A**).

2.2.2 Identification of Vx3-bound proteins by mass spectrometry

To identify endogenous proteins modified with K63-polyUb and bound by Vx3, we immunoprecipitated Vx3 and associated proteins using GFP-Trap resin under partially denaturing conditions and utilized LC-MS/MS to identify the tryptic peptides. We performed this protocol on three HeLa stable cell lines: HeLa-Vx3NB as a control, HeLa-Vx3, and HeLa-Vx3 stably co-expressing VMP1-iRFP to determine if additional proteins associate with Vx3 due to VMP1 overexpression. Results of the proteomics analyses showed that the most prominent hits were transmembrane proteins known to localize at the plasma membrane (**Table 3A**). They included transferrin-receptor (TfR), MHC class I HLA-A (MHC-I), integrin-β1 (ITGB1), and caveolin-1 (CAV1). By contrast, we did not recover any ER-resident membrane proteins. Overexpression of VMP1 led to identification of additional proteins associated with Vx3, the majority of which are also transmembrane proteins. This is consistent with the increased number of cytosolic Vx3-EGFP foci observed with VMP1 overexpression. Notably, peptides from VMP1 were only identified in immunoprecipitates from the VMP1-iRFP expressing cells (**Table 2**), supporting that overexpressed but not endogenous VMP1 is potentially modified by K63-polyUb and bound by Vx3. In contrast, despite its colocalization, ATG9A was not found in the Vx3 pulldown. The high affinity between Vx3 and K63-polyUb allowed us to perform Vx3 pulldowns under stringent,

semi-denaturing conditions. We suspect that the majority of the proteins identified by LC-MS/MS were directly modified by K63-polyUb. We were able to confirm a few hits where high quality antibody is readily available. By immunostaining HeLa-Vx3 cells, we observed that a small fraction of endogenous TfR accumulated in Vx3 foci that also were positive for ATG9A, whereas the vast majority of TfR localized in the perinuclear region and cytosol (**Fig 2.7A**; **Table 1**). Similarly, a subpopulation of MHC-I was in Vx3 foci (**Fig 2.7B**; **Table 1**). Both endogenous TfR and MHC-I were also enriched in Vx3 foci that accumulated upon overexpression of VMP1-iRFP (**Fig 2.7C**). We also evaluated the ubiquitination status of Vx3-bound proteins by treating Vx3 immunoprecipitants with deubiquitinating enzymes (DUBs). Vx3 immunoprecipitated high molecular weight forms of TfR (**Fig 2.7D**). Upon treatment with AMSH (a K63-linkage specific DUB)[137] or USP2cc (a linkage non-specific DUB) [138], the smear of high molecular weight material was converted to free monomeric TfR, corresponding to polyUb removal; OTUB1 (a K48-linkage specific DUB) [139] had no effect (**Fig 2.7D**).

2.2.3 Caveolae components and VAMP proteins accumulate in Vx3 foci

Vx3 immunoprecipitation coupled to mass spectrometry analysis allowed us to identify K63-polyubiquitinated targets, which were significantly enriched in plasma membrane proteins (**Tables 2-3a**). Here, we carried out a second round of LC-MS/MS to identify additional Vx3-associated proteins from scaled-up samples. In addition to HeLa-Vx3 and HeLa-Vx3NB cells, we also conducted experiments on HeLa-Vx3 cells treated with the transfection reagent L3000 to induce for an autophagy response as described in **Fig. 2.1C**. With this setup, we identified a list of thousands peptides isolated by Vx3 immunoprecipitation, making their functional annotation and biochemical validation challenging. Nonetheless, by focusing on the most abundant Vx3-bound

peptides, the top two hundred hits could be sorted into the following categories: plasma membrane, caveolae, trafficking, quality control, and E3 ligases (**Table 3A-B**). Similar to the first proteomic analysis, the transmembrane proteins TfR and MHC-I were identified among the most enriched Vx3-associated proteins that fall under the "plasma membrane" category. However, autophagy induction by L3000 did not lead to the identification of additional Vx3-bound proteins.

This second mass spectrometry analysis revealed a strong enrichment of additional caveolae-associated proteins (**Table 3A**), such as the integral caveolin membrane protein CAV1, which is the major constituent of caveolae, CAV2, another member of the caveolin family, CAVIN1, an adapter known to stabilize caveolins at the plasma membrane during caveolae biogenesis, and ANKRD13A, a Ub-binding protein that mediates endolysosomal targeting of CAV1 [140,141]. We stained HeLa-Vx3 with a CAV1 antibody and found that a subpopulation of intracellular CAV1 accumulates at Vx3 foci (**Fig 2.8A**), supporting that CAV1 is a K63-polyubiquitinated cargo [142].

Other identified transmembrane proteins (annotated as "trafficking") included members of the synaptobrevin/vesicle-associate membrane protein (VAMP) and secretory carrier membrane protein (SCAMP) families known to regulate membrane trafficking at post-Golgi compartments (**Table 3A**). VAMP2, VAMP3 and VAMP7 are v/R-SNARE proteins involved in fusion of post-Golgi carriers with the plasma membrane or lysosomes. Previous studies have also reported the involvement of VAMP3 and VAMP7 in specific steps of the autophagy pathway. VAMP3 participates in autophagosome biogenesis by mediating homotypic fusion of ATG9-containing vesicles [119], whereas VAMP7 is required for both autophagosome biogenesis and lysosome fusion events [97,143]. VAMP2 and VAMP3 have been described to have redundant roles in mediating fusion of vesicles with the plasma membrane [144]. Moreover, Snc1, the yeast orthologue of VAMP2, has been shown to be modified by K63-polyUb on Lys49, Lys63 and Lys75 and recognized by the

Ub-binding adaptor β'-COP for its recycling to the plasma membrane [145]. We confirmed that both VAMP3 and VAMP7 accumulated at Vx3-EGFP foci (**Figs 2.8B** and **2.8C**). However, similar to what was observed for other ubiquitinated cargo (i.e., TfR, MHC-I and CAV-1), only a small fraction of VAMP3 or VAMP7 colocalized with Vx3 foci, while the bulk of the two v/R-SNAREs partitioned between the plasma membrane and intracellular structures that were negative for Vx3 (**Figs 2.8B** and **2.8C**). An amino acidic sequence alignment (not shown) showed that Lys49, Lys63 and Lys75 are highly conserved among VAMP family members (i.e., VAMP1, VAMP2, VAMP3, VAMP4, VAMP5, VAMP7 and VAMP8). Vx3 foci comprise numerous proteins modified by K63-polyUb; we found that loss of VAMP2, VAMP3 and VAMP7 expression did not impair Vx3 foci formation (**Fig 2.8D**). Similarly, siRNA-based knockdown of other VAMP proteins did not affect Vx3 foci formation (see **Table 4**). Thus, VAMP2, VAMP3, and VAMP7, albeit found enriched in our proteomics analysis, do not appear to play a role in regulating membrane fusion events required for Vx3 foci formation. These data indicate that many transmembrane proteins known to traffic through the post-Golgi endomembrane system are subjected to K63-polyubiquitinayion and accumulate in intermediate trafficking compartments disrupted by Vx3.

2.3 Vx3 foci are clusters of vesicles at the ER–endolysosome interface

To investigate the nature of the Vx3 containing foci, we performed correlative light-electron microscopy (CLEM) of HeLa-Vx3 co-expressing VMP1-iRFP and mCherry-ATG9A. Structures containing EGFP, mCherry and iRFP were first identified and imaged by confocal microscopy with Airyscan detection to enhance resolution and were then analyzed by transmission electron microscopy (TEM). We found that Vx3 foci correspond to heterogeneous clusters of small vesicles with different electron densities and sizes (50-150 nm in diameter) (**Fig 2.9A**). As was observed

from TEM of serial sections, these clusters appear complex as some contain double-membrane vesicles, MVB-like compartments, and tubules (**Fig 2.9B**). Airyscan confocal images showed that mCherry-ATG9A is found adjacent to and only partially overlapping with Vx3-EGFP (**Fig 2.9C**), indicating that ATG9A-positive subdomains are distinct from the Vx3-bound structures; on the other hand, Vx3-EGFP and VMP1-iRFP signals showed largely coincident staining patterns (**Fig 2.9C**), supporting that vesicles with overexpressed VMP1, but not ATG9A, contain K63-polyUb.

The appearance of electron lucent or dense core vesicles resembling post-Golgi carriers of the endomembrane system led us to investigate colocalization between Vx3 with Golgi and endosomal membrane markers. Our results showed that Vx3 foci are negative for the Golgi markers GM130 and TGN-38 (**Figs 2.10A**). Staining with early endosome antigen 1 (EEA1) or Rab11A showed that Vx3 foci did not colocalize with markers of endocytic recycling (**Fig 2.10B**). Rather, Vx3 foci colocalized with the late endosome markers Rab7 and CD63 (**Fig 2.10C**; **Table 1**), or LAMP1 (**Fig 2.10D**).

Overexpression of the GTPase-defective Rab5 mutant Rab5Q79L generates abnormally large (i.e., 1-5 μm diameter) endosomes as a result of enhanced fusion [146]. We took advantage of the enlarged perimeter of Rab5Q79L endosomes to visualize localization of Vx3 relative to the endosome membrane. In HeLa cells co-transfected with Vx3-EGFP and mCherry-Rab5Q79L, Vx3 appeared to localize at one site along the limiting membrane of the enlarged endosome (**Fig 2.11A**). Interestingly, co-expression of the ER retrieval peptide KDEL fused to BFP showed that Vx3 foci contact both the endolysosome and the KDEL-positive ER tubule (**Fig 2.11A**); live-cell imaging showed a direct association between Vx3 foci and ER tubules. When examined by immuno-EM analysis, we found that the Vx3-EGFP-containing membranes were distinct from the enlarged endosomes. The anti-GFP immunogold particles at the clustered endosome-proximal vesicles

appeared on the cytoplasmic side of the membranes (**Fig 2.11B-C**). In a few exceptions, the anti-GFP immunogold particles were also detected on the edges of intraluminal vesicles (**Fig 2.11B-C**). Consistent with the observations from fluorescence microscopy, tubular ER structures were identified in close proximity to the immunogold-labeled clustered vesicles. By immunofluorescence, Vx3 foci were also observed juxtaposed but not completely colocalizing with the ER proteins Sec61b (**Fig 2.12A**) and Calnexin (**Fig 2.12B**) and ER exit sites (ERES) (**Fig 2.12C**). Overall, these experiments indicated that Vx3 associates with K63-polyubiquitinated and VMP1-containing vesicles at the interface between ER and endolysosomes.

2.4 K63-polyubiquitinated cargo traffics to Vx3 foci by an endocytic route

As our data suggest that K63-polyUb is preferentially conjugated onto transmembrane proteins known to cycle between the plasma membrane and early or recycling endosomes, we hypothesized that cargo reaches Vx3 foci through endocytosis.

TfR is a *bona fide* K63-polyubiquitinated endocytic cargo protein. Because TfR is internalized by clathrin-mediated endocytosis, we examined whether acute inhibition of endocytosis by treating cells with the dynamin inhibitor dynasore alters formation of Vx3 foci. Our strategy took advantage of the destabilizing domain called "DD", a variant of FKBP12 [147]. Proteins expressed as fusions with DD are rapidly degraded by the proteasome but can be stabilized by Shield1, a reversible cell-permeable ligand [147]. The Shield1-based system controls the amount of DD-tagged Vx3-EGFP by acting directly on the translated protein; therefore, it can be used to induce Vx3-EGFP stabilization and accumulation in a short interval of time. After just 3 h of Shield1 treatment, we observed a rapid formation of DD-Vx3-EGFP foci, whereas 24 h was needed to detect fluorescent cytosolic foci after Vx3-EGFP induction from the Dox-activated promoter in

HeLa-Vx3 cells. Therefore, we sought to monitor Shield1-induced accumulation of Vx3 foci while concurrently disrupting clathrin-mediated endocytosis by treatment with dynasore [148]. We found that dynasore treatment abolished Shield1-induced formation of Vx3 foci (**Fig 2.13A**). Conversely, treatment with BFA did not reduce Vx3 foci formation following Shield1 addition (data not shown), indicating that transmembrane proteins that enter into Vx3 foci traffic through an endocytic rather than biosynthetic pathway.

Mature TfR resides on the plasma membrane, but after endocytosis it is typically trafficked to early and recycling endosomes before returning to the cell surface. We fused a HaloTag to the extracellular domain of TfR to enable selective labeling of the receptor on the plasma membrane by using a fluorescent cell-impermeant Halo ligand, thus facilitating visualization of the endosomal and distinguishing it from the newly-made subset of the intracellular receptor. We observed that DD-Vx3-EGFP foci that formed early upon Shield1 addition did not colocalize with internalized TfR-Halo (**Fig 2.13B**). Instead, colocalization between DD-Vx3-EGFP and endocytosed TfR-Halo only occurred at a late time point (between 12-16 h; **Fig 2.13B**), indicating that trafficking of internalized TfR to the Vx3 foci was relatively slow. This behavior was confirmed by uptake of Alexa640-labeled transferrin ligand (Tf-640) added to the cell medium, which showed that internalized Tf-640 accumulated in Vx3 foci with similar kinetics (**Fig 2.13C**). These results indicate that K63-polyubiquitaned cargo in Vx3 foci originate from the endocytic compartment.

Previous studies have reported that treatment of cells with wortmannin, a small-molecule inhibitor of the PI3K activity, resulted in the appearance of TfR in swollen late endosomes as a consequence of increased receptor internalization together with a blockade of receptor recycling [149,150]. Wortmannin addition drastically increased the number of Vx3 foci that corresponded to pre-

lysosomal hybrid membranes staining for both LAMP1 (late endosome) and Rab11a (recycling endosome) markers (**Fig 2.14A**); these wortmannin-induced Vx3-positive structures also stained for TfR (**Fig 2.14B**). Similar results were observed when HeLa-Vx3 cells were treated with SAR405 [151], a more potent and selective Vps34 inhibitor (data not shown). In addition, Vx3 foci colocalizing with ATG9A also contained 2xFYVE [152], a probe for PI3P (**Fig 2.14C**), indicating that K63-polyubiquitinated cargo accumulate with PI3P-enriched membranes. As a control, treatment with wortmannin was seen to abolish formation of 2x-FYVE foci while Vx3 and ATG9 colocalization was retained (**Fig 2.14C**). These results suggest that PI3P generation may be important for downstream sorting of K63-polyubiquitinated cargo.

2.5 Vx3 inhibits delivery of ubiquitinated transmembrane proteins to lysosomes

The findings described above suggested the possibility that the clusters of vesicles trapped by Vx3 might ordinarily function as "hotspots" where K63-polyUb dependent membrane fusion occurs to deliver cargo to lysosomes. To investigate the relationship between Vx3 foci and lysosomes, we used Lysotracker Red, which labels intracellular acidic compartments, and DQ-BSA Red, a fluorogenic protein derivative that, after endocytic uptake from culture medium, signals active intralysosomal proteolysis. Although Vx3 foci are marked by CD63 and LAMP1 (**Figs 2.10E** and **2.10F**; **Table 1**), they are distinct from structures stained by Lysotracker or DQ-BSA, indicating the foci do not include mature lysosomes (**Fig 2.15A**).

Transmembrane cargo degradation typically occurs via sorting into intraluminal vesicles of maturing endosomes to generate MVBs that will ultimately fuse with lysosomes. Rab5 to Rab7 conversion is used in the progression from early to late endosomes and, in concert with active cargo sorting into intraluminal vesicles by the ESCRT machinery, are crucial events that precede

lysosomal fusion [153]. Thus, we sought to interfere with endosome maturation by siRNA-mediated depletion of Rab7a. We found that loss of Rab7a expression increased formation of Vx3-EGFP foci (**Fig 2.15B**), in agreement with a block of downstream lysosomal targeting. Similarly, when the ESCRT function was impaired by overexpression of retroCHMP3, a fragment of CHMP3 that competes for ESCRT-III assembly and thereby inhibits cargo sorting, we observed an increase in the number of Vx3 foci (**Fig2.15C**). RNAi of USP8 (**Table 5**), a deubiquitinating enzyme that regulates cargo degradation through interaction with ESCRT-0 [51], also promoted accumulation of Vx3 foci (**Fig 2.15D**). These results suggest that a subset of K63-polyubiquitinated cargo sequestered in Vx3 foci are substrates of the ESCRT-mediated cargo sorting and degradation pathway.

To uncover the fate of K63-polyubiquitinated cargo downstream of the Vx3-blocked step, we set out to develop a method to induce its release from Vx3 in the foci. Our strategy took advantage of the Shield1-based system DD system described above to induce degradation of DD-Vx3-EGFP. We optimized conditions in which small Vx3 foci were generated over 24 h using Shield1 and a low dose of Dox; with this protocol, DD-Vx3-EGFP formed cytosolic puncta similar to Vx3-EGFP (**Fig 2.16A**). Dox and Shield1 were then removed by changing the medium, and after 10 h most of the DD-Vx3-EGFP was degraded as seen from a decrease of the cells' EGFP fluorescence to background levels (**Fig 2.16A**).

To monitor the fate of K63-polyubiquitinated cargo upon its release from Vx3, we needed to differentiate the cargo (e.g., TfR) trapped in Vx3 foci from the large population residing on recycling endosomes or the plasma membrane. To do this, we expressed TfR-Halo and supplied the cells with PA-JF646, a photoactivatable and cell-permeable HaloTag ligand. The TfR-Halo proteins at selected Vx3 foci were photoactivated by 405 nm laser irradiation and then monitored

over time following Dox and Shield1 washout. Live-cell imaging revealed that the TfR-Halo in the foci disassembled into small fluorescent structures that moved away from the initial photoactivation site (**Fig 2.16B**). Strikingly, photoactivated TfR-Halo seen to leave the Vx3 foci then colocalized with acidic lysosomes identified with Lysotracker (**Fig 2.16B**). Indeed, we had often observed in live cells that both Lysotracker and DQ-BSA signals contacted and remained associated with DD-Vx3-EGFP foci for 15-20 minutes before dissociating again. The transfer of photoactivated TfR to Lysotracker-positive structures occurred at the sites where Lysotracker contacted DD-Vx3 foci, suggesting that proximity or fusion with the lysosome allows TfR-containing vesicles to leave the Vx3-induced cluster (**Fig 2.16 D**). In contrast, photoactivated ATG9A-positive signals moved away from the DD-Vx3 foci very rapidly and did not colocalize with Lysotracker (**Fig 2.16E**), indicating that ATG9A was not incorporated into lysosomes.

We expected that the C-terminal tail of TfR would be exposed to the lumen of acidic lysosomes after membrane fusion. Therefore, to monitor fusion between TfR-containing vesicles and lysosomes, we fused pHuji, a pH-sensitive red fluorescent protein whose fluorescence decreases 20-fold from pH 7.5 to 5.5, to the C-terminus of TfR-Halo [154]. After photoactivation, the DD-Vx3 foci showed both pHuji and PA-JF646 fluorescence from the TfR-Halo-pHuji tandem fusion protein. After Dox and Shield1 washout, once TfR-containing vesicles departed the DD-Vx3 foci, the PA-JF646 signal persisted but the pHuji fluorescence disappeared (**Fig 2.16F**), indicating that TfR is incorporated into an acidic compartment upon release from Vx3 foci. Taken together, these results indicate that Vx3 expression blocks fusion of vesicles containing K63-polyubiquitinated cargo — here, exemplified by TfR — with lysosomes.

Discussion

By using Vx3 as a tool to investigate K63-polyUb-dependent signaling in living cells, we have provided evidence that K63-polyUb plays a role in regulating trafficking of transmembrane proteins to the lysosome. The vast majority of proteins identified in our mass spectrometry analyses are transmembrane proteins that are continually endocytosed and recycled to the cell surface, including TfR, MHC-I, CAV1 and VAMP3. In the early endosomes, ubiquitinated cargo can be either incorporated into the lumen of maturing endosomes for degradation or delivered back to the plasma membrane. Previous studies demonstrated that TfR and CAV1 ubiquitination lead to their incorporation into the intraluminal vesicles of multivesicular late endosomes via a mechanism that is dependent on cargo recognition and sorting by the ESCRT machinery [49,142,155]. Here we show that ESCRT-III deficiency causes accumulation of cytoplasmic Vx3 foci, consistent with an enrichment of ubiquitinated substrates that otherwise would be degraded via the MVB pathway. Consist with this, K63-polyubiquitinated cargo bound by Vx3 is also enriched upon loss of USP8, a non-selective endosomal DUB involved in ESCRT regulation and lysosomal turnover of transmembrane proteins [51] (**Fig. 2.15D**). It has been reported that expression of CHMP2B[Intron5], a mutant that disrupts ESCRT-III function, resulted in an extensive accumulation of inclusions containing p62, which is known to preferentially bind K63-polyUb, and dense clusters of vesicular and tubular elements [124]. An emerging model from our data supports a scenario in which, by tightly binding to K63-polyUb, Vx3 inhibits trafficking of endocytic transmembrane cargo to the lumen of endolysosomes. Typically, ubiquitinated endocytic cargo are sorted in subdomains of the endosomal membrane and incorporated into intraluminal vesicles; these multivesicular regions mature or detach from early endosomes to form mature MVBs, which in turn deliver their lumenal

contents to lysosomes for degradation. We propose that Vx3 accumulates cargo destined for degradation via the MVBs, most likely by directly competing with ESCRT proteins for binding to K63-polyUb.

Endocytic cargo are typically marked by K63-polyUb and recognized by multiple low-affinity UBDs contained within ESCRT components; these UBDs may cooperate to achieve high-avidity binding of the K63-polyubiquitinated cargo [28,47]. Thus, by acting as a competitive inhibitor, Vx3 might reduce interaction of ESCRT proteins with ubiquitinated cargo, thereby impairing their sorting and formation of intraluminal vesicles. Our results suggest that, as a consequence of the block to ESCRT-mediated MVB formation, the ubiquitinated cargo are diverted to an alternative proteolytic route that employs machinery from selective autophagy (i.e., p62 (SQSTM1), a receptor for autophagic cargo, the autophagy core transmembrane protein ATG9A, and the autophagosome membrane marker LC3).

Typically, plasma membrane proteins are degraded by endocytosis, while autophagy degrades cytoplasmic proteins, large particles, or organelles. However, autophagy as a degradation pathway of endocytosed cargo also has been reported [113,120]. Thus, a possibility arising from our work is that transmembrane proteins found enriched in Vx3 foci are cargo that normally undergo K63-polyUb-dependent lysosomal targeting via either an endocytic or autophagic pathway. An example of such a cargo is connexin-43, a transmembrane protein involved in assembling gap junctions at the cell surface [113,114]. Connexin-43 was not associated with Vx3 in our experiments, but most likely that is because HeLa cells lack gap junctions. In rat kidney cells, connexin-43 is primarily targeted by an ESCRT-dependent pathway, wherein Hrs and TSG101 shuttle the ubiquitinated protein from an early endosome to a late multivesicular endosome for degradation [156]. Upon starvation, connexin-43 is internalized via AP2 and traffics together with ATG9A and ATG16L1

into large and complex protein/vesicular plaques that are typically removed from the cytoplasm via a p62 and LC3-dependent autophagy [113,114]. Interestingly, connexin-43 targets to lipid rafts by interaction with CAV1, and it has been suggested that caveolae might be involved in connexins trafficking [157]. Our data show an enrichment of ubiquitinated cell surface proteins and caveolae components in Vx3 foci. Future studies will be needed to investigate further the requirement of caveolae during Vx3 foci formation and test if the K63-polyubiquitinated cargo identified by Vx3 follow a similar trafficking itinerary to that observed for connexins.

Autophagosome formation and maturation involves multiple entry points for endocytic vesicles [117]. Fusion of autophagosomes with early endosomes and MVBs is required for maintaining the flux throughout autophagy. Amphisomes are hybrid vesicular compartments with characteristics intermediate of autophagosomes and late multivesicular endosomes that originate along the multi-step process of autophagosome maturation [125]. One possibility arising from our work is that K63-polyUb serves as a signal for autophagosome fusion with MVBs. The appearance of ubiquitinated transmembrane proteins in clusters of vesicles showing heterogeneous morphology, size, and electron-density most likely reflects a mixture of vesicular elements that arise from the intersection between the endocytic and autophagic routes. Consistently, double-membrane and MVB-like structures were observed within the Vx3-positive vesicular clusters, although the vast majority of vesicles have single membranes. We showed that K63-polyUb-decorated vesicles co-clustering with ATG9A are found juxtaposed to degradative endolysosomes, consistent with the idea of fusion block imposed by Vx3. This idea is supported by evidence that vesicles containing ubiquitinated cargo, such as K63-polyubiquitinated TfR, fuse with acidic lysosomes following degradation of Vx3 to release the block. Moreover, we showed that Vx3 expression causes a defect

in autophagosome maturation, as indicated by the accumulation of LC3-positive compartments at a stage prior to autophagosome acidification.

ATG9A has been implicated in the early events of autophagosome formation, but its cellular function and trafficking remain elusive. ATG9A-containing vesicles may also play a role during autophagosome maturation, as suggested by previous reports of ATG9A-mediated sorting of ferritin receptor into MVB-like compartments [158], and the involvement of ATG9A in the formation of intraluminal vesicles in the late multivesicular endosomes during cell development in *Drosophila* [159]. Therefore, one possibility is that Vx3 slows the flux through autophagy by blocking ESCRT-mediated cargo internalization and biogenesis of fusogenic MVBs.

Recycling endosomes also contribute to autophagy, as they have been proposed to act as a primary membrane source for autophagosome biogenesis. More recently, ESCRT dysfunction has been linked to defects in phagophore closure [160-162], the last step in autophagosome formation, which has been largely uncharacterized. An alternative model arising from our study is that K63-polyubiquitinated transmembrane proteins are re-routed from early endosomes to the sites of phagophore nucleation following trafficking of ubiquitinated TfR and ATG9A through the endosomal recycling compartment. However, our data argue against this model because knockdown of essential early autophagy genes did not show a similar increase in Vx3 foci (see results in Chapter 3), as seen after ESCRT dysfunction. In addition, our studies showed colocalization of Vx3 foci with CD63, LAMP1 and Rab7 (late endosomal markers), but not Rab11 (recycling endosomal marker) or phagophore markers (e.g., ATG13), thus suggesting that K63-polyubiquitinated proteins do not contribute to autophagosome formation, but rather represent cargo destined to endolysosomal targeting.

It was previously found that siRNA-mediated depletion of ESCRT subunits inhibits autophagic degradation and leads to accumulation of Ub and p62 inclusions; the inclusions also contained membrane-free aggregates and clusters of endosomal and autophagic vesicles [124]. Our results show that overexpression of Vx3 results in a similar phenotype, most likely by acting as a competitive inhibitor of the ESCRT function *in vivo* (discussed above). However, a central conundrum still remains if autophagy requires K63-polyUb for the downstream lysosomal targeting of endocytosed cargo. ESCRT dysfunction resulting from competition by Vx3 might re-route endocytic transmembrane cargo to an autophagy pathway where the coalescence of vesicular intermediates containing ubiquitinated cargo and ATG9A could help to concentrate K63-polyUb conjugates, which in turn can serve as a scaffold for recruitment of p62 or other autophagic cargo receptors. The Vx3 sensor allows us to detect and characterize intracellular K63-polyUb-positive signals in aggregates or clusters that can be recognized by microscopy as foci, but it does not tell us about when those proteins were ubiquitinated. During selective autophagy, autophagic adaptors have been proposed to bind polyUb and recruit LC3-positive membranes to cargo. More recently, a role for Ub in signaling autophagy of ruptured endosomes or lysosomes also has been documented [102]. At least five autophagic adaptors containing UBDs have been described [106]. That K63-polyubiquitination of transmembrane proteins of endocytic origin may serve as a scaffold for autophagosome recruitment via autophagic adaptors and subsequent lysosome targeting seems plausible. Further investigation is needed to address whether the K63-polyUb-dependent trafficking of transmembrane proteins to the lysosomes is strictly dependent on autophagy; future experiments in cells that are deficient for essential autophagy genes (e.g., ATG5 or LC3) will be performed to track the itinerary of ubiquitinated cargo downstream of the Vx3 block and to monitor their delivery to lysosomes.

Material and methods

Plasmids, transfection, and knockdown

Vx3NB and Vx3K0 in pEGFP were subcloned into pcDNA5/FRT/TO plasmids with a N-terminal 3xFLAG tag. HA-Vx3NB-EGFP and HA-Vx3K0-EGFP were made non-fluorescent with S65T/G76A-EGFP; they are referred to as HA-Vx3NB and HA-Vx3. VMP1 was amplified from the pMRXIP-hVMP1-GFP plasmid (a gift from N. Mizushima, University of Tokyo, Japan) and subcloned into pQCXIP retrovector as a fusion with C-terminal HA and iRFP (Addgene #45459; iRFP682 was a gift from V. Verkhusha, Albert Einstein College of Medicine). mRFP-EGFP-LC3 was a gift from T. Yoshimori (Addgene # 21074, Osaka University). mCherry-Rab5 (Addgene #49201) and BFP-KDEL (Addgene#49150) were a gift from G. Voeltz, University of Colorado. Rab5 was mutated to Q79L. mCherry-Sec61b (Addgene #121160) was a gift from C. Mayr. ATG9A was cloned from cDNA into mCherry-C2 and pFN21A HaloTag. TfR-HaloTag was cloned from TfR-mCherry (Addgene #55144; a gift from M. Davidson, Florida State University) and additionally modified with pHuji on the C-terminus (Addgene #61505; D. Perrais, University of Bordeaux, Interdisciplinary Institute of Neuroscience). pEGFP-VAMP7 (Addgene #423116) was a gift from T. Galli, University of Paris Descartes. GFP-2x-FYVEE was a kind gift from H. Stenmark, University of Oslo. Retro-CHMP3 plasmid was a generous gift from W. Sundquist, University of Utah. The DD-tagged 3xFLAG-Vx3-EGFP was constructed by subcloning the FKBP12-variant destabilizing domain (i.e., FKBP12 E31G, F36V, R71G, K105E; ordered as a gene block from Integrated DNA Technologies, Inc.) upstream of the 3xFLAG sequence.

DNA plasmids were transfected for 24 h using Lipofectamine 2000 or Lipofectamine 3000 accordingly to manufacturer's instructions (Thermo Fisher Scientific). For RNAi treatment, HeLa-Vx3 were seeded at 5 x 10^4 cells/well in 24-well plates in complete medium and transfected with

6 pmol siRNA for 72 h using Lipofectamine RNAiMAX. Where indicated, Vx3-EGFP expression was induced by addition of 1 μg/ml Dox in the last 24 h. siGenome SMART pool siRNA against VAM2, VAMP3, VAMP7, USP8 and Rab7a were purchased from Dharmacon.

Cell culture and stable cell lines

HeLa, COS-7, Flp–In T-REx HeLa and Flp–In T-REx 293 cells were maintained in DMEM (Gibco) supplemented with 10% (v/v) FBS (Atlas Biologicals), 2 mM L-glutamine (Hyclone), and 100 U/mL penicillin-streptomycin (Hyclone). Cell lines were regularly tested for mycoplasma contamination using PCR Mycoplasma Detection Kit (G238, Applied Biological Materials Inc.).

To generate stable cell lines, HeLa-Vx3NB, HeLa-Vx3, HEK293-Vx3NB, and HEK293-Vx3, 3xFLAG-Vx3NB-EGFP or 3xFLAG-Vx3-EGFP in pcDNA5–FRT/TO plasmids were co-transfected with pOG44 recombinase-containing plasmid into parental Flp–In T-REx HeLa or 293 cells (Invitrogen). Inducible stable cell lines were established following selection and clonal expansion in complete medium containing 0.3 mg/mL hygromycin. Clones were analyzed for inducible expression of Vx3-EGFP and its localization in cytoplasmic foci after addition of 1 μg/mL doxycycline (Dox) for either 24 h or 48 h.

To create HeLa-Vx3NB-VMP1 and HeLa-Vx3-VMP1 cells which stably express Vx3 and VMP1, Phoenix cells were co-transfected with retroviral plasmid pQCXIP-VMP1-HA-iRFP and VSV-G envelope expressing plasmid pCS1.G (a gift from J. DeLuca, Colorado State University). The resulting retrovirus was used to infect HeLa-Vx3NB and HeLa-Vx3 cells grown under 1 μg/mL puromycin selection.

Autophagy induction

To monitor autophagy of damaged, internalized membranes, HeLa-Vx3 were infected with RFP-containing *Salmonella* (a gift from J. Brumell, University of Toronto) for 1 h, as described or treated with 3 µL of Lipofectamine 2000 for 4 h. For *Salmonella* growth assays performed in the presence or absence of Vx3-EGFP. Flp–In T-REx 293 cells were infected as previously described [134], lysed in 0.3% Triton X-100 in PBS and plated on agar plates at different times post-infection.

DD-Vx3 system

To tune DD-Vx3-EGFP expression, the plasmid was transiently transfected into parental Flp–In T-REx HeLa for 24 h; 1 ng/mL (low dose for slow formation of Vx3-EGFP foci formation, ~ 24 h) or 1 mg/mL (high dose for rapid formation of Vx3-EGFP foci, ~ 3 h) Dox and 1 µM Shield-1 were added simultaneously for the indicated times to induce expression and localization of Vx3-EGFP into cytoplasmic foci. To evaluate Vx3-EGFP foci formation, Flp–In T-REx HeLa cells transiently transfected with DD-3xFLAG-Vx3-EGFP were pre-treated with 80 µM dynasore before treatment with 1 mg/mL Dox and 100 µM Shield-1 for an additional 3 h. To induce Vx3-EGFP, DOX and Shield1 were washed-out and cells cultured in regular media up 12-16 h. To visualize lysosomes in live-cell experiments Flp–In T-REx HeLa cells were treated with Lysotracker-Red or DQ-BSA-Red according to the manufacturer's instructions.

Immunofluorescence, confocal microscopy, and quantitation

The following antibodies were used for this study: anti-ATG9A (clone EPR 2450[2], Abcam; 1:200 dilution), anti-calnexin (clone W17077C, Biolegen; 1:100 dilution), anti-CD63 (clone

H5C6, Biolegend; 1:200 dilution), anti-EEA1 (clone 14, BD Biosciences; 1:200 dilution), anti-Galectin-3 (clone A3A12, Abcam; 1:100 dilution), anti-GM130 (clone EP892Y; dilution 1:200), anti-K63-polyUb (clone Apu3, Millipore; 1:400 dilution), anti-HA7 (Sigma-Aldrich clone HA-7; 1:1,000 dilution), anti-LAMP1 (clone H4A3, Iowa Hybridoma; 1:100 dilution), anti-LC3 (clone 4E12, MBL; 1:100 dilution), anti-MHC-I/HLA-A,B,C (clone W6/32, Biolegend; 1:100 dilution),anti-p62/SQSTM1 (Abcam #56416; 1:500 dilution), anti-Rab7 (clone D95F2, CST; 1:200 dilution), anti-Rab11 (clone D4F5, CST; 1:100 dilution), anti-Sec31A (clone 32, BD Biosciences; 1:200 dilution), anti-TGN38 (clone 21-G, Santa Cruz; 1:200 dilution), anti-TfR/CD71 (clone CY1G4, Biolegend; 1:100 dilution), anti-VAMP3 (ThermoFisher #PA1-767A; 1:200 dilution), anti-VMP1 (clone D6N4G, CST; 1:200), and anti-TGN38 (clone 21-G, Santa Cruz; dilution 1:100), and CAV1 AF647 (clone 7C8, Santa Cruz; 1:50 dilution) antibodies.

We fixed cells onto coverslips at <80% confluence with 2.5% paraformaldehyde in PBS for 10 min at 37 °C and preserve them in PBS at 4 °C. For immunostaining, cells were permeabilized with 0.1% Triton X-100 for 10 min at RT and blocked for 1 h with 1% BSA in PBS before incubation with primary antibodies diluted in blocking buffer for 2 h at 25 °C or overnight at 4 °C. Anti-ATG9A antibody was preferably incubated at RT for 2h. For immunostaining with anti-CD63, anti-Rab7, and anti-Rab11 antibodies, we adapted a protocol previously described. Staining with anti-LC3 antibody was performed as previously reported.

We collected fixed-cell images and live-cell time-lapse images using a Zeiss LSM 880 confocal microscope equipped with conventional GAsP and Airyscan detectors using a plan-Apochromat 63x/NA 1.40 oil immersion objective. Airyscan superresolution images were acquired with the settings recommended by the manufacturer. After acquisition, Airyscan images were processed to enhance resolution using the Airyscan processing tool in ZEN Black software (Version

14.0.9.201). Images of Tetraspeck beads were used as reference for channel alignment of three-color images through ZEN Black.

For colocalization quantification, images were processed in Slidebook 5.0 software (3i) as described [163]. Quantification in Fig 2.4A was performed with the Image Analysis Wizard module in Zen Blue software (Version 2.3) by applying a constant threshold of fluorescence intensity to mask LC3 puncta in all the images analyzed.

Statistical analysis

Statistical calculations were performed with GraphPad Prism software and are described in the relevant figure legends. *P* values less than 0.05 were considered significant.

Correlative light electron microscopy (CLEM)

CLEM experiments were performed with HeLa cells stably expressing Vx3-EGFP and VMP1-iRFP and transiently transfected with mCherry-ATG9A. The cells were grown on etched-grid glass bottom dishes (No.1.5; MatTek Corporation). A two-step fixation protocol was used. The first round of fixation was performed with 2% paraformaldehyde and 0.2% glutaraldehyde in 0.1 M sodium cacodylate buffer, pH 7.4. This low percentage of glutaraldehyde did not alter EGFP, mCherry, or iRFP fluorescence signals; therefore, cells triply-expressing Vx3-EGFP, mCherry-ATG9A and VMP1-iRFP were identified by fluorescence and differential interference contrast (DIC) microscopy using a 20X plan-Apochromat 20x/NA 0.8 objective to mark their positions relative to the etched grid. Next, 0.18 μm-thick z-section images of Vx3−ATG9−VMP1-containing structures were obtained using the Zeiss Airyscan superresolution mode with a plan-

Apochromat 63x/NA 1.40 oil immersion objective. Subsequently, cells were subjected to a second fixation procedure with Karnovsky fixative (2% paraformaldehyde/1.5% glutaraldehyde in 0.1 M sodium cacodylate buffer) for subsequent EM analysis.

The cells were stored in cacodylate buffer after fixation. For CLEM, the samples were processed as described [164]. Briefly, the cells were post-fixed in 1% osmium tetroxide, dehydrated in ethanol, and flat-embedded in epoxy resin. Pyramids were trimmed using the etched grid as a guide to localize the cells of interest. Thin sections were cut with a diamond knife, picked up on Pioloform-coated one-slot grids, and stained with uranyl acetate and lead citrate. The sections were examined using a JEM-1400 electron microscope (JEOL, Tokyo, Japan).

Immunogold electron microscopy

HeLa-Vx3 were grown on 3 mm sapphire discs and transiently transfected with mCherry-Rab5Q79L for 24 h in the presence of 1 μg/mL Dox. Trypsinized cells were pelleted and resuspended in cryo-protectant (2% sucrose, 150mM mannitol in growth media). Cells were high pressure frozen using a Wohlwend Compact 02 high pressure freezer (Technotrade International, Manchester, NH) as described previously [165]. Cells grown on Frozen specimens were then freeze-substituted in anhydrous acetone containing 0.25% glutaraldehyde/0.1% uranyl acetate, and then by embedded in Lowicryl HM20 resin and UV-polymerized at low temperature (-45ºC). Serial thin sections (60-80 nm) were cut using a Leica UCT ultramicrotome and collected on Formvar-coated nickel slot grids.

Thin sections were immunolabeled using an anti-GFP primary in 1% nonfat dry milk blocking solution, and a 15nm gold-conjugated goat-anti-rabbit seconday, followed by post-staining with

2% (aqueous) uranyl acetate and Reynold's lead citrate, as previously described [165]. Sections were imaged on a FEI Tecnai T12 Spirit transmission electron microscope, operating at 100 kV.

Immunoprecipitation and DUB assays

Vx3 stable cells were induced with 1 μg/mL Dox for 48h and lysed in RIPA lysis buffer (50 mM Tris-Cl pH 7.6, 300 mM NaCl, 1% NP-40, 0.1% sodium deoxycholate, 1 mM EDTA) with 10 mM iodoacetamide, 4 mM 1,10-phenanthroline, and a protease inhibitor cocktail (P8340, Sigma-Aldrich). For GFP IP, 15 uL GFP Trap agarose resin (ChromoTek) was used per 10 cm dish of cells. For binding, salt was increased to 500 mM NaCl, and samples were incubated at 4°C for 1-2 h on a tube revolver. The resin was then washed with TBS (50 mM Tris pH 7.6, 150 mM NaCl). Samples were first eluted in 1.5x resin volume of elution buffer (50 mM Tris pH 7.6, 3.3% SDS, 2 mM DTT) at room temperature followed by a second round of elution by heating at 70°C. The majority of the ubiquitinated proteins were in the first elution, and the second elution mostly contained Vx3. For FLAG IP, Anti-FLAG M2 Affinity Gel (Sigma-Aldrich) was used according to manufacturer's instructions. The lysis buffer included 10 mM iodoacetamide, 4 mM 1,10-phenanthroline, and a protease inhibitor cocktail.

For DUB assays, IP'd samples were directly digested while still bound to resin. After washing, the resin was resuspended in digestion buffer (PBS pH 7.4, 0.3 mg/mL ovalbumin, 0.05% Brij35, 5 mM DTT). Digestions were incubated with 10 μM of different DUBs at 37°C for at least 1.5 h with shaking: OTUB1 (a gift from Cynthia Wolberger, Johns Hopkins University), GST-AMSH (a gift from Tingting Yao), and USP2cc26 (a gift from Bob Cohen). The samples were then eluted with 2x Laemmli Sample Buffer. This method was taken from S. Lian Master Thesis "Probing unconventional vesicular trafficking with K63-polyubiquitin sensors", Colorado State, 2019.

Mass spectrometry

For each cell line, 4 x 10 cm dishes were grown and co-IP'd. The elutions were precipitated in 80% acetone at -80 °C overnight. The protein pellets were recovered by centrifuging at 10,000 x g, 4 °C for 30 min and resuspended in 2x Laemmli sample buffer. To fractionate the samples, 90% of the elutions were run on a 4-15% SDS-PAGE gel (456-1083, Bio-Rad) past the stacking gel. The gel was then stained (0.05% Coomassie Blue R250, 10% acetic acid, 50% MeOH) for 1 h and destained (10% acetic acid, 50% MeOH) for 3 h with a solvent change each hour to remove SDS. Each sample was extracted and separated into two pieces to separate proteins <70 kDa and >70 kDa. The gel was dehydrated, reduced, and alkylated: 100% acetonitrile for 5 min at room temperature, 10 mM DTT with 0.1 M ammonium bicarbonate for 20 min at 55°C, 100% acetonitrile for 5 min, 55 mM iodoacetamide for 20 min at room temperature, and 100% acetonitrile for 5 min. The samples were then rehydrated and digested with 1:30 trypsin (V5111, Promega) in 0.1 M ammonium bicarbonate with 0.01% ProteaseMAX (V2071, Promega) at 37°C overnight. Afterwards, the reactions were stopped with 10% TFA, and the supernatant was collected. Remaining peptides left in the gel were further extracted by shaking the gel pieces in 50% acetonitrile and 0.1% TFA for 2 h and 100% acetonitrile for 5 min. These solutions were combined and dried down in a vacuum centrifuge. This method was taken from S. Lian Master Thesis "Probing unconventional vesicular trafficking with K63-polyubiquitin sensors", Colorado State, 2019.

Western blot analysis

Samples were incubated in 1x Laemmli sample buffer at room temperature, separated by SDS-PAGE, and transferred to PVDF in 1x Towbin buffer (with 0.1% SDS and 20% MeOH for blotting LC3). The following primary antibodies were used at 1:1000 dilution: anti-LC3 (L7543, Sigma-Aldrich), anti-TfR (D7G9X, CST) and anti-VMP1 (clone D6N4G, CST). Fluorescent secondary antibodies were imaged with an Odyssey CLx scanner (LI-COR Biosciences) and densitometry was performed in Image Studio Lite (LI-COR Biosciences). This method was taken from S. Lian Master Thesis "Probing unconventional vesicular trafficking with K63-polyubiquitin sensors", Colorado State, 2019.
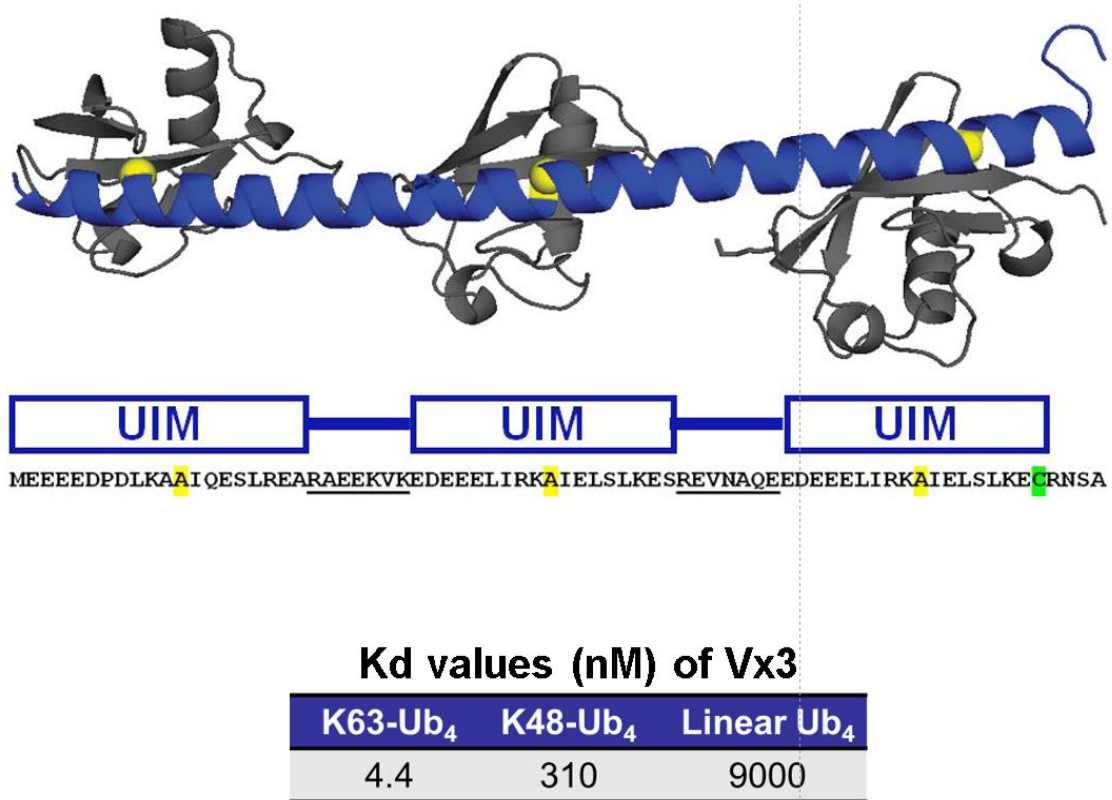
Figure 2.0: Vx3 binds K63-polyUb with high affinity and specificity *in vitro*. Top panel: Structural model of Vx3 interaction with K63-tri-Ub. Vx3 (*blue*) consists of three tandem Ubiquitin-Interacting Motifs (tUIMs) connected by two seven-residue linkers that position each UIM binding site (yellow spheres) for avid interactions with K63-linked Ub moieties (gray). Below is the amino acidic sequence of Vx3. Bottom panel: Affinities of Vx3 for tetra-Ub chains of different linkage-types. Adopted from Sims *et al*. (2012).
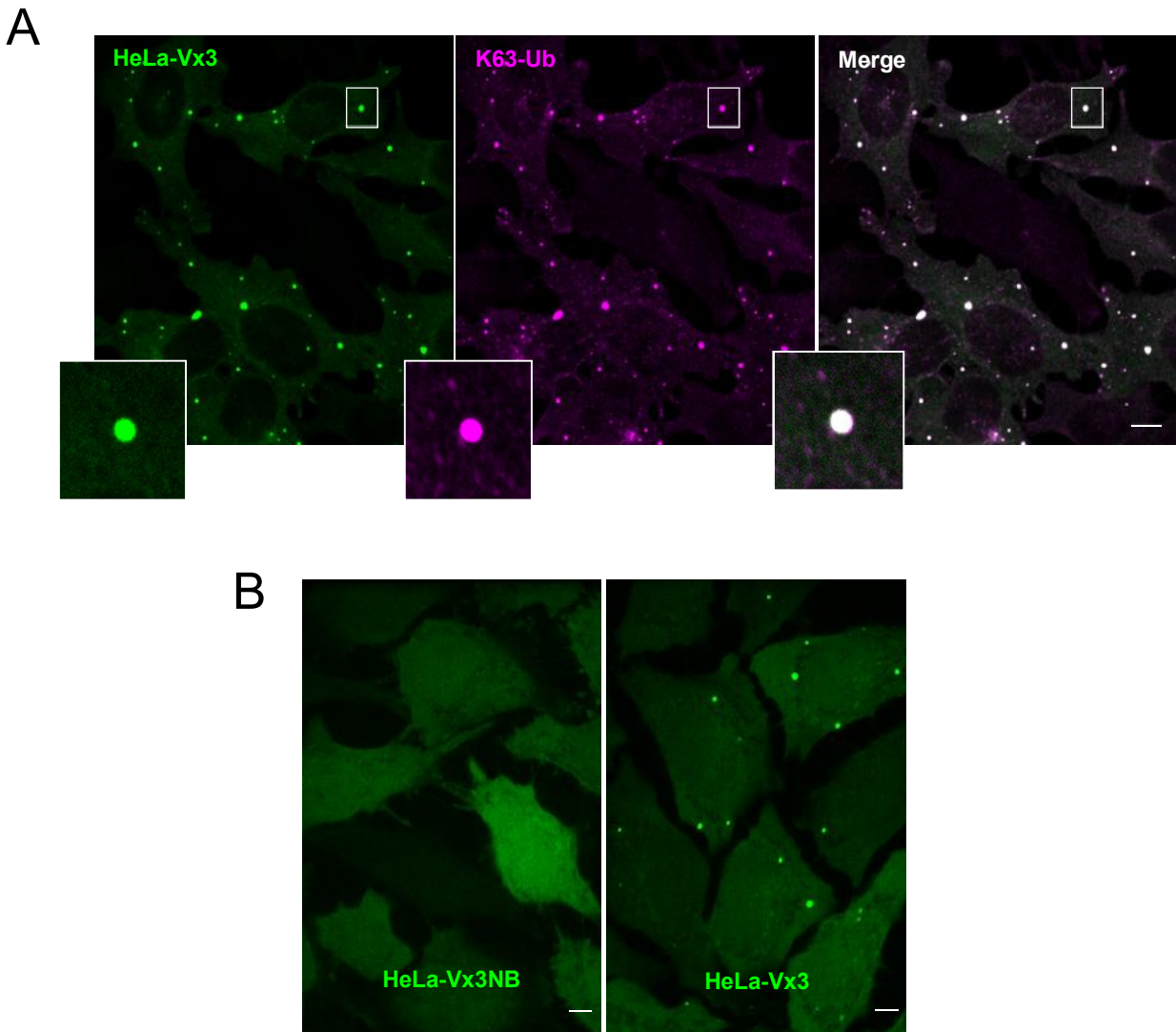
Figure 2.1: Vx3 accumulates into cytosolic foci enriched for K63-polyUb. A) Maximum projection image of HeLa-Vx3 cells treated with 1 µg/mL Dox for 24 h to induce expression of Vx3-EGFP (*green*); cells were fixed and stained with an anti-Ub K63-specific (clone Apu3) antibody (*magenta*). **B)** HeLa-Vx3NB and HeLa-Vx3 cells were treated with 1 µg/mL Dox for 24 h to induce expression of the EGFP-tagged sensors (*green*). Scale bars: 5 µm.
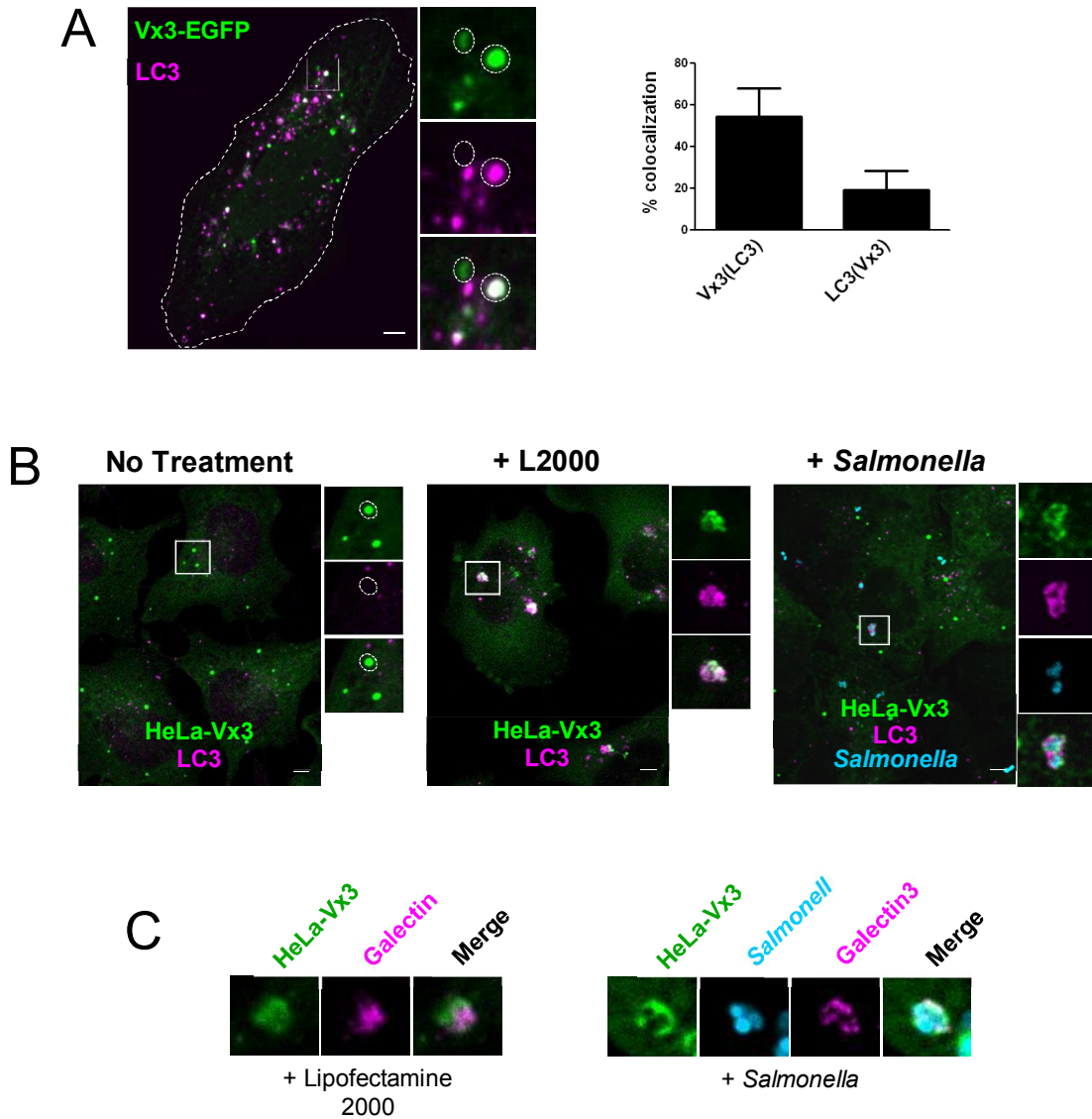
Figure 2.2: Vx3 colocalizes with LC3 upon autophagy induction. A) A HeLa cell transiently transfected to express Vx3-EGFP (*green*) for 24 h and then stained with an anti-LC3 antibody (*magenta*); dashed line indicates cell boundary. Magnified images of the boxed area indicate positions of selected Vx3 foci (white dotted circles) and illustrates partial colocalization with LC3. Measurements from >100 cells showed that whereas 54% of Vx3 foci colocalized with LC3 (Vx3[(LC3)]), 19% of LC3 foci co-localized with Vx3 (LC3[(Vx3)]). **B)** HeLa-Vx3 were treated with 1 μg/mL Dox for 24 h before addition of L2000 for 4 h or infection with *Salmonella* for 1 h. Cells were stained with an anti-LC3 antibody. Zoomed panels from L2000 treatment or *Salmonella* infection show overlap between Vx3 (*green*) and endogenous LC3 (*magenta*). No overlap between Vx3 and LC3 is observed in zoomed areas of untreated or nutrient-starved HeLa-Vx3 (see white dotted outlines of Vx3 foci projected onto the LC3 channel). **C)** HeLa-Vx3 (*green*) treated as in (B) and stained with an anti-Galectin3 antibody (*magenta*). Scale bars: 5 μm.
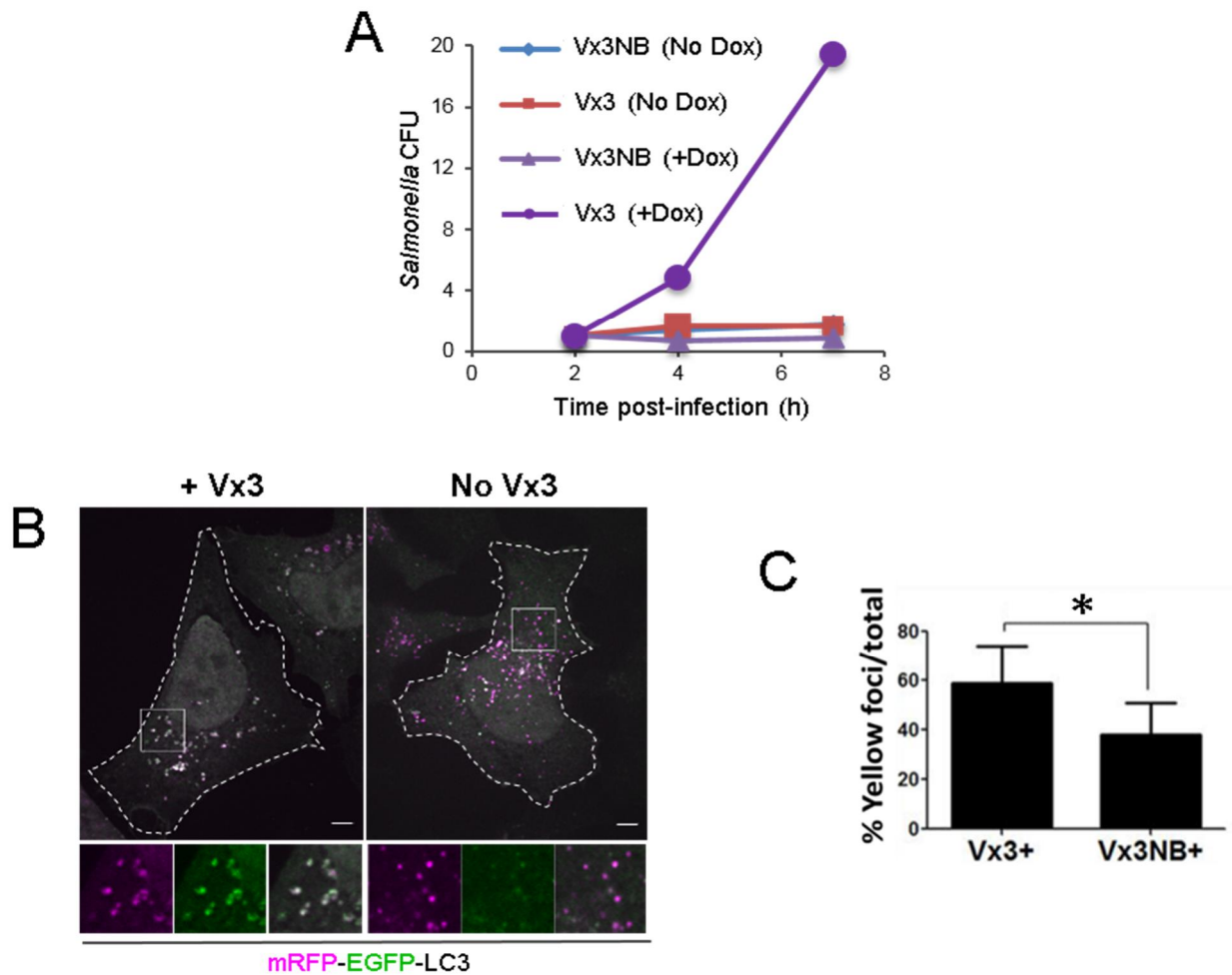
Figure 2.3: Vx3 expression interferes with selective autophagy A) HEK293-Vx3NB and Vx3 cells, untreated or treated with 1 µg/mL with Dox for 48 h, were infected with RFP-containing *Salmonella* for the indicated times. Cells were lysed 2 h, 4 h and 7 h post-infection, plated on selective agar plates and bacterial colony-forming units (CFU) were counted. *Salmonella* growth was less restricted in cells expressing Vx3: Error bars indicate the SD from the mean of triplicate experiments (*n* = 3). **B)** Single z-section image of HeLa cells transiently co-transfected with mRFP-EGFP-LC3 (EGFP, *green*; mRFP, *magenta*) and HA-Vx3. Cells were treated with the autophagy inducer Torin1 (250 nM) plus lysosomal protease inhibitors E64d (10 µg/mL) and pepstatin A (10 µg/mL). The dashed line marks the contour of the cell. Scale bar: 5 µm. **C)** Quantification obtained with >60 cells per condition shows that HA-Vx3 expression reduced the matured autophagosomes (autolysosomes; *magenta*) from 59% to 38% when compared to control cells without HA-Vx3. Error bars indicate the SD from the mean. Unpaired two-tailed *t*-test, *$p < 0.0001$.
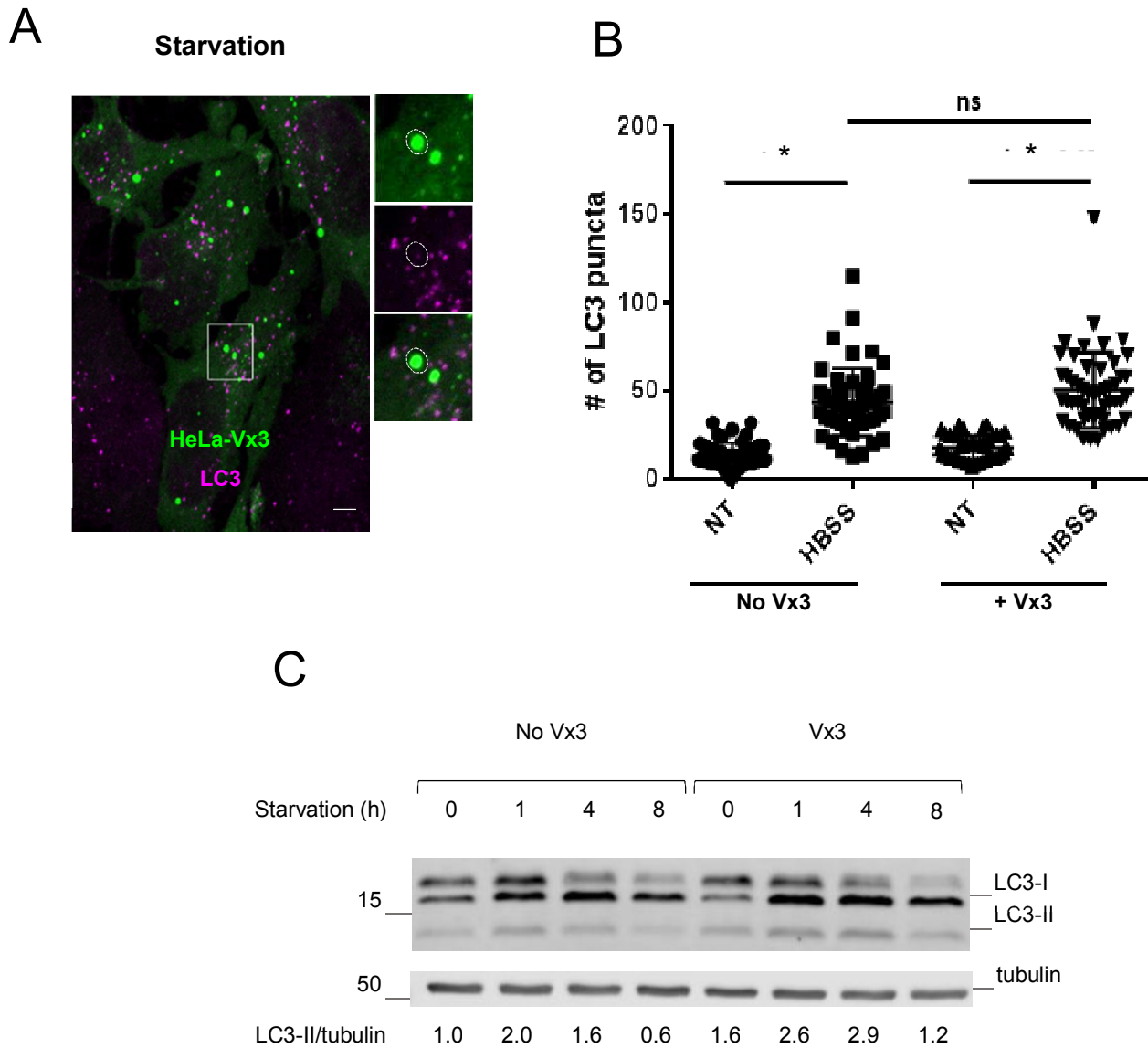
Figure 2.4: Vx3 expression does not perturb starvation-induced autophagy. A) HeLa-Vx3 were treated with 1 μg/mL Dox for 24 h before nutrient starvation with Hank's balanced salt solution (HBSS) for 1 h. No overlap between Vx3 and LC3 is observed in zoomed areas of untreated or nutrient-starved HeLa-Vx3 (see white dotted outlines of Vx3 foci projected onto the LC3 channel). Scale bar: 5 μm. **B)** HeLa-Vx3 untreated or treated with 1 μg/mL Dox for 24 h were cultured in DMEM or HBSS for 1 h and stained for LC3 to visualize nutrient starvation-induced autophagosomes. Quantification of LC3 dots was done by counting a total of 50 cells per condition. Error bars indicate the SD from the mean. Unpaired two-tailed *t*-test, ns: p > 0.05, *$p < 0.05$. **C)** Western blot analyses with an LC3 antibody of HeLa-Vx3 lysates untreated or treated with 1 μg/mL Dox for 48 h before starvation in HBSS medium. This western blot analysis was performed by Sharon Lian.
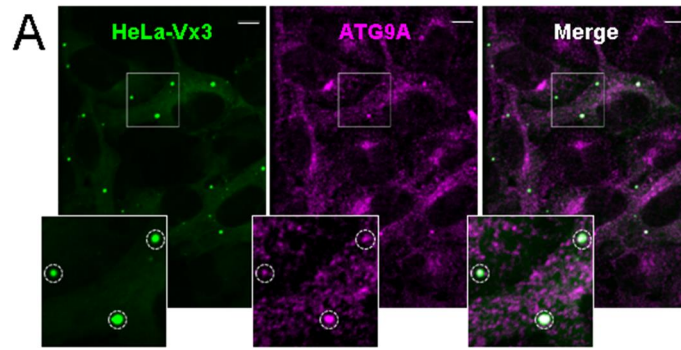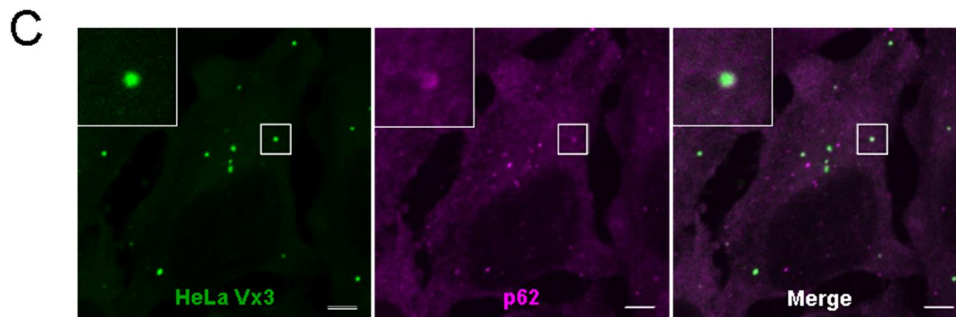
Figure 2.5: Vx3 foci colocalize with markers of autophagy. A) Vx3 (*green*) colocalization with endogenous ATG9A (*magenta*) in HeLa-Vx3 cells treated with 1 µg/mL Dox for 24 h. Inset panels show Vx3 foci (dotted circles) projected onto the ATG9A channel to visualize colocalization. **B)** Colocalization of endogenous proteins involved in early autophagy with HeLa-Vx3 foci. **C)** Maximum projection image showing colocalization of Vx3 (*green*) and p62. HeLa-Vx3 cells were cultured with 1 µg/mL Dox for 24 h before and staining with anti-p62 antibody (*magenta*). Scale bars: 5 µm.
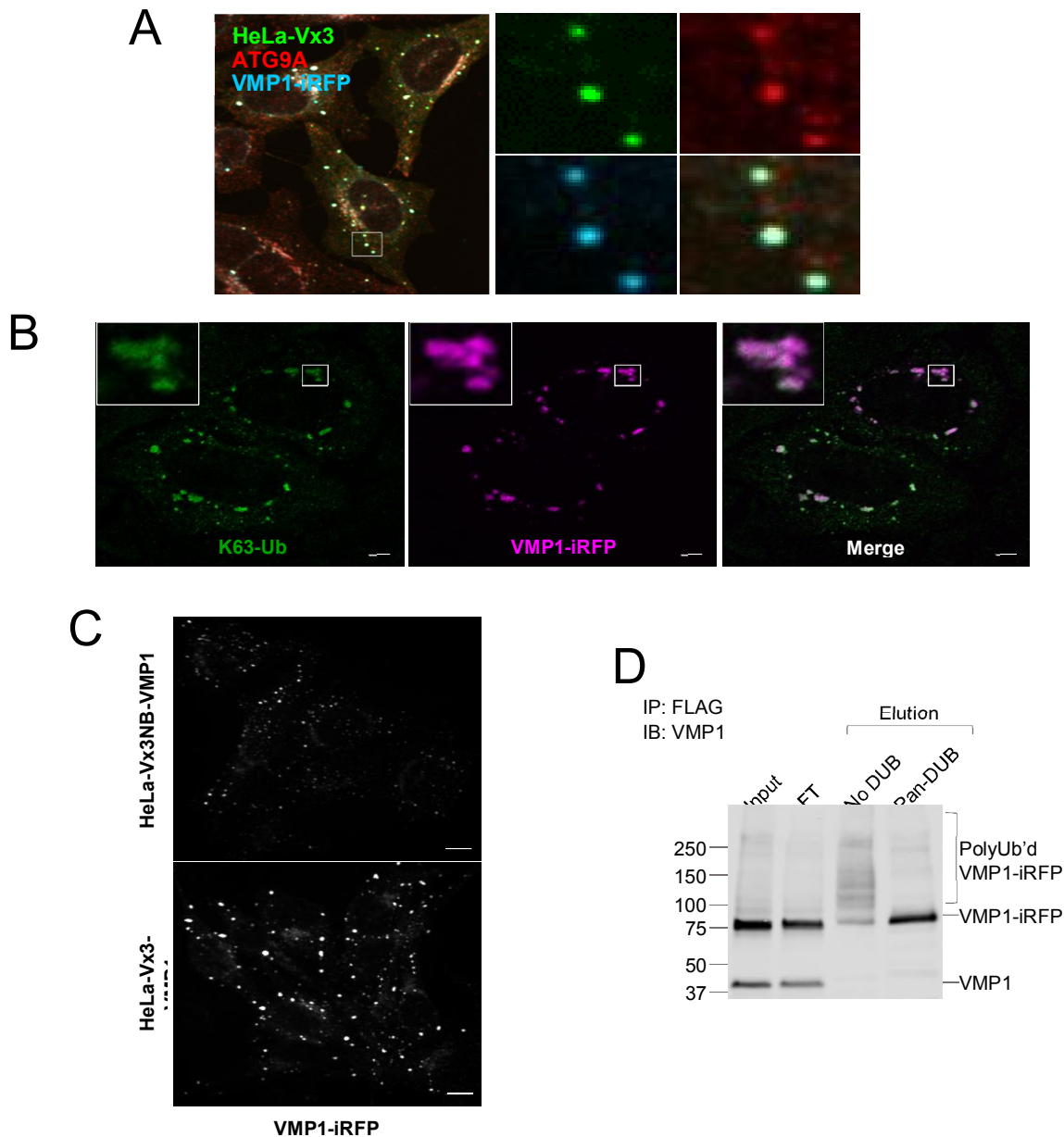
Figure 2.6: Overexpressed VMP1-iRFP is K63-polyubiquitinated. A) HeLa-Vx3 cells stably transduced with VMP1-HA-iRFP (*blue*) [HeLa-Vx3-VMP1] were treated with Dox for 24 h to express Vx3 (*green*) and stained with an antibody against ATG9A (*magenta*). **B)** HeLa cells were transiently transfected with VMP1-iRFP and stained for with an anti-Ub K63-specific (clone Apu3) antibody (*magenta*). Scale bar: 5 μm. **C)** VMP1-iRFP (*white*) foci in HeLa-Vx3NB-VMP1 and HeLa-Vx3-VMP1 cells treated with 1 μg/mL Dox for 24 h to induce expression of Vx3NB and Vx3, respectively. Scale bar: 8.3 μm. **D)** HeLa-Vx3-VMP1 cells were treated with Dox for 48 h. After FLAG IP to capture Vx3, the elutions were treated with a pan-specific DUB. Anti-VMP1 antibodies detect both endogenous VMP1 and VMP1-iRFP. This experiment was performed by Sharon Lian.
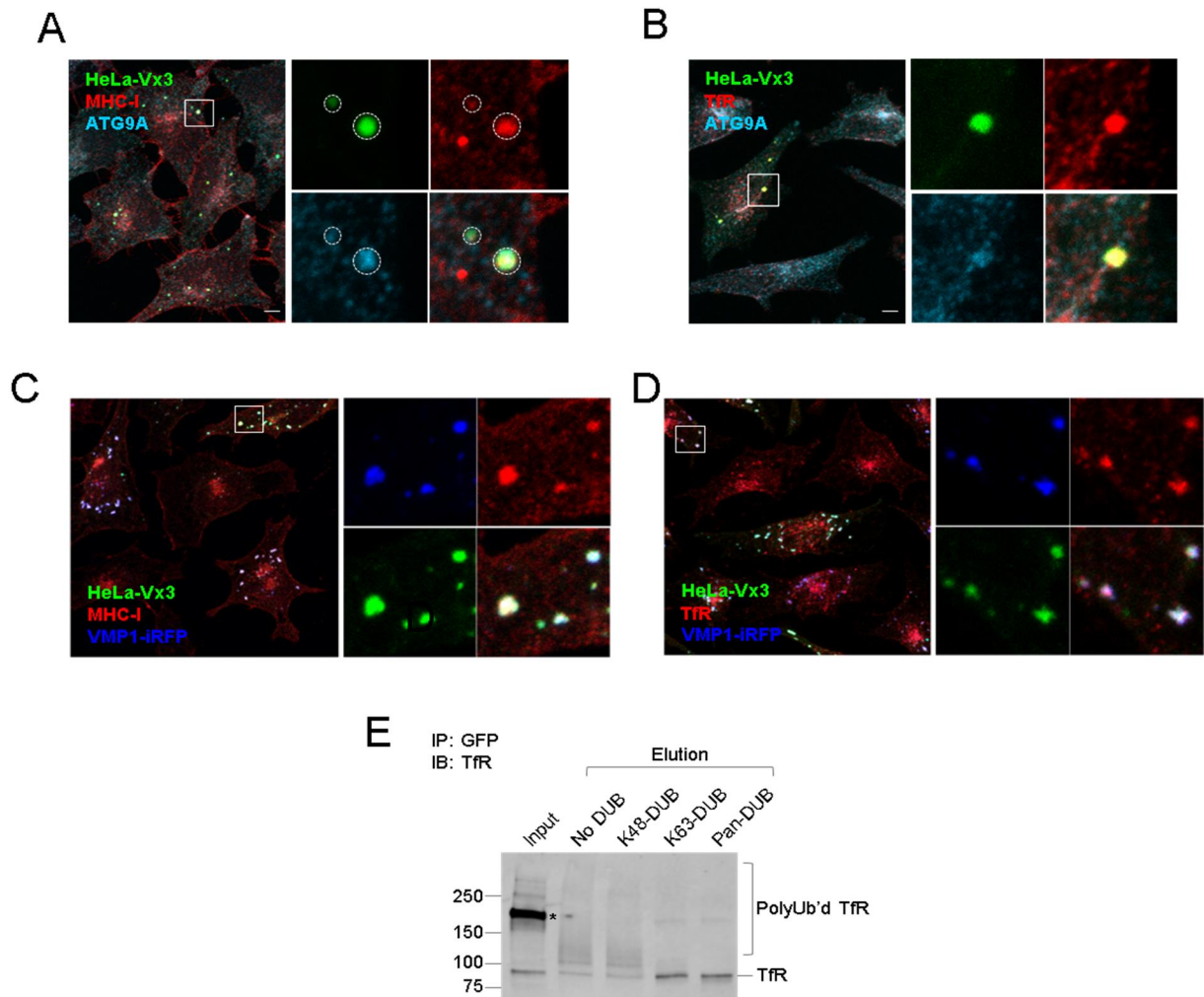
Figure 2.7: Plasma membrane proteins are K63-polyubiquitinated. A) Maximum projection image of HeLa-Vx3 cells (Vx3, *green*) treated with 1 μg/mL Dox for 24 h and stained with anti-MHC-I (*magenta*) and anti-Atg9A (*blue*) antibodies. Vx3 foci (dotted circles) are projected onto the TfR and ATG9A channels to visualize colocalization in the magnified panels. **B)** Same as in (A), but immunostaining with TfR (*magenta*) and ATG9A (*blue*) antibodies. Scale bars: 5 μm. **C)** HeLa-Vx3-VMP1 were treated with Dox for 24 h to express Vx3 (*green*) and stained with an antibody against MHC-I (*red*). VMP1 foci are shown in *blue*. **D)** Same as in (C) but immunostaining with TfR (*red*). Scale bars: 5 μm. **E)** HeLa-Vx3 cells were treated with 1 μg/mL Dox for 48 h before IP with an anti-GFP nanobody. Elutions were treated with linkage-specific or pan-specific DUBs and subjected to immunoblot analysis with anti-TfR antibodies. Ubiquitinated TfR appears as a high molecular weight smear. Residual dimeric TfR, indicated by an asterisk, is due to incomplete disulfide reduction of the sample. This experiment was performed by Sharon Lian.
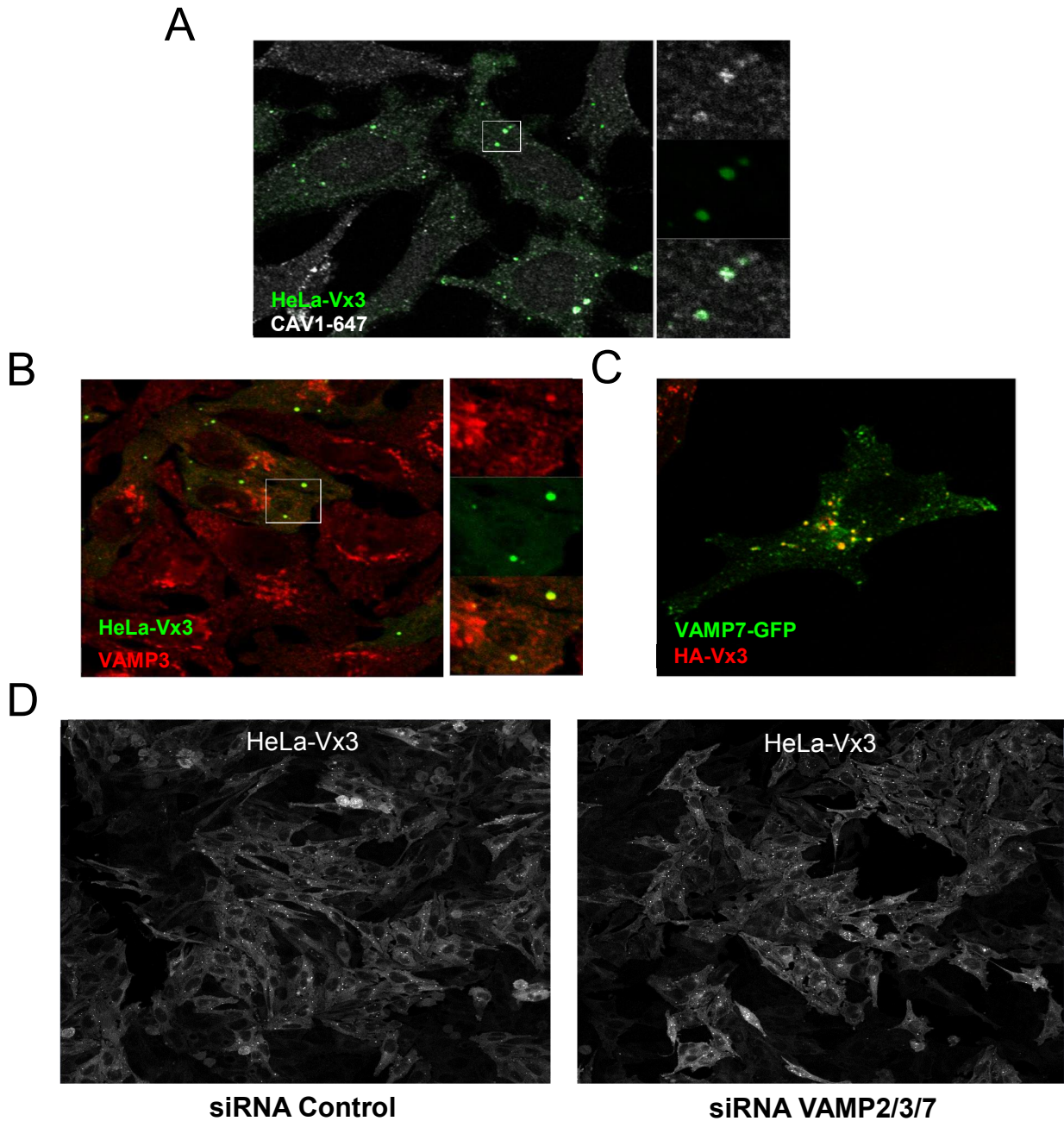
Figure 2.8: Vx3 accumulates caveolae components and VAMPs. A) After 24h DOX, HeLa-Vx3 cells (Vx3, *green*) were fixed and stained with a fluorescently-labeled anti-CAV1 antibody (CAV1-647, *white*). **B)** HeLa-Vx3 cells (Vx3, *green*) were treated with 1 µg/mL Dox for 24 h and stained with an anti-VAMP3 (*red*) antibody. **C)** A HeLa cell transiently transfected with VAMP7-GFP (*green*) and HA-Vx3 for 24 h and stained with an anti-HA antibody (*red*). **D)** HeLa-Vx3 cells were transfected with either control siRNA or siRNAs against VAMP2, VAMP3 and VAMP7 for 72 h and then stained with an anti-ATG9A antibody. At 48 h after siRNA transfection, Vx3-EGFP (upper panel, *white*) expression was induced by addition of 1 µg/mL Dox. Maximum projections of 5x5 tiled images are shown.
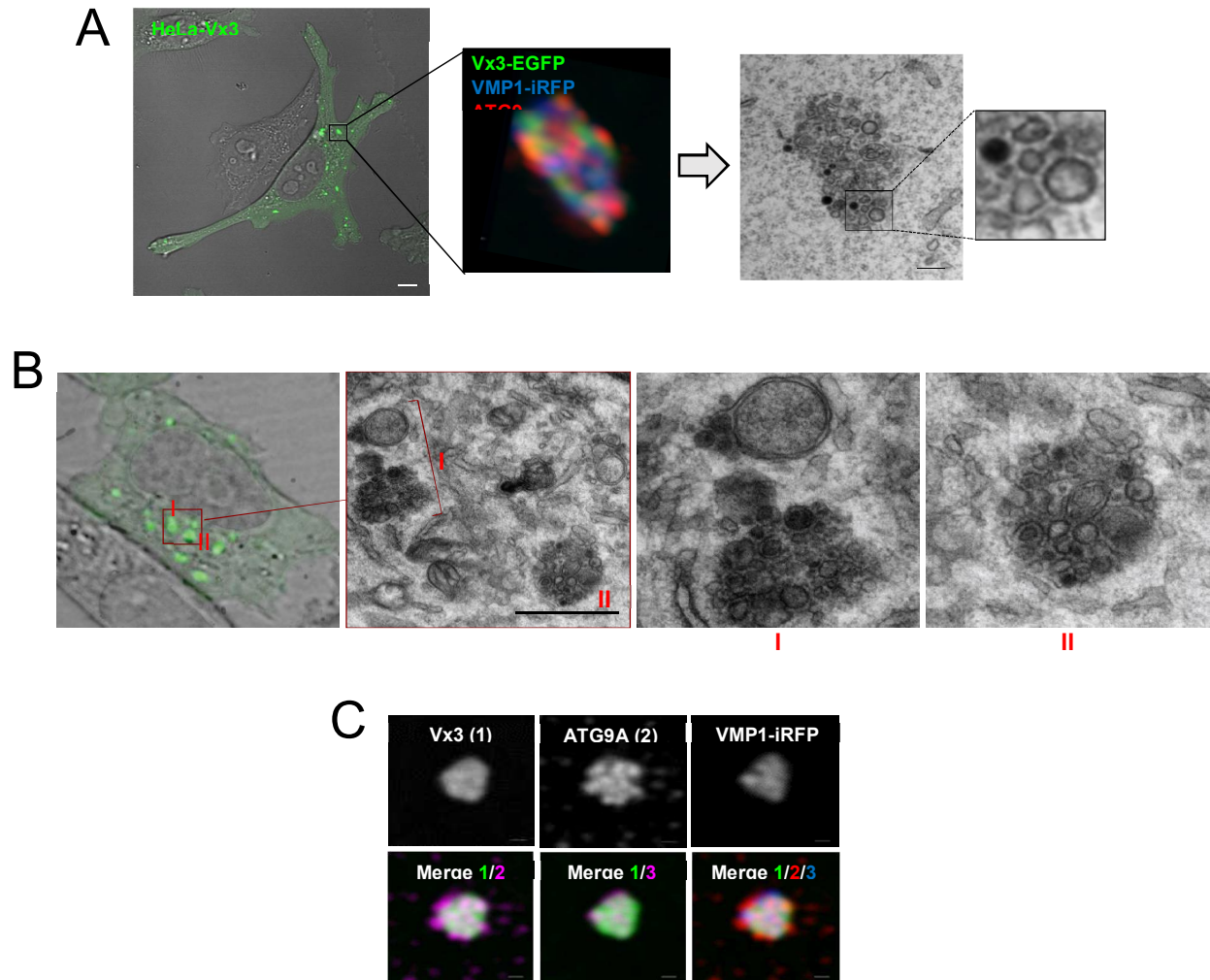
Figure 2.9: CLEM and Airyscan superresolution of Vx3 foci. A) Analysis by CLEM shows that clusters of vesicles comprise HeLa-Vx3-VMP1 foci. HeLa-Vx3-VMP1 cells were transiently transfected with mCherry-ATG9A and treated with 1 µg/mL Dox for 24 h. Triply-expressing Vx3-EGFP (*green*), mCherry-ATG9A (*red*) and VMP1-iRFP (*blue*) foci were first imaged with Airyscan superresolution and subsequently identified in 100 nm thin sections for TEM. Scale bars: 5 µm and 0.5 µm. **B)** CLEM images illustrating membrane complexity of HeLa-Vx3-VMP1 foci. Low magnification TEM of 100 nm thin sections of areas containing fluorescent Vx3 foci. Insets (I) and (II) show the presence of double membranes, ER tubules and clusters of vesicles that correspond to the Vx3−ATG9A−VMP1 foci identified (left panel) from Vx3 fluorescence (*green*). Scale bar: 1 µm. **C)** Airyscan image (single z-section) of a Vx3−ATG9A−VMP1 focus from a HeLa-Vx3-VMP1 cell prepared as in (A). Single-color images of each channel are shown in *white* (top row). Pairwise combinations between Vx3 (*green*) and ATG9 (*magenta*) or VMP1 (*magenta*) show that Vx3−VMP1 exhibit a similar staining pattern when compared to Vx3−ATG9A; a three-color merged image is also shown (bottom row: Vx3 (*green*), ATG9 (*red*), and VMP1 (*blue*)). Scale bar: 0.1 µm.
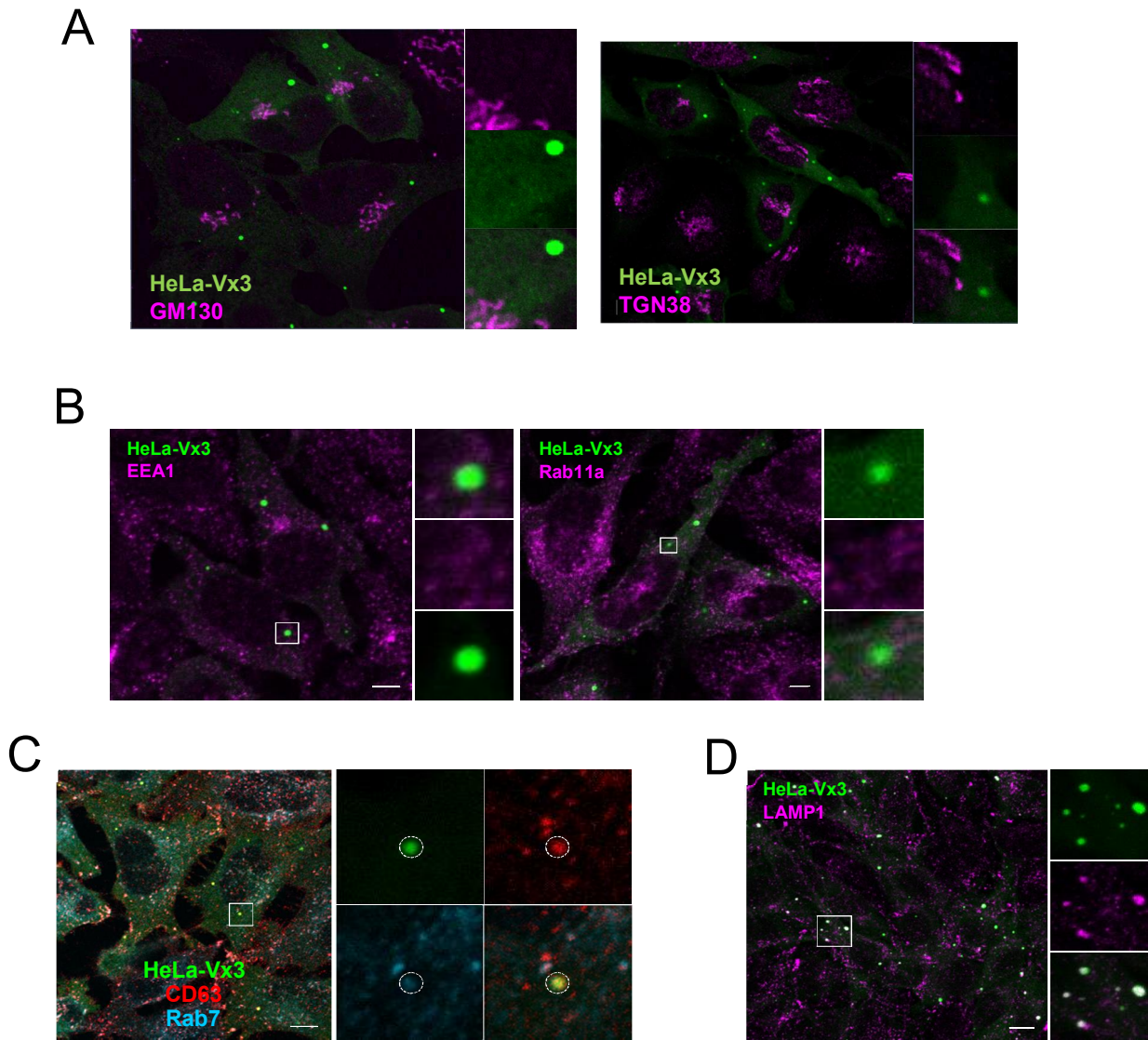
Figure 2.10: Vx3 colocalizes with late endocytic markers. A) HeLa-Vx3 cells (Vx3, *green*) were treated with 1 µg/mL Dox for 24 h and stained with an anti-GM130 antibody (left panel, *magenta*) or anti-TGN38 antibody (right panel, *magenta*). **B)** HeLa-Vx3 cells (Vx3, *green*) were treated with 1 µg/mL Dox for 24 h and stained with an anti-EEA1 antibody (left panel, *magenta*) or anti-Rab11a antibody (right panel, *magenta*). Scale bar: 5 µm. **C)** HeLa-Vx3 cells (Vx3, *green*) were treated with 1 µg/mL Dox for 24 h and co-stained with anti-CD63 (*red*) and anti-Rab7 (*blue*) antibodies. The dotted circle around a Vx3 focus is projected onto the other channels to visualize colocalization in the magnified region. Scale bar: 10 µm. **D)** Maximum projection image of HeLa-Vx3 cells (Vx3, *green*) treated with 1 µg/mL Dox for 24 h and stained with an anti-LAMP1 antibody (*magenta*). Scale bar: 10 µm.
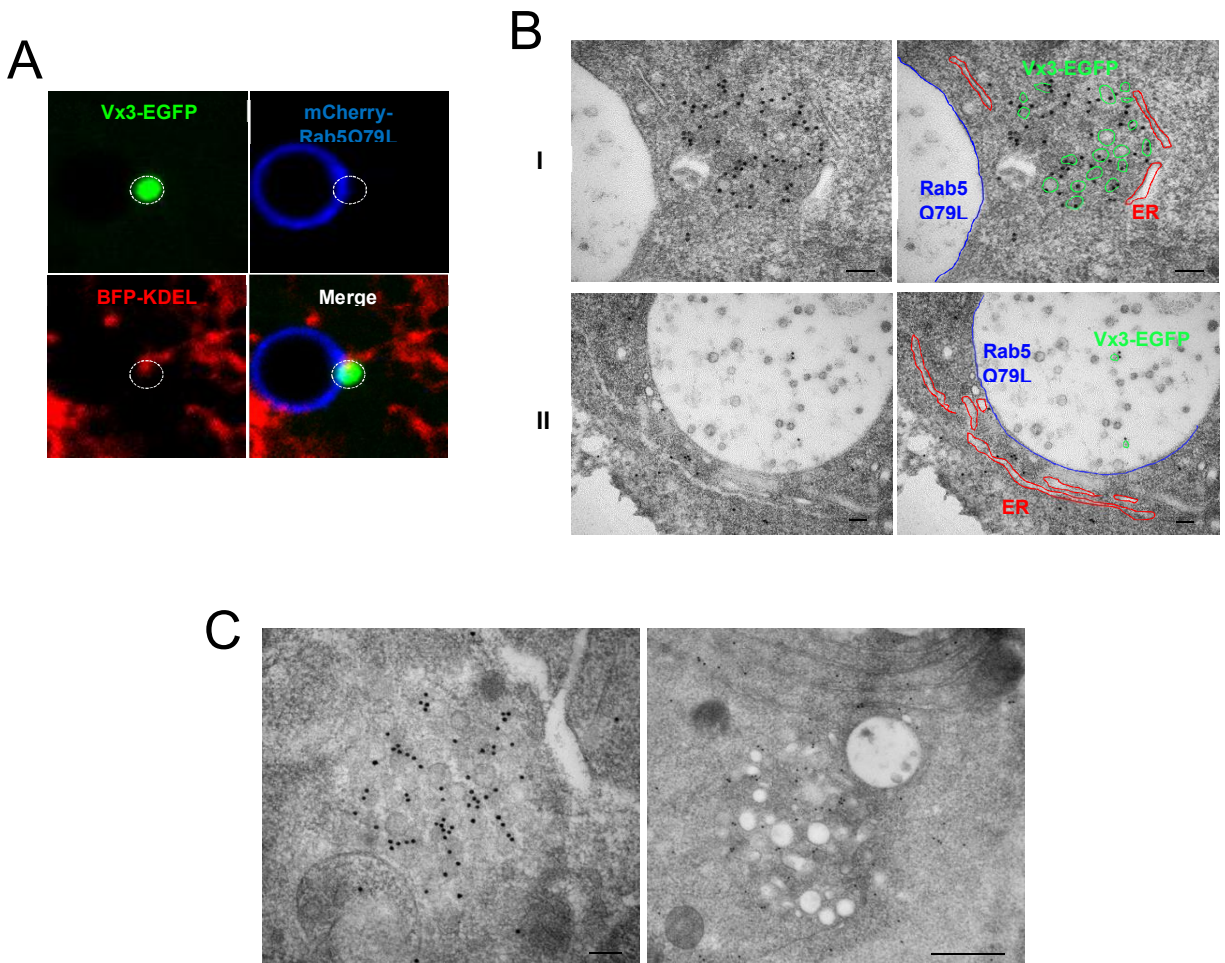
Figure 2.11: K63-polyUb-decorated vesicles localize at the interface between ER end endolysosomes. A) Single frame from Video 1 of HeLa cells transiently co-transfected with BFP-KDEL (*red*), Vx3-EGFP (*green*) and mCherry-Rab5Q79L (*blue*). The dotted circle around a Vx3 focus is projected onto the other channels to visualize juxtaposition with KDEL (i.e., ER tubule) or Rab5 (i.e., late endosome). **B)** Distribution of immunogold-labeled Vx3-EGFP in HeLa-Vx3 cells transiently transfected with mCherry-Rab5Q79L and treated with 1 μg/mL Dox for 24 h. Image (I) shows localization of immunogold-labeled Vx3-EGFP within a cluster of vesicles found close to the edge of an endolysosome. Image (II) shows localization of immunogold-labeled Vx3-EGFP on ER tubules and in the lumen of Rab5Q79L-positive endolysosomes. Panels on the right show likely endolysosome, ER tubule, and Vx3-positive vesicle membranes outlined, respectively, in *blue*, *red*, and *green*. Scale bar: 0.1 μm. **C)** Additional TEM images showing distribution of immunogold-labeled Vx3-EGFP in HeLa-Vx3 cells prepared as described in (B). Scale bars: 0.1 μm (left) and 0.5 μm (right).
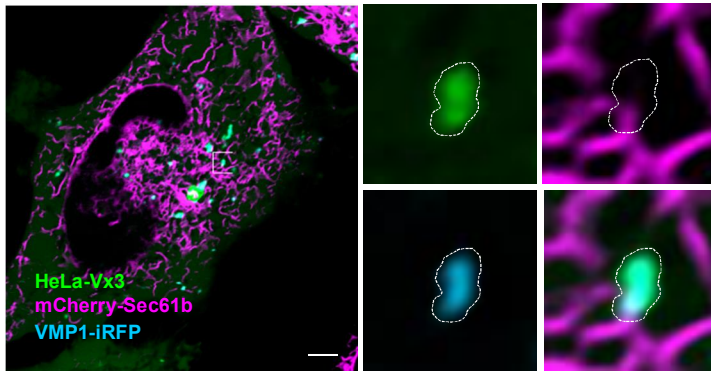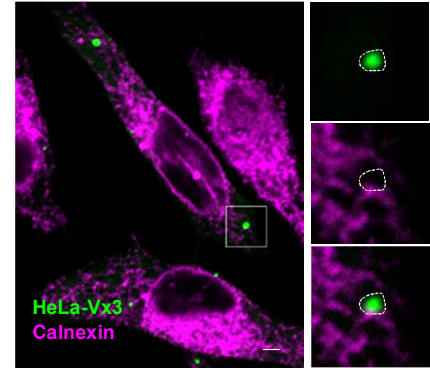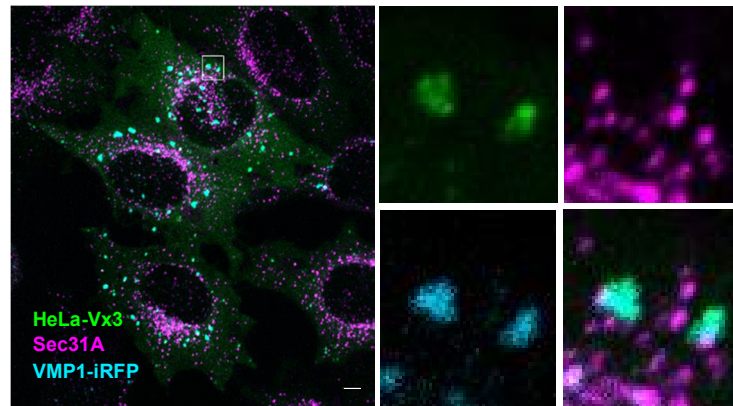
Figure 2.12: Vx3 foci are in close proximity to ER contacts. A) Airyscan image (single z-slice) of a HeLa-Vx3-VMP1 cell transiently transfected with mCherry-Sec61b. Dotted outlines of Vx3 (*green*) foci are projected onto Sec61b (*magenta*) and VMP1 (*blue*) panels in the magnified images to indicate extent of colocalization. Sec61b partially overlaps with Vx3, but unlike VMP1-iRFP, does not completely colocalize with it. **B)** HeLa-Vx3 cells (Vx3, *green*) were treated with 1 µg/mL Dox for 24 h and stained with an anti-calnexin (*magenta*) antibody. Dotted outlines of Vx3 (*green*) foci are projected onto calnexin channel to evaluate colocalization. Calnexin contacts Vx3 foci but it does not overlap completely. **C)** HeLa-Vx3-VMP1 cells were treated with 1 µg/mL Dox for 24 h and stained with an anti-Sec31A (*magenta*) antibody. Sec31A puncta are often found juxtaposed to Vx3 foci. Scale bars: 5 µm.
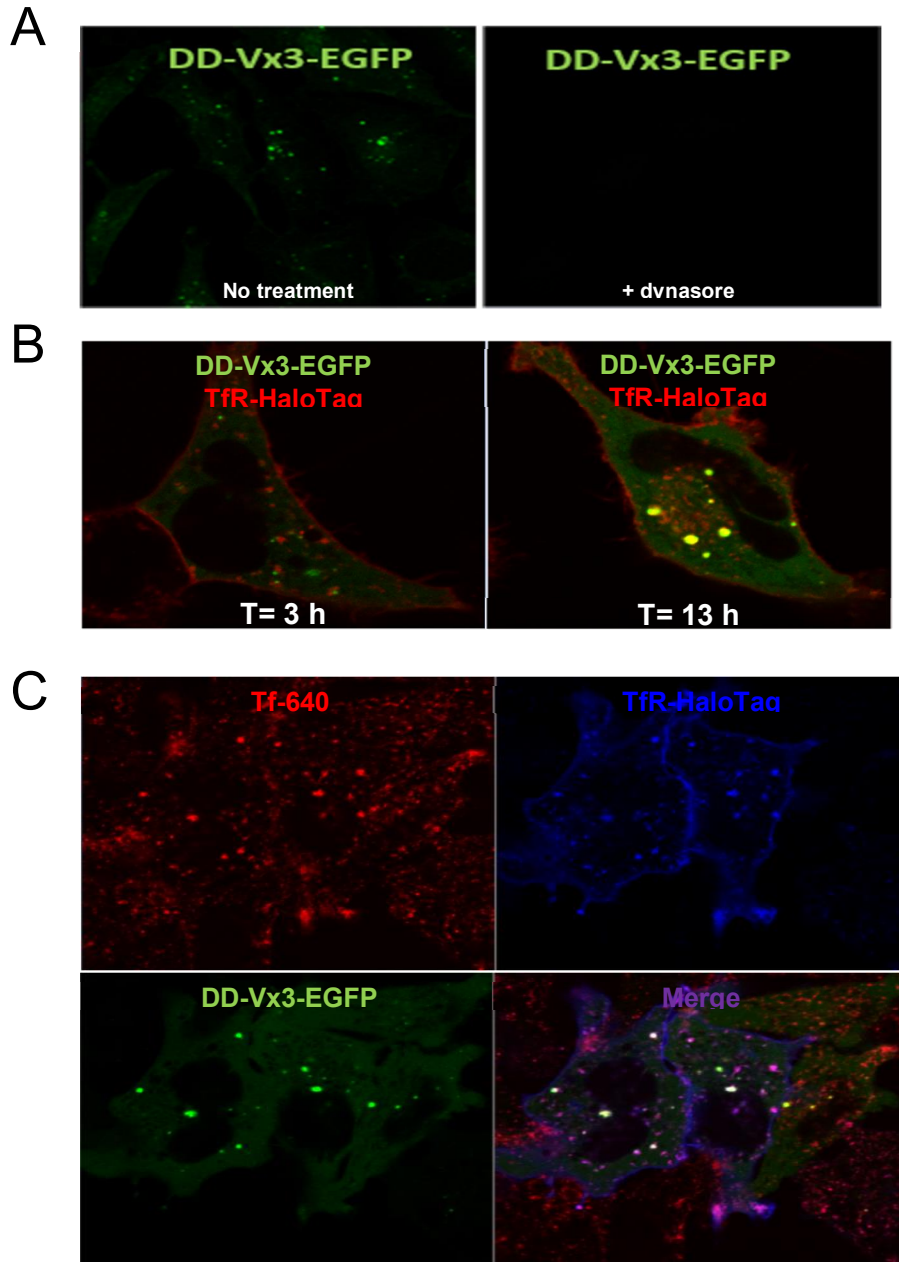
Figure 2.13: K63-polyubiquitinated TfR traffics to Vx3 foci via endocytosis. A) HeLa FRT transfected with DD-Vx3-EGFP (*green*) and treated with 1 µg/mL Dox and 100 µM Shield1 in the presence or absence of dynasore for 3h. **B)** HeLa FRT were co-transfected with DD-Vx3-EGFP (*green*) and TfR-HaloTag (*red*) for 24 h, treated with 1 µg/mL Dox and 100 µM Shield1, and cultured in the presence of a cell-impermeant Halo 660 ligand for 13 h to monitor accumulation of internalized TfR into Vx3 foci. Same cell acquired at 3 h and 13 h time points is shown. **C)** HeLa FRT were co-transfected with DD-Vx3-EGFP (*green*) and TfR-HaloTag (*blue*) as in (B) and treated with a cell-permeable Halo ligand (JF549) and incubated with fluorescently-labeled transferrin (Tf-640, *red*) for 16 h.
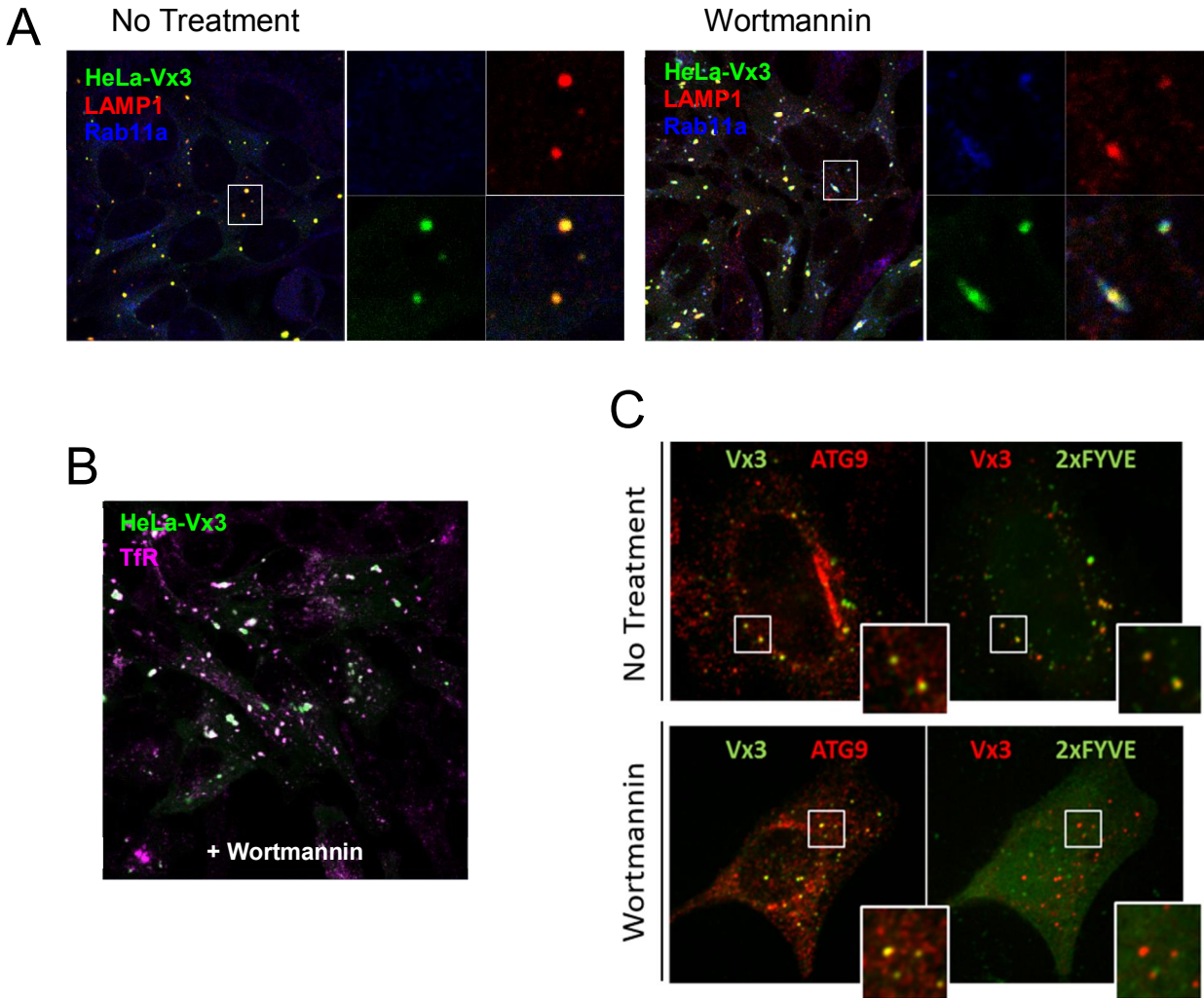
Figure 2.14: PI3K inhibition accumulates K63-polyubiquitinated cargo. A) Comparison of Vx3 foci (*green*) in HeLa-Vx3 with or without treatment with 100 nM Wortmannin for 4 h. Cells were stained with anti-LAMP1 (*red*) and anti-Rab11a (*blue*) antibodies**. B)** HeLa-Vx3 were treated with wortmannin as in (A) and stained with an anti-TfR antibody (*magenta*). **C)** HeLa cells were transiently co-transfected with GFP-2xFYVE and HA-Vx3. After 24h, cells were fixed and stained with anti-ATG9 and anti-HA antibodies. Wortmannin (50nM) treatment for 2h was done as a control.
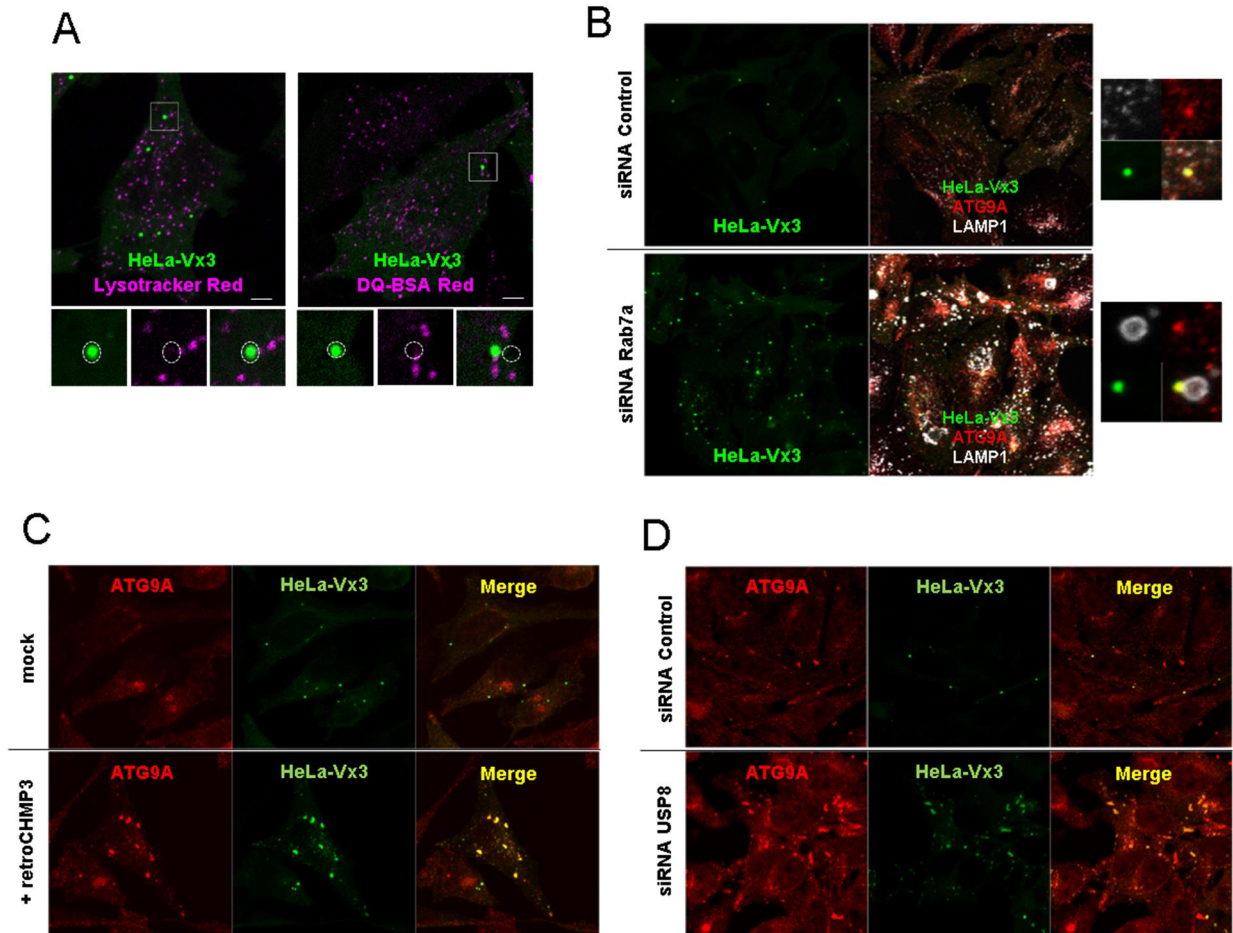
Figure 2.15: ESCRT inhibition accumulates K63-polyubiquitinated cargo. A) HeLa-Vx3 cells (Vx3, *green*) were cultured with 1 µg/mL Dox for 24 h and then treated with 50 nM Lysotracker Red (*magenta*) for 1 h or pulsed with 10 µg/mL DQ-BSA for 1 h and chased for 3 h before fixation. Insets show no staining of Vx3-EGFP foci (*green*) with either Lysotracker or DQ-BSA Red (*magenta*). Scale bar: 5 µm. **B)** HeLa-Vx3 cells were transfected with either control siRNA or siRNA against Rab7a for 72 h and then stained with anti-ATG9A (right panel, *red*) and anti-LAMP1 (right panel, *white*) antibodies. At 48 h after siRNA transfection, Vx3-EGFP (left panel, *white*) expression was induced by addition of 1 µg/mL Dox. Scale bar: 5 µm. **C)** HeLa-Vx3 cells were transfected with a vector containing retroCHMP3 or with empty vector (*mock*) for 24 h before treatment with 1 µg/mL Dox for an additional 24 h. Cells were stained with an anti-ATG9 (*red*) antibody. This image was acquired by Sharon Lian. **D)** Same as (B) but with siRNA against USP8.
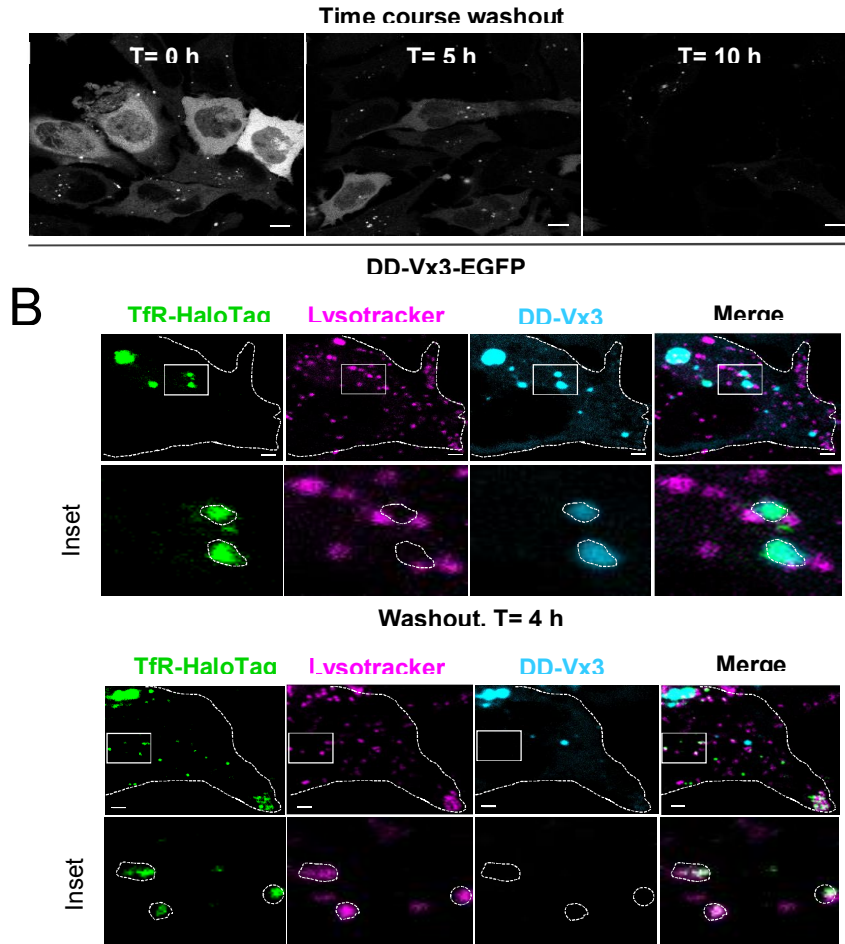
Figure 2.16: TfR-containing vesicles released by Vx3 traffic to the lysosomes. A) Time course (0, 5, and 12 h) of Vx3-EGFP (*white*) disappearance from HeLa FRT cells transfected with DD-Vx3-EGFP. The cells were treated with 1 ng/mL Dox for 12 h then 10 μM Shield1 was added for another 12 h to promote DD-Vx3-EGFP expression and stabilization. At T = 0 h, Dox and Shield1 were washed out and DD-Vx3-EGFP fluorescence was monitored. Representative maximum projection images of the cells show nearly complete loss of Vx3 between 5 and 10 h). Scale bar: 2 μm. This experiment was done by Sharon Lian. **B)** HeLa FRT were co-transfected with DD-Vx3-EGFP and TfR-HaloTag and treated with Dox and Shield1 as in (A). After 24 h, cells were rinsed three times in PBS for drug washout and cultured in medium containing 100 nM PA-JF646 Halo ligand and 25 nM Lysotracker Red. At 4 h after washout, TfR-HaloTag colocalizing with selected DD-Vx3-EGFP foci (inset boxes) was photoactivated and monitored over time. Two representative maximum projection images and corresponding insets from one cell show that, after ~18 h drug washout, Vx3-EGFP (*blue*) was largely degraded and the previously colocalized TfR-HaloTag (*green*) no overlapped extensively with Lysotracker (*magenta*); see Video 2 for more detailed kinetics. Dashed lines mark the cell contours, and outlines of the TfR-HaloTag foci are projected onto the other panels to visualize colocalization with Vx3 and Lysotracker. Scale bar: 2 μm.
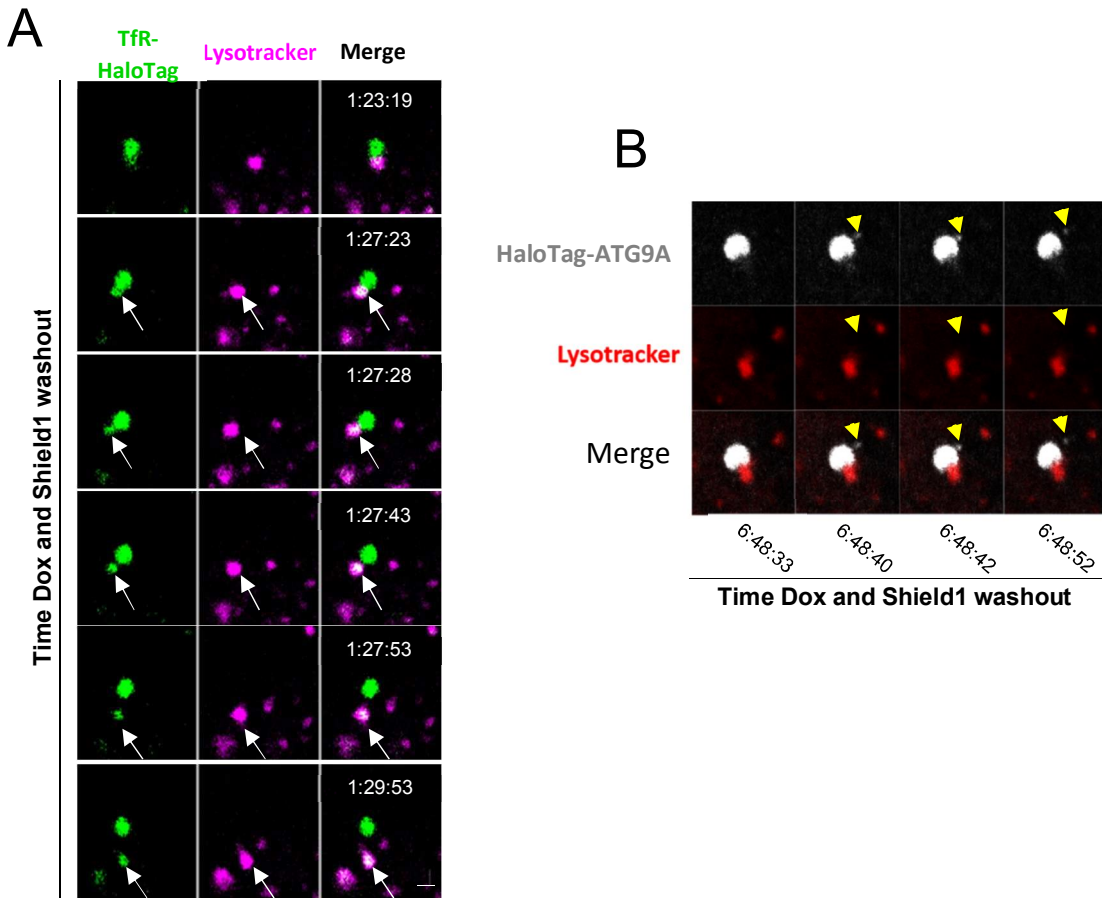
Figure 2.17: TfR but not ATG9A is delivered to the lysotracker-positive vesicles. A) Live-cell imaging of HeLa FRT cells co-transfected with DD-Vx3-EGFP and TfR-HaloTag and treated with Dox and Shield1 as in (**C**). After drug washout, cells were incubated with 25 nM Lysotracker Red and HaloTag-TfR colocalizing with Vx3 foci were photoactivated and then imaged at 1 frame every 5 s. Representative montages of single z-slice, time lapse images show mobilization of photoactivated TfR-HaloTag (*green)* to Lysotracker-positive signals (*magenta*) during a selected time interval (starting approximately 1 h and 23 min after drug washout); also see Video 3. *White arrows* indicate the transfer of TfR from the original Vx3-stabilized cluster to a lysosome. Scale bar: 1 µm. **B)** Live-cell imaging of HeLa FRT cells co-transfected with DD-Vx3-EGFP and HaloTag-ATG9A and treated as described in Fig 5C. Representative montages of single z-slice, time lapse images show the release of photoactivated HaloTag-ATG9A (*white)* independently of Lysotracker-positive signals (*red*) during a 20 s interval starting approximately 6.8 h after drug washout. *Yellow arrows* indicate the appearance of a small ATG9A punctum that moves away from the site of photoactivation.

69
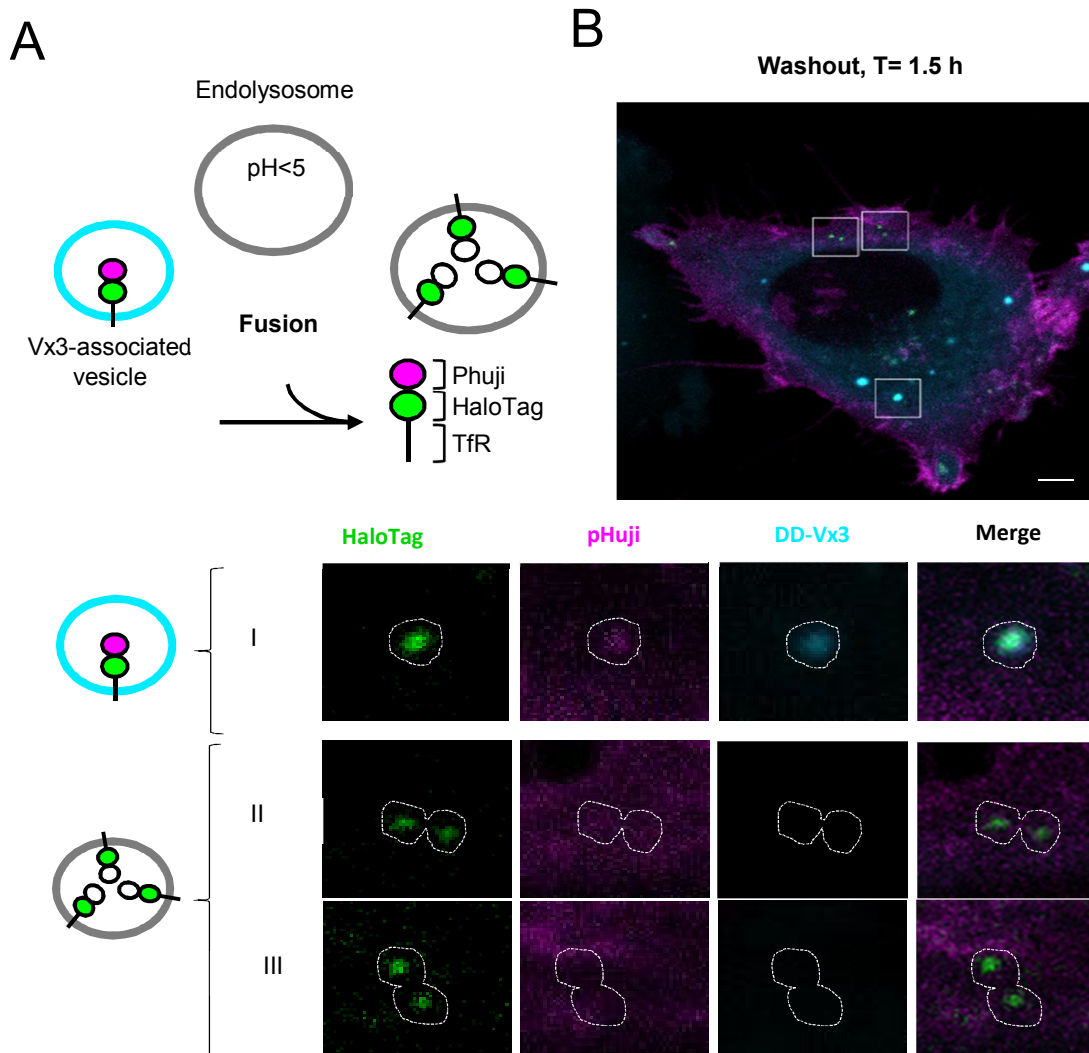
Figure 2.18: TfR-containing vesicles fuse with lysosomes following Vx3 degradation. A) Schematic representation of the fusion event between TfR-HaloTag-pHuji on a Vx3-associated vesicle and a lysosome. TfR in non-acidic vesicles shows both HaloTag (*green*) and pHuji (*magenta*) fluorescent signals; upon release from Vx3 and incorporation into lysosomes, pHuji is quenched at the acidic pH and TfR emits only the HaloTag fluorescence (*green*). **B)** HeLa FRT cells co-transfected with DD-Vx3-EGFP and TfR-HaloTag-pHuji were prepared as in Figs 2.15 and 2.16. After washout, z-stack images were collected and photoactivated TfR released from Vx3 was identified (see insets). Insets from a representative maximum-projection image acquired ~1.5 h post-washout show that photoactivated TfR colocalizing with Vx3 emitted signals from both the HaloTag and pHuji, whereas the photoactivated TfR released from Vx3 only exhibited HaloTag fluorescence. The dotted outlines of TfR-HaloTag are projected onto the other panels to visualize colocalization with pHuji or Vx3. Scale bar: 5 μm.

Table 1: Colocalization between Vx3 and autophagic or endocytic markers. Quantification of colocalization between HeLa-Vx3 foci and endogenous autophagic or endocytic protein markers. Time for Dox treatment to induce expression of Vx3 foci is indicated (24 or 48 h). Asterisk (*) indicates that the cells were transiently transfected with Vx3-EGFP. All quantifications were performed using Fiji (Image J) as described [187]. Mander's coefficients (M2) were calculated using the JaCoP colocalization plug-in. The numbers of total images and total cells analyzed are reported. These analyses were performed by Sharon Lian.

	Total Images	Total Cells	M2
*Vx3-EGFP/LC3	29	32	0.57
HeLa-Vx3/LC3 (24 h Dox)	7	60	0.01
HeLa-Vx3/ATG9 (48 h Dox)	10	82	0.93
HeLa-Vx3/ATG9 (24 h Dox)	10	51	0.82
HeLa-Vx3/p62 (24 h Dox)	10	100	0.96
HeLa-Vx3/VMP1-iRFP (24 h Dox)	10	29	0.71
HeLa-Vx3/TfR (48 h Dox)	9	86	0.78
HeLa-Vx3/MHC-I (48 h Dox)	10	87	0.81
HeLa-Vx3/CD63 (24 h Dox)	10	92	0.80
HeLa-Vx3/CD63 (48 h Dox)	10	121	0.86
HeLa-Vx3/Rab7 (24 h Dox)	10	92	0.79
HeLa-Vx3/Rab7 (48 h Dox)	10	121	0.81

Table 2: Vx3-associated transmembrane proteins identified from the first round of LC-MS/MS. Lysates from HeLa-Vx3NB control, HeLa-Vx3, or HeLa-Vx3-VMP1 cells were immunoprecipitated with GFP-Trap, and captured proteins were identified after trypsin digestion and LC-MS/MS. Shown are selected proteins and corresponding peptide counts from the analysis. These proteins are potentially modified by K63-polyUb. The table was prepared with assistance from Sharon Lian.

Protein Name	Human Gene Descriptions	Stable Cell Line		
		Vx3NB	Vx3	Vx3, VMP1
ATG9A	Autophagy-related protein 9A	-	-	-
VMP1	Vacuole membrane protein 1	-	-	6
TFRC	Transferrin receptor	-	11	32
MHC-I	MHC class I A-69 alpha chain	-	6	11
ITGB1	Integrin beta-1	-	2	5
p62/SQSTM1	Sequestosome-1	-	4	25

Table 3A: Vx3-associated proteins identified from the second round of LC-MS/MS. List of proteins from the top 200 most enriched peptides obtained by GFP co-IP of HeLa-Vx3 cells. Proteins were grouped according to their annotated function or cellular localization: "Caveolae", "Plasma Membrane", "Trafficking". Abundance is based on total spectral counts/protein molecular weight (SC/MW). GG peptide number is indicated along with all ubiquitination sites. General protein descriptions were written based on information available in the databases UniProt (https://www.uniprot.org/), NCBI (https://www.ncbi.nlm.nih.gov/), and GeneCards (https://www.genecards.org/). The table was prepared with assistance from Sharon Lian.

	Gene Name	Abundance (SC/MW)	GG peptide	Description
Caveolae	CAV1	982	19	caveolae biogenesis
	ANKRD13A	370	1	late endosome; binds K63-Ub; CAV1 to lysosome
	CAVIN1	343	4	caveolae biogenesis
	CAV2	153	7	caveolae biogenesis
	FLOT1	129	0	caveolae biogenesis
Plasma Membrane	STOM	391	0	melanosome integral protein
	SLC1A5	327	11	amino acid transporter
	TFRC	299	11	TfR; recycling endosome
	CLIC4	142	1	chloride intracellular channel
	FAT1	133	4	pro-cadherin; cell migration
	HLA-A	130	4	MHC-I; antigen cross-presentation
	LY6K	123	0	cell growth
	MARCKSL1	123	2	cell migration
	ITB1	118	6	ITGB1; cell adhesion
	MYOF	116	2	endocytic recycling
	ITM2B	92	3	neurite outgrowth
	LIMS1	91	0	cell growth
	ATP1B1	88	0	cell adhesion
	ATP1B3	83	0	ion transport
	SLC4A2	80	6	anion transport
Trafficking	RAB7A	477	9	late endosome
	VAMP3	327	11	v-SNARE; recycling endocytic TfR; late endosome to TGN
	ARF3	316	0	GTP-binding; Golgi
	ARF4	273	0	GTP-binding; Golgi
	VAMP7	261	16	v-SNARE; early endosome/autophagosome with lysosome
	VAMP2	190	11	v-SNARE; exocytosis; clathrin-independent endocytosis
	SCAMP3	141	6	post-Golgi recycling
	SCAMP4	109	8	post-Golgi recycling
	SNAP23	116	0	membrane fusion
	MYOF	116	2	exosomes
	SCAMP1	90	7	post-Golgi recycling
	STX6	82	0	t-SNARE; TGN; endosomes
	STX10	78	0	t-SNARE; late endosome to TGN

Table 3B: Vx3-associated proteins identified from the second round of LC-MS/MS. List of proteins from the top 200 most enriched peptides obtained by GFP co-IP of HeLa-Vx3 cells. Proteins were grouped according to their annotated function or cellular localization: "Autophagy", "Quality Control", "E3 ligases". Abundance is based on total spectral counts/protein molecular weight (SC/MW). GG peptide number is indicated along with all ubiquitination sites. General protein descriptions were written based on information available in the databases UniProt (https://www.uniprot.org/), NCBI (https://www.ncbi.nlm.nih.gov/), and GeneCards (https://www.genecards.org/). The table was prepared with assistance from Sharon Lian.

	Gene Name	Abundance (SC/MW)	GG peptide	Description
Autophagy	SQSTM1	1340	4	p62; selective autophagy cargo receptor
	LAMTOR5	177	0	mTOR complex
	TOMM20	147	0	mitophagy
	FUNDC1	123	2	mitophagy
	DIABLO	133	1	mitophagy
	FUNDC2	111	6	mitophagy
	LAMTOR2	111	0	mTOR complex
	TMEM59	105	4	Golgi; unconventional autophagy
	LAMTOR1	85	2	mTOR complex
Quality Control	HSP90AA2P	452	2	chaperone
	UBQLN2	234	3	ERAD
	UBQLN1	213	3	ERAD
	FAF2	146	0	ERAD
	UBQLN4	144	0	ERAD
	DNAJC5	108	1	chaperone
	BAG6	96	0	ERAD
	UBAC2	92	0	ERAD
	SRP72	88	3	cotranslational protein targeting
	SPCS2	88	0	cotranslational protein targeting
	AUP1	85	0	translocation ER to proteasome
E3 ligases	TRIM25	634	6	K63 for NF-κB signaling
	PJA2	355	6	innate immune response
	MIB1	222	18	Notch signaling; K63 endocytosis
	TRIM26	217	1	innate immune response
	RNF5	191	7	K63 for ERAD; K48 by virus
	HUWE1	156	0	K48 on K63 for NF-κB signaling, for proteasome
	ITCH	153	4	K63 seed in K48/K63 for proteasome
	STUB1	120	0	K48 for proteasome; K27 for NF-κB signaling
	KCMF1	117	0	neutrophil degranulation
	DZIP3	105	5	proteasome degradation
	PJA1	89	1	protein sorting
	ZNRF1	84	0	neuronal cell differentiation; K48
	CUL1	83	0	cell cycle progression
	SMURF1	81	0	proteasome degradation

Chapter 3: Molecular machineries required for Vx3 foci formation

Introduction:

Eukaryotic cells use a highly regulated system of tubular and vesicular membranes as intermediates to transport cargo and membrane lipids between different organelles. Nucleation of the pre-autophagosomal structure requires a flux of membrane lipids from multiple sources (i.e., ER, Golgi, recycling endosomes and plasma membrane) [79]. ATG9A, the only transmembrane protein that is part of the core ATG machinery, is conserved from yeast to humans and plays essential roles in all the stages of autophagosome formation and maturation. Although its function remains largely unknown, ATG9A vesicles are thought to deliver essential machineries and lipids to the growing autophagosome. Evidence based on live-cell imaging and colocalization studies using markers of the *trans*-Golgi network (TGN), the early, recycling, and late endosomes, or plasma membrane showed that ATG9A undergoes a complex trafficking pathway through the secretory and endocytic systems [89,90,118] (**Fig 3.0**). ATG9A is internalized from the plasma membrane by clathrin-mediated endocytosis using the adaptor protein AP2 [166,167]. Once inside, ATG9A is transported to recycling endosomes via a conventional route through early endosomes and appears to follow the canonical transferrin receptor internalization pathway [119]. Intracellular ATG9A cycles between the Golgi and recycling endosomes, creating a constant pool of ATG9A vesicles that can be mobilized to the sites of autophagosome formation when necessary. Recycling endosomes have been suggested to act as a platform for autophagosome formation, wherein ATG9A and ATG16L1-positive vesicles coalesce to facilitate initiation of autophagy following nutrient starvation [119,120].

ATG9A vesicles are highly mobile, and their trafficking requires the action of many cellular components such as coat adaptors (e.g., AP2) [166,167] and membrane remodeling factors (e.g.,

SNX18) [168]. Additionally, the retromer, a protein complex whose activity is essential for the recycling of endocytosed cargo to the plasma membrane or retrograde transport to the Golgi, has been implicated in mediating sorting of ATG9A [72]. Previous studies showed that the core retromer subunit mutant VPS35-D20N, which is unable to recruit the WASH complex for the sorting of cargo to subdomains of the early endosomes, leads to autophagy defects as a consequence of ATG9A mistrafficking [72]. Other factors, including TRAPPC8, a subunit of the autophagy specific Rab1 GEF TRAPPIII, have also been reported to contribute to ATG9A exit from the recycling endosomes *en route* to the ER-Golgi intermediate compartment during the initial stages of autophagosome formation [166,169].

By using the K63-polyUb specific sensor Vx3, we had identified proteins modified by K63-polyUb and characterized their intracellular trafficking. The attachment of K63-polyUb to transmembrane proteins of the post-Golgi endomembrane system signals their lysosomal targeting via an autophagy-related vesicular transport. Our results showed that Vx3 expression caused accumulation of cytoplasmic structures enriched for K63-polyubiquitinated transmembrane proteins and ATG9A. We showed that ATG9A itself is not K63-polyubiquitinated, although it tightly associates with ubiquitinated cargo sequestered by the K63-polyUb-specific sensor. Our electron and superresolution fluorescence microscopy analyses also revealed that Vx3 localized on clusters of vesicular elements adjacent to the endolysosome, with ATG9A vesicles co-clustering in subdomains distinct from Vx3. These observations led us to hypothesize that ATG9A might play a role in regulating sorting or transport of K63-polyubiquitinated transmembrane proteins for their lysosomal targeting. The exact function of ATG9A remains elusive. While ATG9A has been found to act at the early stages of autophagosome biogenesis, some reports have suggested a role during late events (i.e., fusion between autophagosomes and lysosomes).

Interestingly, other studies have documented roles for ATG9A that is independent of autophagy; these include the regulation of the cGAS-STING DNA-sensing pathway in an innate immune response [87], and the TBK1-dependent lysosomal trafficking of ferritin [158].

In the present study, we used a siRNA approach to investigate the function of ATG9A with respect to the trafficking of K63-polyubiquitination transmembrane proteins. We also conducted a limited screen using siRNA-mediated knockdown to identify Ub-pathway machineries (i.e., regulators of K63-polyUb conjugation and deconjugation) involved in K63-polyUb-dependent trafficking and Vx3 foci formation. By using Vx3 as a tool to monitor K63-polyubiquitinated cargo within cells, we found that ATG9A, but not other autophagic components, are essential for Vx3 foci formation. Moreover, we show that perturbations of ATG9A trafficking consistently affected Vx3 foci formation. Retromer deficiency impaired formation of Vx3 foci, which supports the involvement of the retromer complex in ATG9A sorting. In our effort to gain more insight into the cellular function of ATG9A, we were able to identify a role for ATG9A in recycling of transmembrane proteins via the retromer, thus establishing a functional link between these proteins during K63-polyUb-dependent sorting of transmembrane proteins into the lysosomes.

Results:

3.1 Vx3 foci formation depends on ATG9A and machineries required for ATG9A trafficking

To determine whether ATG9A is required for Vx3 foci formation, we used RNA-interference to reduce ATG9A expression in HeLa-Vx3 cells. Strikingly, siRNA targeting ATG9A caused a marked decrease of Vx3 foci (**Fig 3.1A**); depletion of ATG9A was confirmed by immunoblotting with an antibody against ATG9A (**Fig 3.1B**). Knockdown of ATG9A also reduced Vx3 and

VMP1-iRFP colocalization (**Fig 3.1C**). On the other hand, Vx3 foci were not affected by knockdown of VMP1 (**Fig. 3.1D**). Also, in contrast to ATG9A, knockdown of other early autophagy regulators had no effect (**Table 4**), suggesting that autophagosome biogenesis is not required for Vx3 foci formation. Additionally, Vx3 foci were not affected by ATG5 knockout (**Fig 3.2A**), which further confirms that LC3 lipidation is dispensable for foci formation.

For selective autophagy, multiple autophagy cargo receptors have been identified that function in part by recognizing (poly)ubiquitin signals. Both our colocalization studies (**Fig 2.5C**; **Table 1**) and mass spectrometry data (**Tables 2** and **3B**) showed association of Vx3 with p62/SQSTM1, a cargo receptor known to be involved in autophagic degradation of polyubiquitinated protein aggregates. We found that knockdown of p62 has no effect on Vx3 foci (**Fig 3.2B**). Furthermore, we employed the previously-developed HeLa cell line ("HeLa penta-KO") that is deficient in the five autophagy receptor proteins p62/SQSTM1, OPTN, NDP52, NBR1 and TAX1BP1 [106]. Transfection of Vx3-EGFP into HeLa penta-KO cells showed a similar Vx3 foci as control cells (**Fig 3.2C**), indicating that neither p62/SQSTM1 nor the other autophagy receptors are required for Vx3 foci formation.

While investigating the ATG9A-dependence of Vx3 foci, we found that perturbation of ATG9A trafficking consistently affected Vx3 foci formation. As described above, the intracellular trafficking of ATG9A is complex. While ATG9A mainly localizes to the Golgi and recycling endosomes, it is also found at the plasma membrane and it is mobilized to autophagic sites during autophagosome biogenesis. Trafficking of transmembrane proteins generally requires sorting motifs that are recognized by adaptor proteins (AP) to direct transport of transmembrane proteins between the various post-Golgi endomembrane compartments. Internalization of ATG9A from the plasma membrane occurs via clathrin-positive carriers using the adaptor protein complex AP2.

Previous studies showed that siRNA-mediated knockdown of AP2A prevents ATG9A redistribution to the sites of autophagosome formation following starvation-induced autophagy in HeLa or HEK293 cells [167]. Recently, an AP2 binding motif in the N-terminus of ATG9A required for its endosomal sorting and autophagosome formation was identified [166]. We found that, as previously described, knockdown of AP2A results in ATG9A mislocalization. Importantly, Vx3 foci were concomitantly reduced in the HeLa-Vx3 cells (**Figure 3.3A**), suggesting that binding of AP2 to an endocytic cargo sorting motif in the ATG9A cytoplasmic tail or, perhaps more directly, within the K63-polyubiquitinated cargo proteins, is required for Vx3 foci formation.

3.1.1 Impairment of ATG9A trafficking via the retromer reduces Vx3 foci formation

The retromer complex assembles onto endosomes and regulates sorting of transmembrane proteins to the appropriate destination. The core retromer subunit VPS35 recruits the WASH complex on endosomes, which in turn promotes actin nucleation to facilitate membrane fission and transport of transmembrane cargo [57]. Two independent studies have reported that VPS35 with the D620N mutation associated with Parkinson's disease confers a decreased affinity of VPS35 for binding to FAM21, a subunit of WASH, resulting in an impaired endosomal recruitment of the WASH complex and a subsequent defect in protein sorting [72,170]. Interestingly, HeLa cells expressing the VPS35 D620N mutant showed mislocalization of ATG9A (i.e., ATG9A accumulates at the perinuclear region) along with an autophagy defect [72].

This crosstalk between ATG9A and the retromer led us to investigate the requirement of the retromer during formation of Vx3 foci. Consistent with a previous study, knockdown of VPS35 resulted in ATG9A accumulation at the perinuclear area [72]. Importantly, we found that Vx3 foci formation was decreased in the absence of VPS35 (**Figure 3.3A**), suggesting that endosomal

sorting by the retromer is required for Vx3 foci formation. Similar to VPS35 knockdown, siRNA targeting WASH1, a core component of the WASH complex, also reduced Vx3 foci formation and perturbed ATG9A localization (**Fig 3.3B**). Modification of WASH1 by K63-polyUb has been reported to activate WASH and facilitate actin nucleation for cargo sorting via the retromer [9]. However, our mass spectrometry data (**Tables 2-3**) did not reveal any peptides from the WASH complex. Furthermore, overexpressed mCherry-tagged WASH1 did not colocalize with Vx3 foci (**Fig 3.3C**). These results suggest that WASH1 does not constitute a major K63-polyubiquitinated substrate bound by Vx3.

Activation of the retromer is initiated by association of the cargo adapter VPS26–VPS29–VPS35 subcomplex to the endosomes through interaction with the GTP-bound form of Rab7a [60]. TBC1D5 is a Rab7a GAP and may act as a negative regulator of the retromer. Loss of TBC1D5 by RNAi has been reported to increase the endosomal localization of the VPS26–VPS29–VPS35 subcomplex, thus leading to an enhanced interaction of the retromer with accessory factors such as the WASH complex [62]. Furthermore, TBC1D5 has been involved in regulating trafficking of ATG9A, as its depletion leads to increased trafficking of ATG9A to the TGN [167]. Our results showed that RNAi-based depletion of TBC1D5 increased Vx3 foci (**Fig 3.4A**) that also stain for ATG9A (data not shown). Altogether, these data provide evidence for a functional relationship between ATG9A and the retromer during Vx3 foci formation.

3.1.2 Impairment of ATG9A trafficking via the TRAPPIII complex increases Vx3 foci

The TRAPPIII complex is a guanine-nucleotide exchange factor (GEF) for Rab1, which has been implicated in regulating autophagy as well as trafficking at the Golgi. In yeast, both Trs85, a subunit of TRAPPIII, and Ypt1 (the yeast paralog of Rab1) have been found to associate with Atg9

vesicles at autophagosome formation sites [171]. Moreover, Trs85 has been shown to facilitate the retrieval of Atg9 from endosomes to Golgi during nutrient-rich conditions [172]. Similar to yeast, TRAPPIII has been shown to regulate ATG9A retrieval to the Golgi. Knockdown of TRAPPC8, the human orthologue of Trs85, was reported to impair autophagy as a consequence of a defective retrieval of ATG9A from RAB11-positive (recycling endosomes) to RAB1-positive (Golgi) compartments [169]. We found that knockdown of TRAPPC8 in HeLa cells caused accumulation of peripheral ATG9A, which corresponded to recycling endosomes, and the loss of the Golgi-localizing ATG9A (**Fig 3.4B**), in agreement with previous reports. Importantly, the absence of TRAPPC8 led to an increase of Vx3 foci number and size (**Fig 3.4C**). Consistently, overexpression of the Rab1A S25N mutant (a GDP-restricted, inactive form) also caused formation of larger Vx3 foci when compared to wild-type Rab1A (**Fig 3.4 D**). These results suggest that the Rab1 GEF TRAPPIII acts downstream of Vx3's block, possibly at the intersection between the retrieval of ATG9A and targeting of K63-polyUb-decorated vesicles to lysosomes.

3.2 ATG9A plays a role in recycling of transmembrane proteins

We showed that loss of ATG9A impairs Vx3 foci formation. Only a subpopulation of TfR and MHC-I is ubiquitinated and bound by Vx3, while the vast majority of TfR and MHC-I is located on the plasma membrane and, after internalization, reaches the recycling endosomal compartment before returning to the cell surface. Surprisingly, knockdown of ATG9A also reduced intracellular staining of TfR and MHC-I in HeLa cells (**Figure 3.5A**). This effect was partly reversed by addition of the lysosomal inhibitors E64d and pepstatin A (data not shown), suggesting that loss of ATG9A caused missorting of transmembrane proteins to the lysosomes for degradation. Loss of SNX3 or VPS35, two components of the retromer, have also been reported to cause missorting

of TfR to lysosomes [71]. In addition to its role in endosome-to-Golgi retrieval of hydrolase receptors, the retromer complex has also been shown to regulate other endosomal recycling pathways, including endosome-to-plasma membrane sorting of integrins [57]. Importantly, both CI-M6PR, a known retromer cargo, and VPS35 have been shown to colocalize with ATG9A under normal conditions and display a similar pattern of redistribution during autophagy [90]. Interestingly, we found that trafficking of CI-M6PR was altered in the absence of ATG9A, resulting in the dispersal of the CI-M6PR to peripheral structures (**Figure 3.5B**); this is in agreement with previous reports of consequences of compromised retromer function [9]. The molecular function of ATG9A remains unknown. Our results support a role for ATG9A in transmembrane protein trafficking that is independent of autophagy, and establish a functional crosstalk between ATG9A and the retromer complex during endosomal recycling of transmembrane proteins.

3.3 Identification of E2 and E3 Ub enzymes required for Vx3 foci formation

Our discovery that conjugation of K63-polyUb onto transmembrane proteins is dependent on ATG9A trafficking offered an opportunity to explore Ub enzymes that may be required for this pathway. For this purpose, we employed RNAi to knockdown Ub pathway enzymes that have been linked to membrane trafficking or that associate with ATG9A based on published studies. A categorized list of siRNA targets (grouped as E2 Ub conjugating, E3 Ub ligase enzymes, and DUBs) that were chosen to examine their effect on Vx3 foci formation is shown in **Table 5**.

3.3.1 Vx3 foci formation depends on the E2 Ub-conjugating enzymes UBE2O and UBE2N

The retromer directs cargo from endosomes to the Golgi or plasma membrane for recycling, while the ESCRT complex sorts ubiquitinated cargo into the MVB pathway for lysosomal degradation.

K63-polyUb is thought to serve as a signal for sorting transmembrane cargo into MVB for degradation [28]. However, recent reports show that K63-polyUb also regulates retromer activity and recycling of transmembrane proteins [9]. Modification of WASH1 by K63-polyUb was shown to require the E2 Ub-conjugating enzyme UBE2O to activate the WASH complex and facilitate actin polymerization on endosomal tubules for the retrograde transport of CI-MPR [9]. Similar to loss of WASH1, knockdown of UBE2O affected ATG9A trafficking (**Fig 3.6A**) and reduced formation of Vx3 foci (**Fig 3.6B**). Its absence also led to p62 accumulation (**Fig 3.6C**), indicating a block of autophagy. These data suggest that generation of K63-polyUb by UBE2O is required for Vx3 foci formation, although its effect might be an indirect consequence of an impaired retromer function and ATG9A missorting.

Although transmembrane protein recycling and degradation are opposing activities that can coexist for the same endosome, they are thought to occur in separate subdomains. A recent report using *C. elegans* showed that loss of *ube2N*, the E2 Ub-conjugating enzyme responsible for generating K63-polyUb, impairs recycling of several retromer-dependent cargo as a consequence of an impaired subdomain separation on endosomes [173]. Given that UBE2N is known to assemble K63-polyUb, we tested its requirement during Vx3 foci formation. Our results showed that siRNA-mediated depletion of UBE2N in HeLa-Vx3 caused a reduction but not a complete abolishment of Vx3 foci (**Fig 3.6B**), likely due to either incomplete protein knockdown or the existence of functional redundancy among E2s. However, in contrast to UBE2O knockdown, its loss did not grossly affect ATG9A or p62 staining. Together with the findings described above, these data pinpoint a role for K63-polyUb in cargo selection at the crossroad between degradation and retrograde transport.

3.3.2 The E3-Ub ligases TRIM27 and NEDD4L are required for Vx3 foci formation

As expected, we found that the E3 Ub ligase TRIM27 affected formation of Vx3 foci. In association with the E2 UBE2O, the MAGE-L2-TRIM27 complex can activate WASH through conjugation of K63-polyUb on WASH1 to facilitate actin polymerization and endosome-to-Golgi trafficking of the CI-MPR protein [9]. In the absence of MAGE-L2 or TRIM27, we observed accumulation of ATG9A at the perinuclear region (data not shown) and the concomitant reduction of Vx3 foci (**Fig 3.7A**), indicating that signaling by K63-polyUb is required for ATG9A recycling and Vx3 foci formation.

Based on previous reports indicating a key role for yeast Rsp5 in mediating K63-polyubiquitination of endocytic cargo [28], we sought to investigate members of the human Nedd4 E3s. Rsp5 is the unique yeast member of the Nedd4 family of HECT E3 ligase, which in humans comprises several enzymes whose functions have been reported to regulate various Ub-mediated protein sorting processes at the plasma membrane and *trans*-Golgi. We found that siRNA-based depletion of the E3 ligase NEDD4L (also known as NEDD4-2) caused a decrease in Vx3 foci formation (**Fig 3.7B**), which is different from the effects seen upon loss of other members of the Nedd4 family (see **Table 5**). We observed that knockdown of NEDD4L caused accumulation of perinuclear ATG9A and reduction of the total levels of TfR (**Fig 3.7 B**), indicating their mistrafficking and thus suggesting a general role for NEDD4L in transmembrane protein trafficking. Overall, these results uncovered a role for the E3 ligase NEDD4L in regulating trafficking of ATG9A and K63-polyubiquitinated cargo.

3.3.3 Vx3 foci formation depends on USP7 and USP9x function

While screening for DUBs affecting Vx3 foci formation, we found that knockdown of USP7 or USP9x dramatically reduced the appearance of Vx3 foci (**Figs 3.8A** and **3.8B**). USP7 has been shown to regulate WASH-mediated endosomal actin assembly and protein recycling by counteracting TRIM27 auto-ubiquitination and degradation [174]. Its loss was reported to impair the WASH complex activation and retrieval of CI-M6PR [174]. Thus, similar to WASH1 loss, we found that knockdown of USP7 abolished Vx3 foci, supporting a role for the retromer/WASH complexes in Vx3 foci formation

The DUB USP9x was selected as a target gene for our RNAi screening due to its reported association with VMP1 and p62 during selective autophagy [175]. Moreover, USP9X was recently reported to interact with NEDD4L to regulate canonical Wnt activation by controlling ubiquitination of the Wnt signaling protein DVL2 [176]. Our results showed that knockdown of USP9x also affected formation of Vx3 foci. Therefore, it is plausible that this effect might be a consequence of an impaired NEDD4L-USP9X regulatory axis that regulates K63-polyUb conjugate levels. Although these results suggest an involvement of USP7 and USP9x during Vx3 foci formation, the exact role of these DUBs in regulating signaling by K63-polyUb and whether they act on the same transmembrane protein substrates is not known.

Discussion

We have shown previously (**Chapter 2**) that ATG9A closely associates with K63-polyubiquitinated transmembrane proteins. By superresolution fluorescence microscopy we revealed that ATG9A accumulating in Vx3 localize to distinct subdomains of the vesicular clusters that constitute Vx3 foci. Whereas the data indicated that ATG9A vesicles are found co-clustering with K63-polyUb-decorated vesicles, they did not reveal anything about the functional relationship between ATG9A and K63-polyUb. Here we made an effort to address ATG9A's function in Vx3 foci formation by employing an RNAi strategy to knockdown ATG9A and other cellular machineries implicated in membrane trafficking during autophagy or endocytosis. By using Vx3 as a probe to detect ubiquitinated cargo *in vivo*, we uncovered requirements for ATG9A and the retromer complex in regulating K63-polyUb-dependent trafficking of transmembrane proteins to the lysosomes.

ATG9A constitutively cycles to and from recycling endosomes, Golgi, and plasma membrane. However, upon autophagy induction, it is mobilized to peripheral structures corresponding to the sites of autophagosome assembly [90]. While ATG9A's role in mammalian cells remains unknown, it has been postulated that ATG9A contributes to autophagosome formation and maturation by delivering lipids and other components. In this study, we report that ATG9A is necessary for Vx3 foci formation, as its loss caused a nearly complete abolishment of cytoplasmic inclusions containing K63-polyubiquitinated cargo. Our data show that this effect is not a consequence of impaired autophagosome formation, as knockdown of other early autophagy proteins essential for phagophore nucleation (e.g., ULK1 or ATG14) or LC3 conjugation (e.g., ATG5 or ATG16L1) did not alter Vx3 foci formation. Roles for ATG9A independent of autophagy have been described during the innate immune response to double-stranded DNA through trafficking of STING and

86

assembly of a complex with TBK1 [87]. More recently, ATG9A has been involved in an alternative lysosomal transport pathway for ferritin that requires FIP200, VPS34 and TAX1BP1, but lacks involvement of the LC3 lipidation machinery [158]. This latter mechanism was also shown to be dependent on TBK1, as TBK1 inhibition affected ATG9A localization and lysosomal targeting of ferritin [158]. Interestingly, our unpublished data showed that TBK1 knockdown also reduced formation of Vx3 foci. Further studies will be needed to characterize the requirement of TBK1 activity in regulating ATG9A during Vx3 foci formation.

We propose that ATG9A plays a major role in regulating formation or localization of K63-polyubiquitinated cargo upstream of their lysosomal targeting. Although our data support an intertwined relationship between ATG9A vesicles and ubiquitinated transmembrane proteins, how formation of Vx3 foci is achieved remains a conundrum. Two fundamental questions arise from this work: *What is being delivered by ATG9A vesicles to the vesicular and tubular inclusions marked by Vx3*? *Why is ATG9A required for Vx3 foci formation?* As one approach to address these, future experiments will employ stable isotope labeling with amino acids in cell culture (SILAC) coupled with tandem mass spectrometry to compare ATG9A-positive vesicles isolated from Vx3NB and Vx3-expressing cells.

Based on current evidence, several possibilities are discussed below.

I) <u>ATG9A vesicles deliver E3 Ub ligases to regulate K63-polyubiquitination of transmembrane protein cargo</u>. Currently, there is no evidence in the literature for a direct interaction between ATG9A and E3 Ub ligases. In our effort to identify potential E3 ligases that could directly K63-polyubiquitinate transmembrane proteins, we found that loss of Nedd4L, a member of the HECT-type Nedd4 E3 Ub family known to be involved in endosomal sorting to the lysosome, affected formation of Vx3 foci. However, this effect might be an indirect consequence of perturbed ATG9A

trafficking, as indicated by the mislocalization of ATG9A observed upon Nedd4L knockdown. ATG9A can be potentially modified by Ub for endocytosis; large-scale ubiquitin proteomics studies have indeed identified two ubiquitination sites within its C-terminal region [177,178]. We propose that NEDD4L affects Vx3 foci formation by either regulating ubiquitination of ATG9A or machinery that governs ATG9A trafficking. A similar phenotype was observed upon loss of the RING-type Ub ligase TRIM27, an E3 enzyme involved in regulating the retromer-dependent endosomal sorting of transmembrane proteins, including ATG9A (see discussion below). The human genome encodes more than 600 E3 Ub ligase genes, with a large subset of them being implicated in regulating various aspects of membrane protein trafficking. A very recent quantitative mass spectrometry analysis of ATG9A-positive compartments identified the E3 Ub ligases TRIM25 and HUWE1 among the highest hits of peptides enriched by immunoisolation of ATG9A vesicles from amino acid-starved cells [179]. Intriguingly, both these E3 ligases were also identified in our proteomics analysis of Vx3-immunoprecipitated proteins. Future RNAi experiments to deplete TRIM25 or HUWE1 will investigate the requirement, if any, of these Ub ligase enzymes during Vx3 foci formation. The identification of E3 Ub ligases associated with ATG9A vesicles will ultimately shed light on the Ub machinery required for the lysosomal targeting of transmembrane proteins via a K63-polyUb-dependent mechanism.

II) <u>ATG9A facilitates internalization and trafficking of K63-polyubiquitinated cargo from the plasma membrane to the Vx3 foci.</u> We showed that Vx3 foci do not form when we acutely inhibited endocytosis by treating HeLa cells with the dynamin inhibitor dynasore, corroborating result reported here shows that depletion of AP2A, an endocytic adaptor that interacts with clathrin, also abolishes formation of Vx3 foci. These observations are consistent with the idea that K63-polyubiquitinated cargo that traffic into Vx3 foci originate from the plasma membrane. A similar

endocytic route is also used by ATG9A. A study using TIRF microscopy showed that ATG9A redistributes close to the plasma membrane upon dynasore treatment. Moreover, AP2A depletion also caused mislocalization of ATG9A, along with an autophagy defect [166]. A role for ATG9A in endocytic cargo internalization has been suggested in previous reports of autophagy-mediated degradation of connexin-43 in rat kidney cells. During starvation, the recruitment of ATG9A and ATG14 to the plasma membrane activates the PI3K kinase VPS34, thereby promoting internalization of connexin-43 into gap junction plaques that are subsequently degraded via autophagy [114]. Internalization of ubiquitinated connexin-43 has been also reported to depend on Eps15 [113], an endocytic adaptor that contains two UIMs for Ub and K63-polyUb binding.

Our study demonstrates that K63-polyubiquitinated cargo that originate from the plasma membrane accumulate in Vx3 foci via an ATG9A-dependent manner. *When and where are these proteins are ubiquitinated?* One possibility is that K63-polyUb conjugation occurs at the plasma membrane and that Eps15 and ATG9A may act in concert to facilitate cargo internalization and targeting to the lysosome. However, using Vx3 as a probe to monitor such events upstream of Vx3 foci formation (i.e., trafficking of small K63-polyUb vesicles) might be ineffective because weakly-fluorescent structures (e.g., very small vesicles or structures sparsely decorated with Vx3) would be very difficult to detect, and relatively weak signals might be lost quickly due to photobleaching. Future studies will evaluate the contribution of Eps15 in the formation of Vx3 foci. In addition, the presence of K63-polyubiquitinated proteins on the plasma membrane can be assessed by cell surface biotinylation followed affinity isolation to help determine if K63-polyUb conjugates are at the plasma membrane.

III) ATG9A concentrates K63-polyubiquitinated cargo for their endosomal sorting via the retromer–WASH axis. Along the endosomal membrane, ubiquitinated proteins are generally

recognized by ESCRT machinery before their sorting into intraluminal vesicles of maturing endosomes. Alternatively, cargo can be de-ubiquitinated before sorting by ESCRT-associated DUBs (e.g., USP8 and AMSH) and undergo recycling via the retromer–WASH supercomplex. Dysfunction of the retromer has been reported to induce ATG9A mistrafficking and cause inhibition of autophagy [72]. Additionally, ATG9A has been reported to strongly colocalize with VPS35, the cargo-recognition subunit of the retromer [167]. We found that depletion of either VPS35 or WASH1, a subunit of the WASH complex, results in impaired ATG9A trafficking whereby ATG9A accumulates at a juxtanuclear area of the cell; this aberrant localization agrees with previous observations from others [72]. Notably, we found that loss of VPS35 or WASH1 also reduces Vx3 foci formation. Retromer deficiency provokes dysfunctional autophagy, possibly because ATG9A is a retromer cargo that traffics to the autophagosomes [72]. Given that perturbation of ATG9A levels or localization consistently affects Vx3 foci formation, the retromer effect on Vx3 foci could be explained by an erroneous trafficking of ATG9A rather than a direct dysregulation of K63-polyubiquitinated cargo sorting by the retromer.

Our work indicates that ATG9A is crucial for Vx3 foci formation, yet its function and the functional relationship with the retromer complex remains unclear. We have seen that depletion of ATG9A causes a nearly complete loss of intracellular TfR, indicative of that receptor missorting to the lysosomes. Similarly, the absence of ATG9A also induces mislocalization of CI-M6PR, a prototypical retromer cargo, supporting the idea of a functional interaction between ATG9A and the retromer. The current model for retromer-mediated cargo sorting argues that the retromer interacts with the cytosolic domains of cargo and, together with the WASH complex, mediates enrichment of selected cargo within the maturing endosomal membrane into subdomains for recycling [57]. Therefore, one possibility is that ATG9A plays a role to concentrate or segregate a

subset of retromer cargo before their transport via tubulovesicular carriers. Our work indicated that Vx3 expression prevents ESCRT-dependent incorporation of K63-polyubiquitinated cargo into invaginations of the late endosome, thereby re-routing them to an alternative proteolytic route (**Figs 2.15** and **2.16**). One model emerging from this study is that K63-polyubiquitinated cargo are sorted into recycling subdomains by the concerted action of ATG9A and the retromer complex before they pinch off into vesicles from tubular structures that emanate from the body of the endosome. Thus, trafficking of K63-polyubiquitinated cargo into Vx3 foci can depend on the presence of both ATG9A and the activity of the retromer–WASH supercomplex, and that their absence precludes the appearance of K63-polyUb into vesicular intermediates that are detectable by the Vx3 probe. Transmembrane proteins in the early endosomes are either destined for lysosomal degradation via the MVB pathway or recycled to their point of origin by the retromer activity. Although these processes have opposing roles, they occur on adjacent subdomains along the limiting membrane of the same endosome. A recent report showed that *ube2N*, the E2 Ub-conjugating enzyme responsible for generating K63-polyUb in *C. elegans*, is important for maintaining the separation between the degradative and recycling subdomains [173]. Our data support the idea that Vx3 expression might disrupt subdomain separation, thereby leading to the re-routing of K63-polyubiquitinated cargo from an ESCRT-dependent degradative compartment to an ATG9A and retromer-dependent transport pathway to the lysosome.

In conclusion, we have uncovered a functional relationship between ATG9A and the retromer complex during general recycling of endocytic transmembrane proteins that may extend beyond their involvement in K63-polyUb-dependent trafficking of cargo to the lysosome. Whether ATG9A and the retromer complex cooperate to control trafficking of endocytic cargo at the

intersection between degradative (e.g., endocytosis and autophagy) and recycling pathways, and

how K63-polyUb conjugation and deconjugation determine this decision, remain to be determined.

Material and methods

Material and methods are overlapping with the ones described in Chapter 2. Following is a list of plasmids, cell lines, siRNAs, and antibodies used exclusively in the experimental session of Chapter 3.

Plasmids

The following plasmids were exclusively used in this study: mCherry-hWASH was a kind gift from A. Gautreau, Institut Polytechnique de Paris; pEGFP-LC3 (Addgene #21073) was a gift from T. Yoshimori, Osaka University; Myc-Rab1-WT and Myc-Rab1-S25N plasmids were gifts from T. Herbert, McGill University (Addgene #46776 and 46777, respectively).

Cell lines

The follow cell lines were exclusively used in this study: ATG5 KO MEF cells were provided by N. Mizushima (University of Tokyo) and HeLa PENTA-KO cells were a generous gift by R. Youle (NIH).

Antibodies

The follow antibodies were exclusively used in this study: anti-myc (clone 9E10, Millipore; 1:200 dilution) and anti-CI-M6PR (clone 8f67, DHSB; 1:100 dilution) antibodies.

RNAi experiments

The following siGenome SMART pool siRNA against AP2A, ATG9A, MAGEL2, NEDD4L, p62

(SQSTM1), TBC1D5, TRAPPC8, TRIM27, USP7, USP9x, VPS35, and WASH1 were purchased

from Dharmacon and exclusively used in this study.
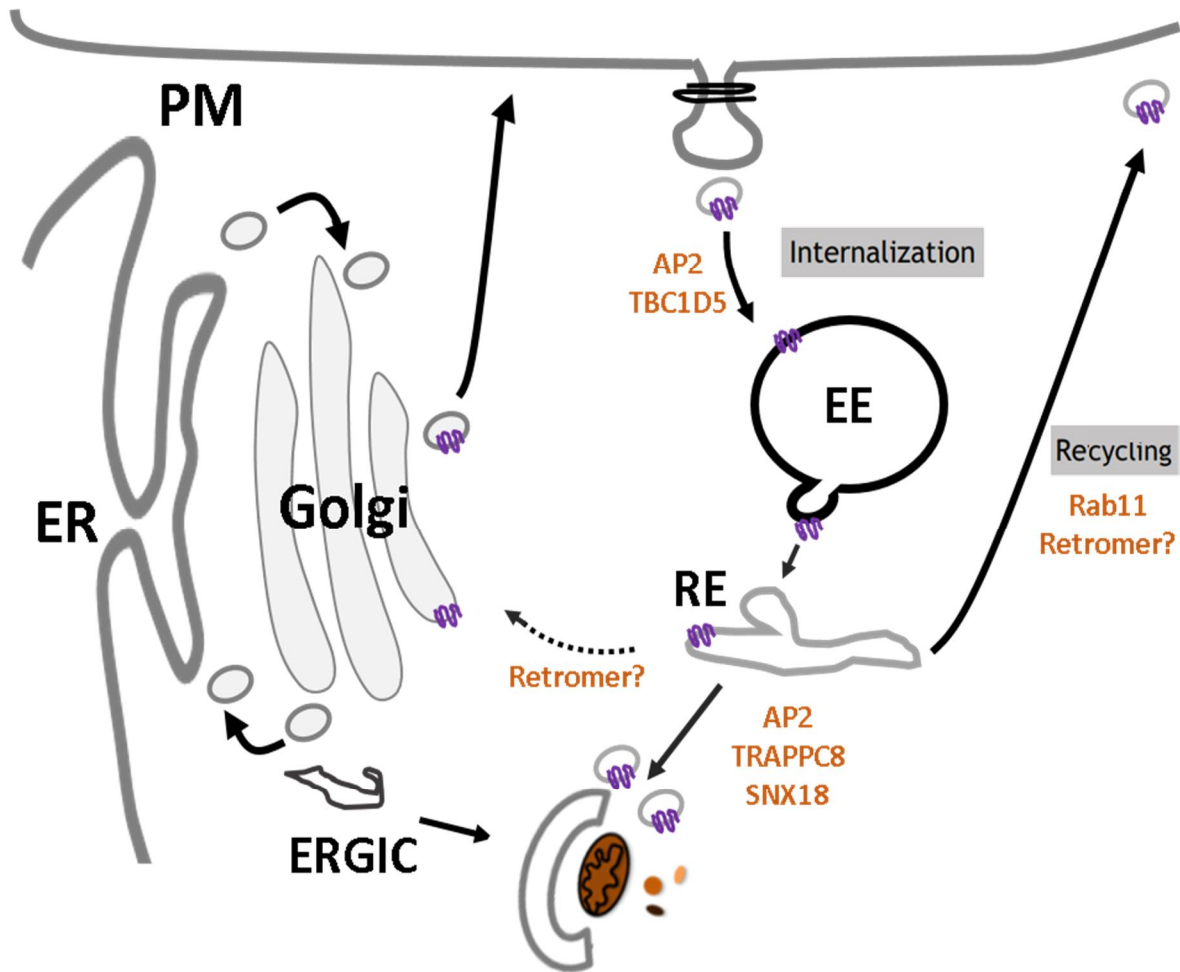
Figure 3.0: Model of ATG9A trafficking in mammalian cells. Trafficking of ATG9A (*purple*) is complex and involves transport through multiple organelles of secretory and endocytic systems. At a steady state ATG9A mainly localizes at the juxtanuclear recycling endosomes and Golgi. Upon autophagy activation, ATG9A vesicles are mobilized to the site of phagophore nucleation and growth. Known regulators of ATG9A trafficking are highlighted (*orange*). The exit of ATG9A from the recycling endosome is required for autophagosome biogenesis. The retromer has been implicated in ATG9A sorting. However it is not clear whether it mediates direct transport of ATG9A to the phagophore, or the ATG9A retrieval to Golgi or plasma membrane. See text for further details. PM= plasma membrane; ER= Endoplasmic Reticulum; EE= early/sorting endosomes; RE= Recycling endosomes.
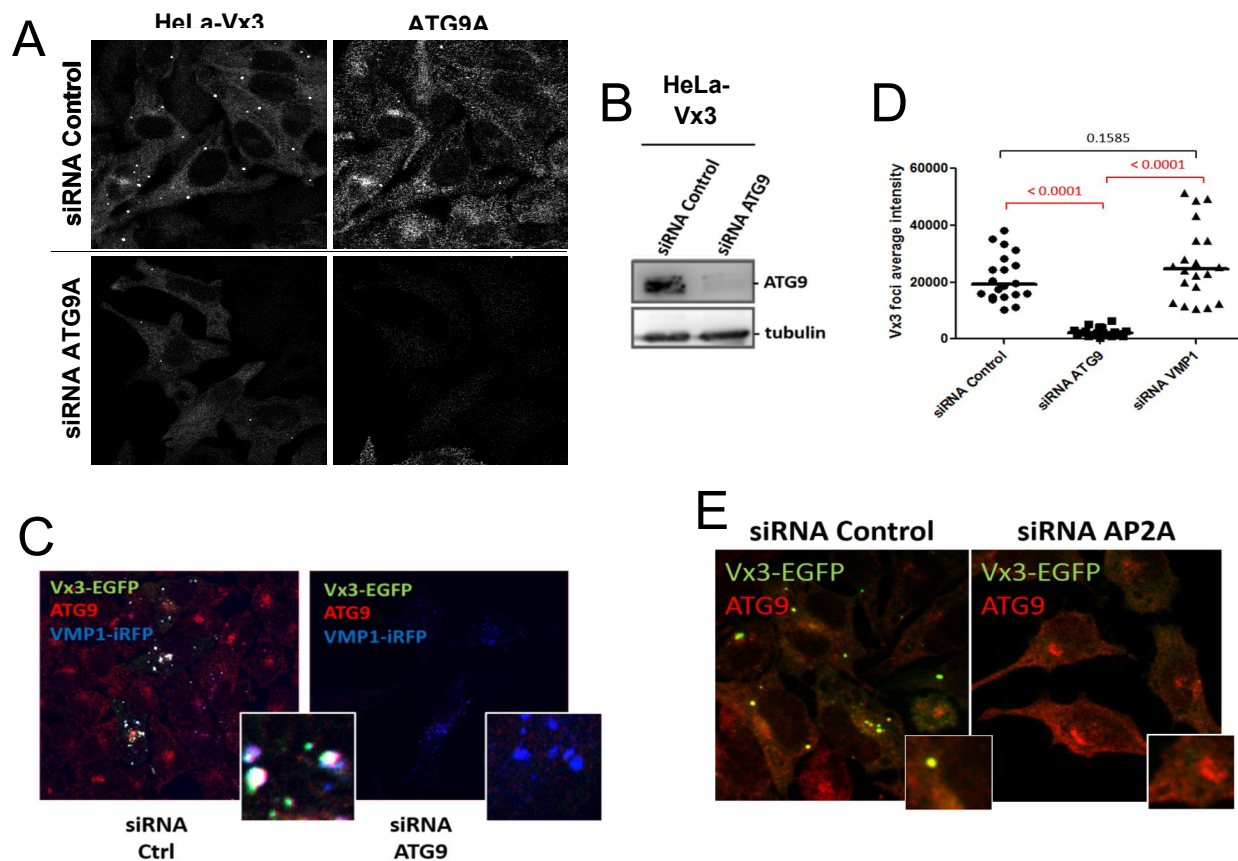
Figure 3.1: Loss of ATG9A or perturbation of ATG9A trafficking reduces Vx3 foci formation. A) HeLa-Vx3 were treated with either control siRNA or siRNA against ATG9 for 72h. Vx3-EGFP expression was induced for 24h by treatment with DOX (1 μg/mL) and stained with an anti-ATG9A antibody. **B)** Cell lysates were analyzed by western blot using antibodies against ATG9 and tubulin as a loading control. **C)** HeLa-Vx3-VMP1 cells stably were treated with either control siRNA or siRNA against ATG9 for 72h, treated with DOX, and stained as in (A). **D)** Analysis of 20 cells per knockdown condition shows that Vx3 foci average intensity in HeLa-Vx3-VMP1 is significantly reduced by knockdown of ATG9 when compared to siRNA-VMP1 or control cells. **E)** HeLa stably expressing Vx3-EGFP were treated with either control siRNA or siRNA against AP2 for 72h. Vx3-EGFP (*green*) expression was induced for 24h with DOX (1 μg/mL). Cells were stained with anti-ATG9 antibody (*red*).
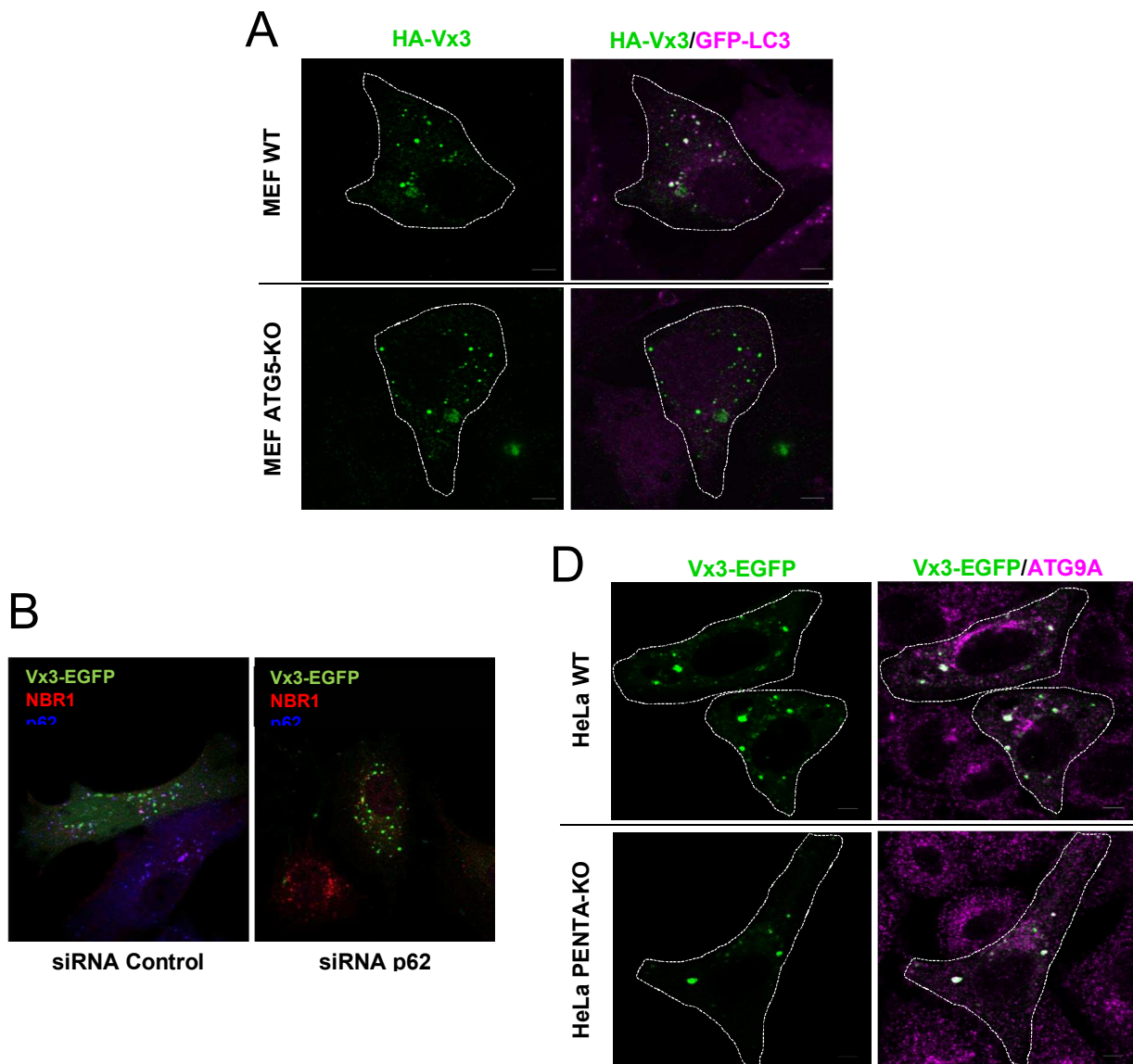
Figure 3.2: Vx3 foci formation does not require LC3 conjugation or autophagy cargo adaptors. A) ATG5-KO and WT MEF cells stably expressing GFP-LC3 (right panel, *magenta*) were transiently transfected with HA-Vx3 for 24 h and stained with an anti-HA antibody (*green*). The absence of ATG5 did not affect formation of Vx3 foci. Dashed lines mark the cell contours. Scale bar: 5 μm. **B)** HeLa cells were treated with either control siRNA or siRNA against p62 for 72h. Vx3-EGFP transiently-transfected for 24h and cells were stained with an anti-NBR1 (*red*) and anti-p62 (*blue*) antibodies. **C)** PENTA-KO and WT HeLa cells were transiently transfected with Vx3-EGFP (*green*) for 24 h and stained with an anti-ATG9A antibody (*magenta*). The absence of all five autophagy cargo adaptors (i.e., p62, NBR1, OPTN, TAXBP1, NDP52) does not affect Vx3 and ATG9A colocalization. Dashed lines mark the cell contours. Scale bar: 5 μm.
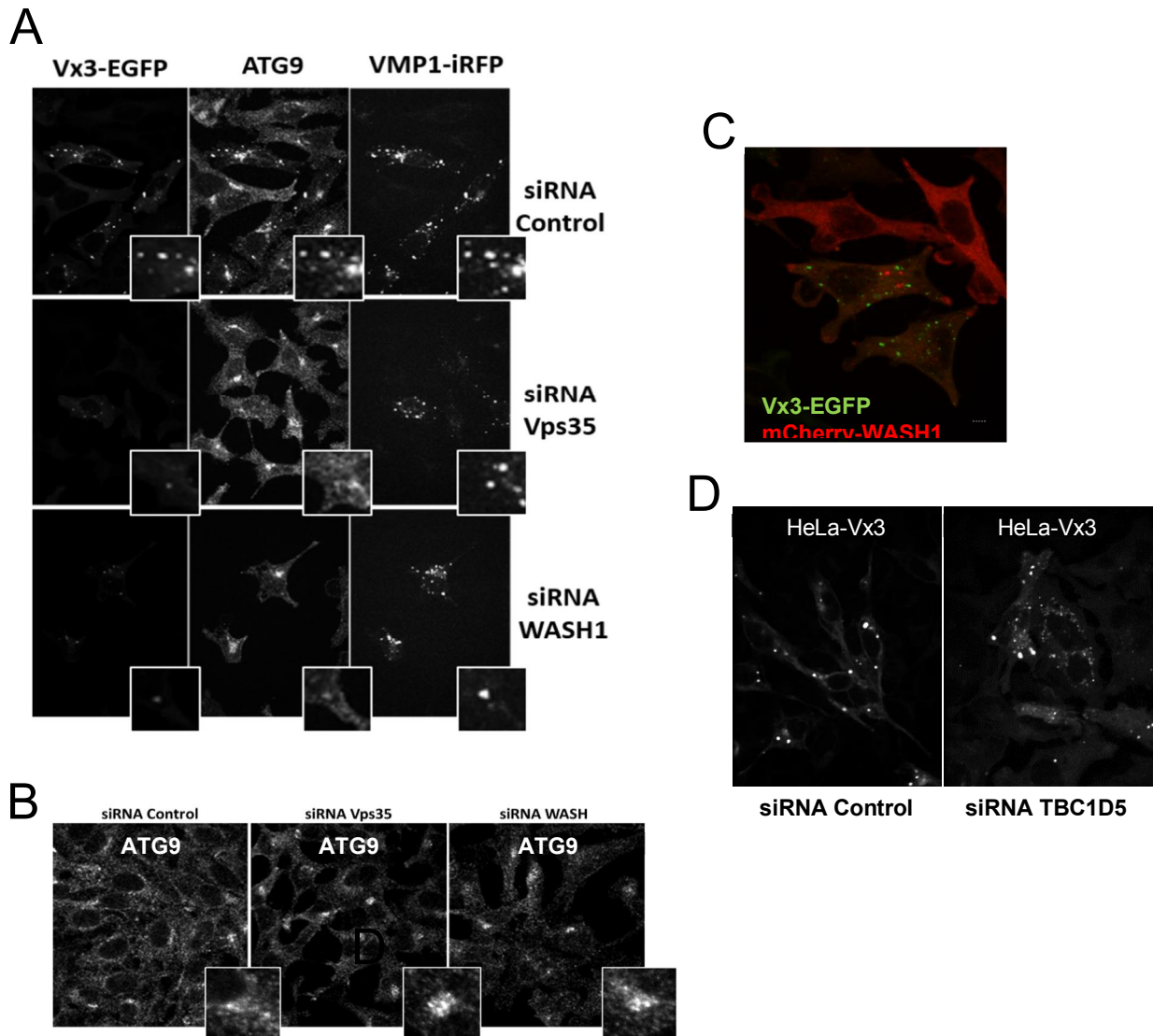
Figure 3.3: Retromer dysfunction mislocalizes ATG9A and reduces Vx3 foci formation.
A) HeLa-Vx3-VMP1 were treated with either control siRNA or siRNA against Vps35 or WASH1 for 72h. Vx3-EGFP expression was induced for 24h with DOX (1 μg/mL). Cells were stained with anti-ATG9 (middle panel) antibody. **B)** HeLa cells were treated with either control siRNA or siRNA against Vps35 or WASH1 for 72h and stained with anti-ATG9 antibody. **C)** HeLa-Vx3-VMP1 cells were transiently transfected with WASH1-mCherry (*red*) for 24 h and cultured in the presence of DOX (1 μg/mL) for additional 24 h to induce expression of Vx3-EGFP (*green*). **D)** HeLa-Vx3 were treated with either control siRNA or siRNA against TBC1D5 for 72h before addition of DOX (1 μg/mL).
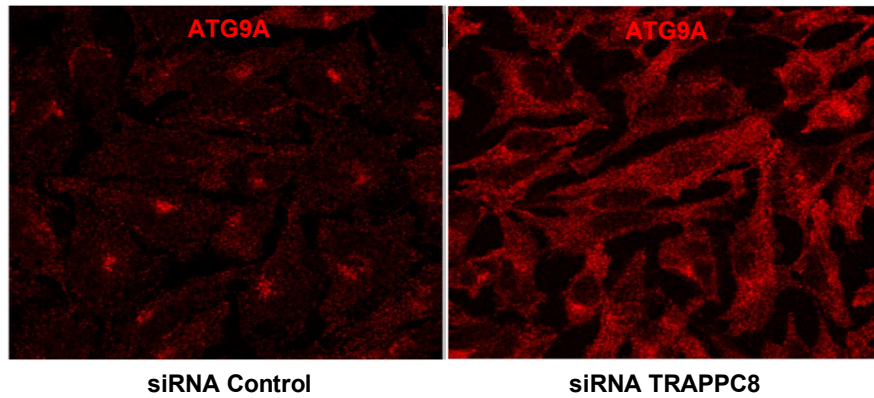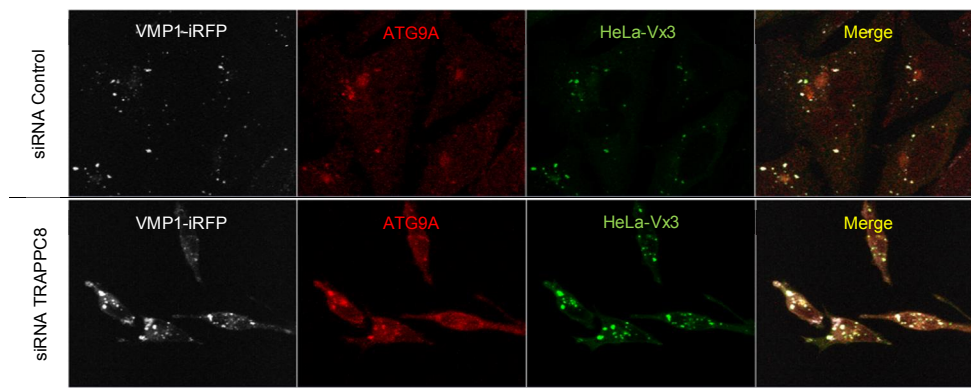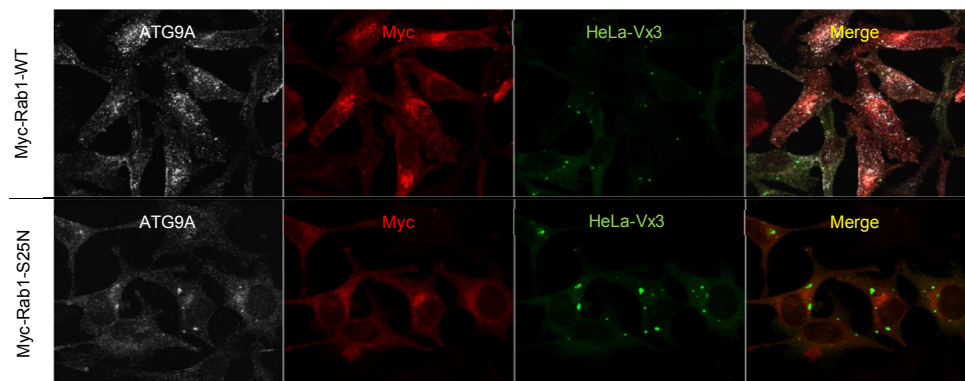
Figure 3.4: Augmentation of Vx3 foci as a consequence of TRAPPIII deficiency. A) HeLa-Vx3-NB were treated with either control siRNA or siRNA against TRAPPC8 for 72h and stained with an anti-ATG9A (*red*) antibody. **B)** siRNA-based depletion of TRAPPC8 for 72 h in HeLa-Vx3-VMP1 before addition of DOX (1 µg/mL) to induce Vx3-EGFP (*green*) expression and staining with an anti-ATG9A (*red*) antibody. **C)** HeLa-Vx3 were transiently transfected with Myc-Rab1 WT or S25N mutant for 24 h and cultured in the presence of DOX (1 µg/mL) to induce formation of Vx3-EGFP (green) foci for additional 24 h. Cells were stained with anti-myc (*red*) and ATG9A (*white*) antibodies.
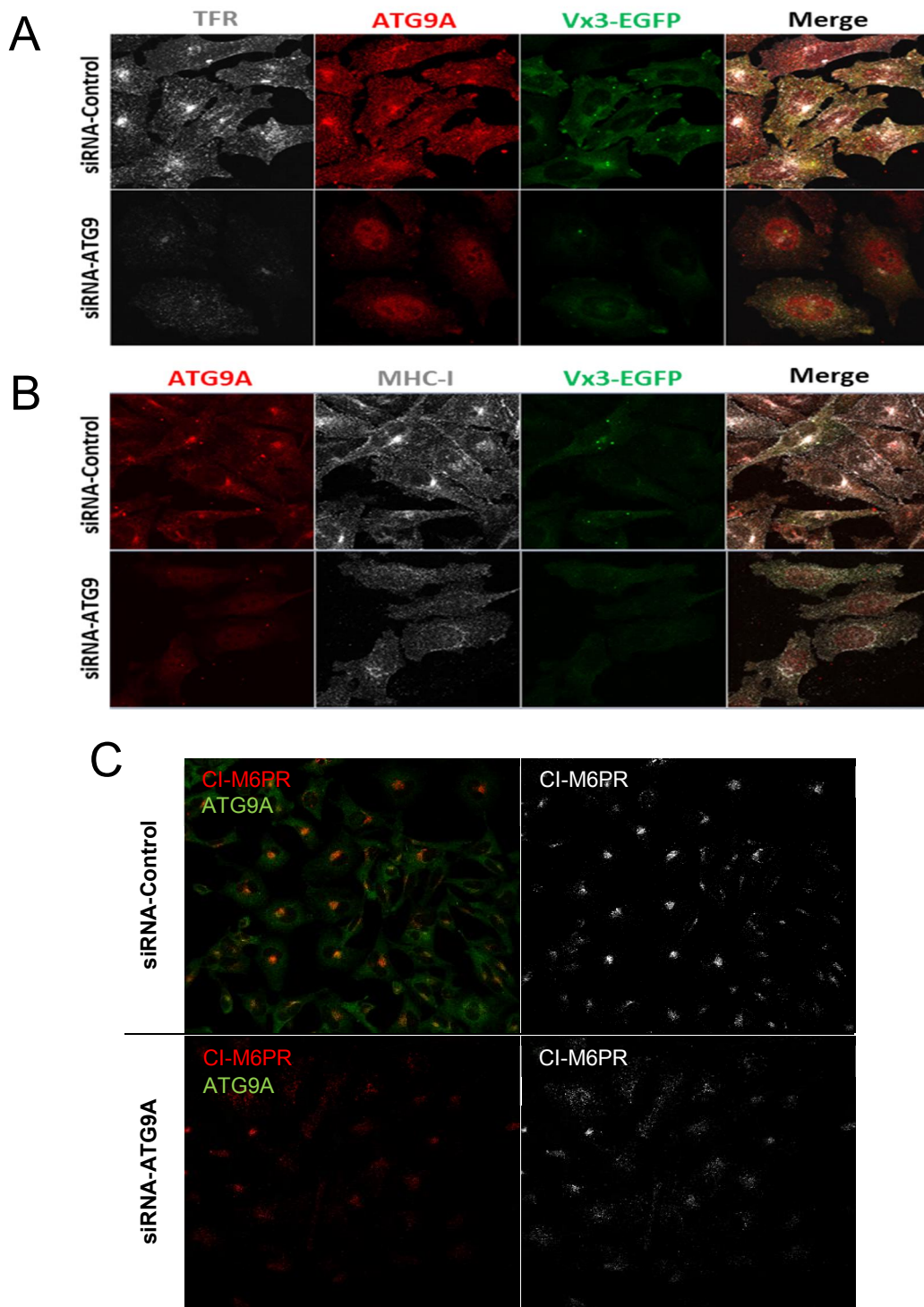
Figure 3.5: Knockdown of ATG9A perturbs endosomal recycling of retromer cargo. A) Maximum projection image of HeLa-Vx3 (*green*) cells were treated with either control siRNA or siRNA against ATG9 for 72h. Cells were stained with antibodies against ATG9A (*red*) and TfR (*white*). **B)** Same as in (A) with immunostaining of ATG9A (*red*) and MHC-I (*white*). **C)** Same as in (A) and (B) with staining of ATG9A (*green*) and CI-M6PR (*red*, left panel; *white*, right panel); single z-stack image.
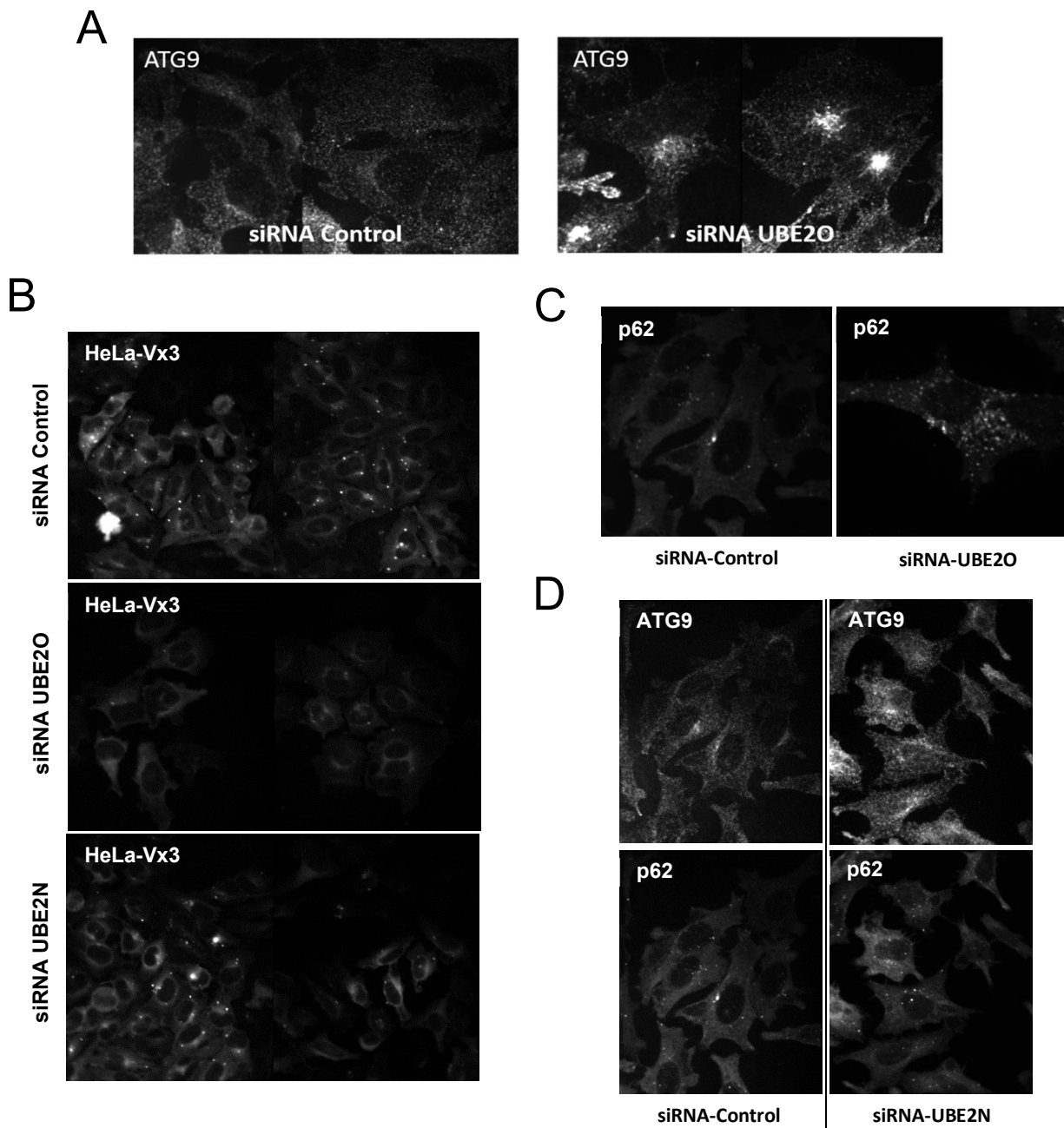
Figure 3.6: E2 Ub conjugating enzymes required for Vx3 foci formation. A) HeLa-Vx3NB
were treated with either control siRNA or siRNA against UBE2O for 72h and stained with anti-
ATG9A antibody. **B)** Hela-Vx3 were treated with siRNA or siRNA against UBE2O or UBE2N
for 72h. DOX (1 µg/mL) was added 24 h prior to fixation. **C)** Same as (A) with staining using
an anti-p62 antibody. **D)** HeLa-Vx3NB were treated with either control siRNA or siRNA
against UBE2N for 72h and stained with antibodies against ATG9A or p62.
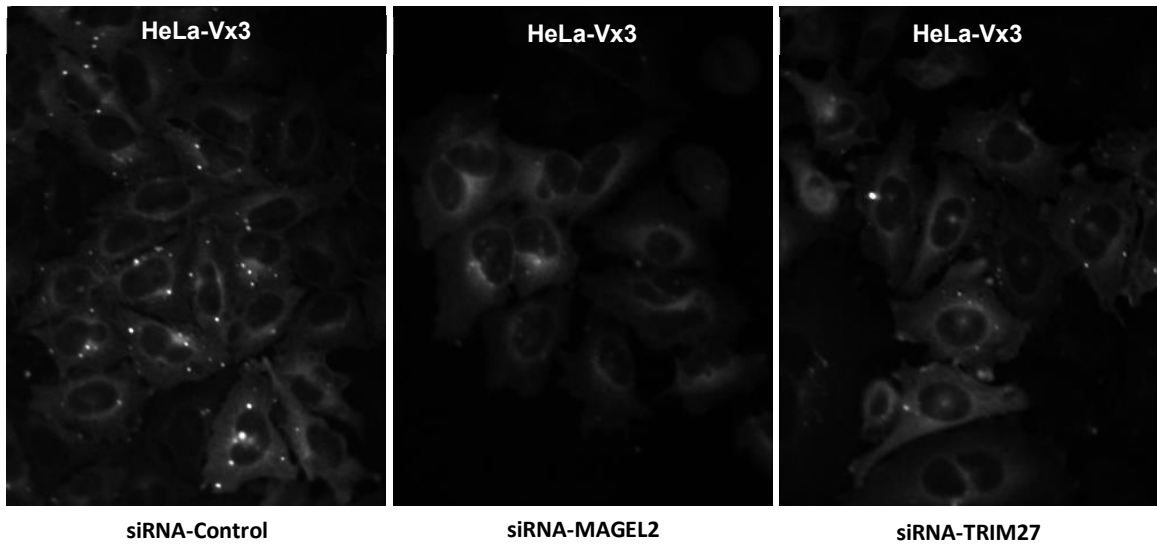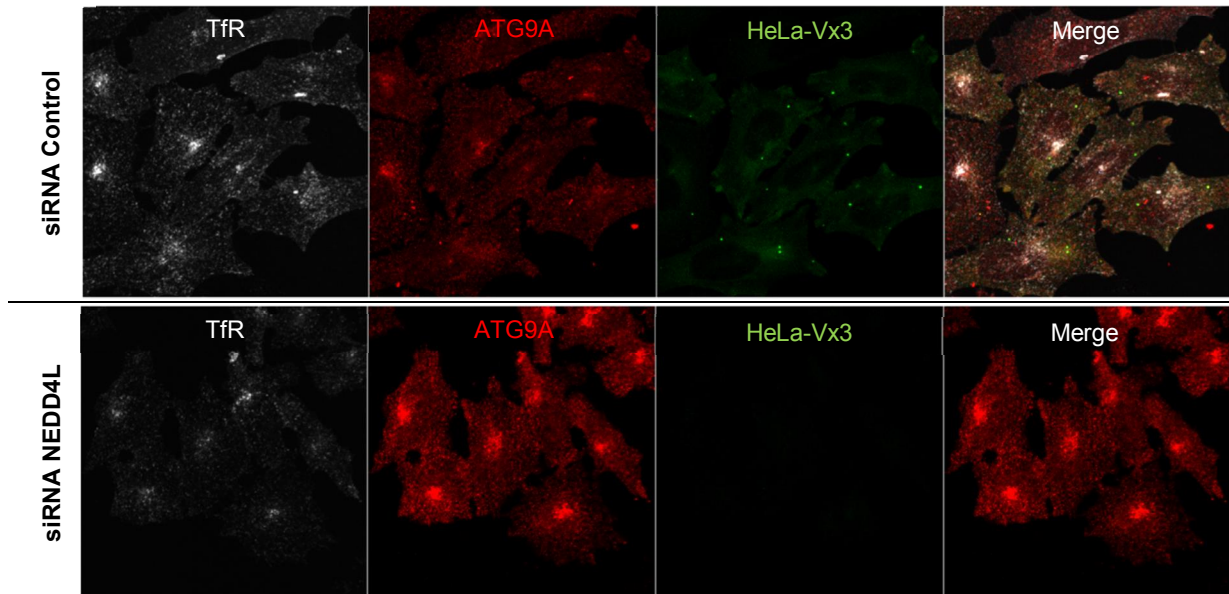
Figure 3.7: E3 Ub ligases required for Vx3 foci formation. A) HeLa-Vx3NB were treated with either control siRNA or siRNA against MAGE-L2 or TRIM27 for 72 h. Cells were cultured with DOX (1 µg/mL) for 24 h to induce Vx3-EGFP expression. **B)** Maximum projection image of HeLa-Vx3 (*green*) cells treated with either control siRNA or siRNA against NEDD4L for 72h. Cells were stained with antibodies against ATG9A (*red*) and TfR (*white*).
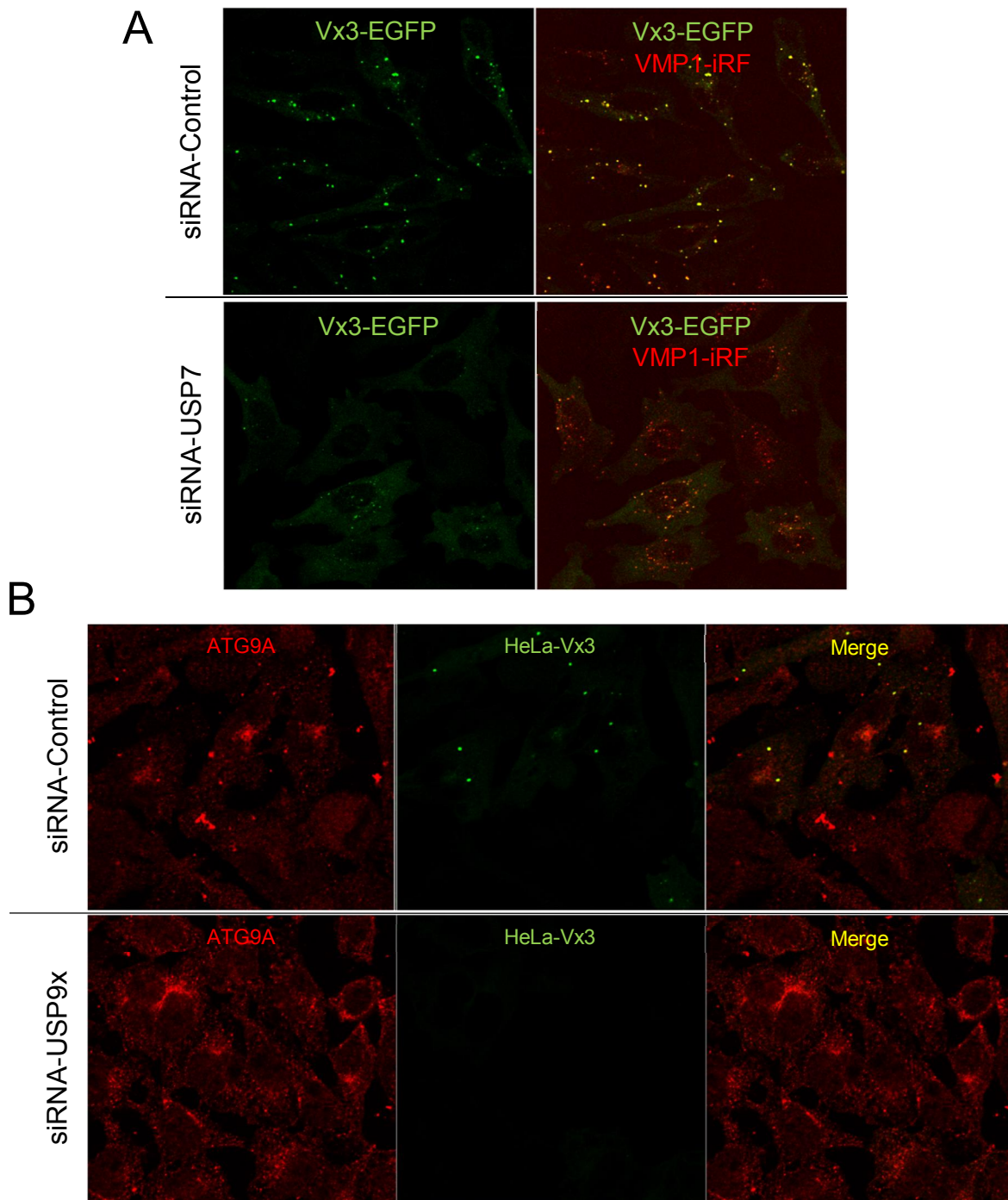
Figure 3.8: Loss of USP7 or USP9x alters Vx3 foci formation. A) HeLa-Vx3-VMP1 were treated with either control siRNA or siRNA against USP7 for 72 h. Cells were cultured with DOX (1 μg/mL) for 24 h to induce Vx3-EGFP (*green*) localization onto VMP1-iRFP signals (*red*). EGFP (left panel) and merge channels (right panel) are shown. **B)** HeLa-Vx3 were treated with either control siRNA or siRNA against USP9x for 72 h. Cells were cultured with DOX (1 μg/mL) for 24 h to induce Vx3-EGFP (*green*) before fixation and staining with an anti-ATG9A antibody.

Table 4: RNAi screen to identify machineries involved in Vx3 foci formation. List of siRNA targets used to examine effect on Vx3 foci formation upon their loss. Autophagy factors and trafficking machineries were chosen because of their role during autophagosome formation/maturation and general membrane fusion or transport, respectively. RNAi against VAMPs were performed based on their presence in the second mass spectrometry experiment. General protein descriptions were written based on information available in the databases UniProt (https://www.uniprot.org/), NCBI (https://www.ncbi.nlm.nih.gov/), and GeneCards (https://www.genecards.org/). For siRNA depletion of autophagy genes that showed no effect on Vx3 foci, the knockdown efficiency was tested by monitoring LC3 punctae formation in response to autophagy-inducing stresses (e.g., starvation in HBSS). For other RNAi data that showed no effect on Vx3 foci, mRNA or protein levels will need to be evaluated in future experiments.

	siRNA target	Effect on Vx3 foci	Description
Autophagy	ATG9A	Decrease	phagophore nucleation
	ATG14	None	PI3K complex, autophagy initiation
	ATG16L1	None	LC3 lipidation, phagophore elongation
	FIP200	None	phagophore nucleation, ULK1 complex
	Beclin-1	None	PI3K complex, autophagy initiation
	p62	None	autophagy cargo adaptor, LC3 binding
	NBR1	None	autophagy cargo adaptor, LC3 binding
	VMP1	None	ER contact, autophagosome formation
	WIPI2	Increase	phagophore elongation
	ULK1	None	phagophore nucleation, ULK1 complex
VAMPs	VAMP1	None	synaptic vesicle priming
	VAMP2	None	Golgi to plasma membrane
	VAMP3	None	autophagy, Golgi to plasma membrane
	VAMP4	None	TGN, immature secretory granules
	VAMP5	None	myoblast fusion, GLUT-4 transport
	VAMP7	None	autophagy, lysosome fusion
	VAMP8	None	lysosome fusion
Trafficking	ABCD3	None	transmembrane transporter
	AP2A	Decrease	clathrin adapter
	Myo6	None	motor protein, K63-Ub binding
	RalB	None	GTPase, exocyst assembly
	SNAP25	None	t-SNARE, neurotransmitter release
	STING	None	activation innate immune response
	Stx1a	None	neurotransmitter exocytosis and endocytosis
	Stx16	None	late endosome to TGN
	Stx17	None	autophagosome maturation
	Stx18	None	Golgi to ER
	TBK1	Decrease	serine/threonine kinase, inflammation
	TOLLIP	None	Toll-like receptor
	TRAPPC8	Increase	ER to Golgi, autophagosome assembly
	VPS35	Decrease	retromer core subunit
	WASH1	Decrease	Arp2/3 activation

Table 5: RNAi screen to identify Ub enzymes involved in Vx3 foci formation. List of siRNA targets against E2 Ub conjugating enzymes (E2s), E3 Ub ligases (E3s), and deubiquitinating enzymes (DUBs) used to investigate effect on Vx3 foci formation upon their loss. General protein descriptions were written based on information available in the databases UniProt (https://www.uniprot.org/), NCBI (https://www.ncbi.nlm.nih.gov/), and GeneCards (https://www.genecards.org/). Similar to Table 4, efficiency of siRNA-mediated depletion experiments showing no effect on Vx3 foci must be tested by monitoring mRNA or protein levels of the target genes.

	siRNA target	Effect on Vx3 foci	Description
E2s	UBE2N	Partial decrease	K63-polyUb, DNA repair
	UBE2O	Decrease	E2/E3 hybrid ubiquitin-protein ligase
	UBE2V1	None	K63-polyUb, heterodimer with UBE2N
E3s	AMFR	None	ERAD, proteasome degradation
	GAN	None	Cytoskeleton organization
	HECW1	None	Nedd4 family, DVL1 and SOD1 Ub
	NEDD4	Increase	Nedd4 family, K63-polyUb, endocytosis
	NEDD4L	Decrease	Nedd4 family, plasma membrane Ub
	TRAF6	None	K63-polyUb, complex with UBE2N
DUBs	USP33	None	Autophagosome formation
	USP7	Decrease	WASH1 function
	USP8	Increase	MVB/ESCRT pathway
	USP9x	Decrease	Autophagy, axonal growth

Chapter 4: Conclusions

Several lines of evidence have implicated K63-polyUb in regulating various aspects of membrane trafficking such as endocytosis of cell surface receptors, budding of viral proteins, and autophagy of damaged organelles and invading pathogens. Given the functional versatility of the K63-polyUb modification, several decoders (i.e., readers or receptors) must contribute to selection of a subset of K63-polyubiquitinated conjugates to confer the proper function [131]. One of the best characterized roles for K63-polyUb is the endocytic sorting of transmembrane proteins into intraluminal vesicles of maturing endosomes before their lysosomal targeting. The Endosomal Sorting Complex Required for Transport (ESCRT) complexes play a key role in regulating endocytic cargo sorting to degraded or recycled. ESCRT complexes contain multiple Ubiquitin Binding Domains (UBDs) that associate strongly with K63-polyUb [28]. Additionally, in what has appeared to be an alternative route to degradation, K63-polyUb was shown to act as an "eat me" signal recognized by autophagic cargo adaptors in response to various forms of selective autophagy [105]. Further complicating K63-polyUb function is its involvement in trafficking where it does not solely act as a sorting signal; e.g., K63-polyUb promotes conformational changes in proteins (e.g., WASH1 or ULK1) that controls their activation [9,180].

Although K63-polyUb represents the second most abundant polyUb linkage type after K48, until recently only a handful of proteins had been shown to be K63-polyubiquitinated. Our development of tools [133] to capture K63-polyUb in living cells for proteomics studies has helped to identify K63-polyubiquitinated targets, for instance, in response to oxidative stress [181] or DNA double-strand breaks [182]. K63-polyUb plays a major role in targeting endocytic cargo for sorting into MVBs. However, the proteins actually modified in this pathway is mostly unknown, as most of

the studies of Ub-dependent endocytosis in mammalian cells have employed EGFR as a model substrate.

Using Vx3 as a high-affinity probe to isolate K63-polyubiqutinated conjugates, our mass spectrometry analyses identify an extensive list of proteins (> 5,000) that are potentially modified by K63-polyUb. The complexity of this dataset may be unavoidably exacerbated by the use of non-fully denaturing conditions for Vx3 immunoprecipitation. Although we employed stringent purification protocols based on RIPA buffer containing NP-40 and sodium deoxycholate to eliminate indirect interactions with Vx3, a large number of co-purified partners interacting indirectly with K63-polyubiquitinated proteins may also exist.

The vast majority of proteins identified in our proteomics studies comprises transmembrane proteins that are continually endocytosed and recycled to the cell surface (**Tables 2-3A**). We showed that the prototypical recycling cell surface receptor TfR enriched in the foci is directly modified by K63-polyUb. K63-polyUb might be conjugated to two distinct sets of proteins: endocytic or autophagic cargo, which K63-polyUb may mark for lysosomal targeting, and proteins that depend on K63-polyUb modification to regulate membrane trafficking of cargo. Indeed, our proteomics analyses also identified several factors known to drive membrane trafficking processes; these included: caveolae components, which are associated with plasma membrane microdomains enriched in cholesterol and sphingolipids; SNARE proteins of the VAMP and Syntaxin families, which mediate membrane fusion events; and ARFs or SCAMPs, which regulate post-Golgi membrane protein trafficking. A likely and particularly exciting possibility is that these factors are regulated via specific polyUb-mediated signaling. Examples of concomitant ubiquitination of endocytic cargo and machineries involved in their internalization and sorting (e.g., epsins and Hrs, respectively) have already been described for EGFR endocytosis [183]. Future studies can screen

individual components identified in our analyses by using methods such as immunofluorescence and live-cell imaging to evaluate subcellular localization, and siRNA-mediated knockdown experiments to determine whether their depletion causes trafficking defects of *bona fide* K63-polyubiquitinated cargo. Additionally, future strategies may employ differential density-gradient centrifugation of cell extracts to isolate the membrane fractions associated with Vx3 before performing immunoisolation of K63-polyUb-conjugates for proteomics or biochemical analyses. Analyzing Vx3 vesicles directly may help to avoid the ambiguity of whether the identified hits are cargo associated with Vx3 that is diffused in the cell or accumulated in foci. Additionally, enrichment for ubiquitinated peptides after Vx3 pulldown and trypsinization can employ an anti-GG□K specific antibody that recognizes ubiquitination-site peptides [178], thus minimizing secondary interactors.

By using Vx3 as a tool to visualize K63-specific chains in cells, we discovered that cytoplasmic Vx3 compartments are enriched in K63-polyubiquitinated plasma membrane proteins colocalizing with markers of autophagy and late endosomes. Based on our observations, Vx3 foci may represent an intermediate stage of a transmembrane protein degradation pathway, where both endocytic and autophagy membrane coalesce, at a stage prior to lysosome fusion. We have uncovered three important features of this pathway: 1) the identity of K63-polyubiquitinated cargo; 2) the membrane origin of K63-polyubiquitinated cargo; 3) the final destination of K63-polyubiquitinated cargo. Some aspects of these discoveries are summarized below.

As previously described, most of the proteins identified by mass spectrometry and potentially modified by K63-polyUb appear to be transmembrane proteins known to localize at the cell surface. For many of the identified cargo proteins, their intracellular trafficking has been extensively characterize. This is the case for TfR, a prototypical recycling protein that cycles

between the plasma membrane and the endosomal recycling system. We showed that TfR is a *bona fide* K63-polyubiquitinated cargo. We reveal that it reaches Vx3 foci through an endocytic pathway that originates at the plasma membrane. Live-imaging experiments were able to track the origin of TfR by labeling the receptor at the plasma membrane and following its endocytic itinerary to the Vx3 foci. Only a small population of intracellular TfR is marked by Vx3; these structures contain late endosome markers but not recycling endosome markers, suggestive of degradative compartments. One prominent protein found to accumulate in Vx3 foci is ATG9A, the sole transmembrane core ATG protein, which plays an essential role during autophagy, most likely by delivering lipids or components necessary for the autophagosome growth. Our study shows that ATG9A is related to K63-polyUb, as its depletion lead to the near complete reduction of Vx3 foci. Superresolution microscopy indicated that ATG9A-positive vesicles do not coincide exactly with K63-polyUb, but rather are found juxtaposed to Vx3, suggesting that ATG9A is not itself modified by K63-polyUb. CLEM of Vx3 foci showed that they correspond to heterogeneous clusters of vesicles where endocytic and autophagic elements converge. We propose that Vx3 foci may represent an intermediate stage of transmembrane protein trafficking that is *en route* to the lysosome. Consistently, our fluorescence and electron microscopy data show that Vx3 structures are often in close proximity to endolysosomes. By using a system to inducibly disable Vx3 inhibition, we studied processes mediated by K63-polyUb immediately past the block from Vx3. We provide evidence that K63-polyubiquitinated cargo released by Vx3 is targeted to the highly acidic and degradative lysosomal compartments. We also report that perturbation of lysosomal degradation of membrane proteins via the MVB pathway leads to accumulation of K63-polyubiquinated cargo into Vx3 foci, as observed upon knockdown of USP8 or overexpression of retroCHMP3, a fragment of CHMP3 that competes for ESCRT-III function.

These data support a model (**Fig 4**) in which, by tightly binding to K63-polyUb, Vx3 prevents lysosomal targeting of cell surface proteins that traffic intracellularly via the endosomal system. We propose that Vx3 accumulates cargo destined for degradation via the MVBs, most likely by directly competing with ESCRT proteins for binding to K63-polyUb. This block is likely to provoke the re-routing of K63-polyubiquitinated cargo to an alternative lysosomal proteolysis that employs machinery from selective autophagy. The presence of ATG9A, p62 (also known as SQSTM1), an autophagy cargo adaptor known to bind K63-polyUb, and the autophagic membrane protein LC3 supports the idea that K63-polyubiquitinated cargo diverted from the MVB pathway is destined to an autophagic compartment. However, it is not yet known if the delivery of K63-polyubiquitinated proteins (e.g. TfR) into lysosomes requires additional autophagy machinery.

Previous work demonstrated the appearance of p62-inclusions containing Ub and a mixture of endocytic and autophagic compartments in HeLa cells depleted for ESCRT components or overexpressing CHMP2B[Intron5], a mutant that disrupts ESCRT-III activity [124]. The ESCRTs dysfunction was proposed to inhibit autophagic degradation and lead to formation of large aggregates that eventually might promote neurodegenerative disease [124]. Our results are consistent with these observations of defective autophago-lysosomal degradation of K63-polyubiquitinated cargo. Future work will be needed to test the dispensability of autophagy genes during the K63-polyUb-dependent trafficking of cargo to the lysosome by, for example, tracking delivery of TfR downstream of Vx3 in HeLa cells that are knocked-down for LC3 or other autophagic components.

Endocytosis and autophagy are the main proteolytic pathways for degradation of transmembrane proteins. Although K63-polyUb serves as a common signal for the lysosomal targeting of transmembrane proteins, how cellular K63-polyUb conjugates are differentially recognized by protein effectors to direct their trafficking through either system is not completely understood.

Important factors providing the basis for Ub binding specificity of protein adaptors are Ub linkage-types and Ub chain length [12]. Either feature might promote avidity to enhance UBD-mediated binding to ubiquitinated cargo. Protein homo- or hetero-oligomerization might also boost multivalent recognition of polyUb, as reported for ESCRTs and autophagic cargo receptors. As discussed above, many endocytic proteins contain UIMs. The cooperative binding of the ESCRT-0 proteins Hrs and STAM has been postulated to enhance binding avidity and specificity towards K63-polyubiquitinated transmembrane proteins [28,47]. Moreover, the presence of multiple UIMs within the same protein (e.g., Eps15) could also promote high affinity interaction between endocytic adaptors and ubiquitinated cargo [183]. Finally, an additional feature contributing to binding specificity might be provided by the particular membrane lipid composition of different organelles, as observed in the case of the Hrs interaction with membrane phospholipids (i.e., PI3P) through its FYVE-domain [184]. Endocytic cargo are typically marked by K63-polyUb and recognized by multiple low-affinity UBDs contained within ESCRT components [28]. On the other hand, Ub recognition in selective autophagy of ubiquitinated aggregated proteins seems to be achieved by the ability of p62 to form oligomers with NBR1 and interact with K63-polyUb [104]. Our model supports that K63-polyUb conjugated onto transmembrane protein cargo is preferentially recognized by UBDs contained within ESCRT components, and that competitive inhibition by Vx3 diverts K63-polyubiquitinated cargo to an alternative lysosomal pathway, which is likely dependent on dual recognition of autophagy proteins and cargo polyUb by autophagic adaptors.

Another important aspect of our study is the discovery that cellular compartments enriched for K63-polyUb require the retromer–WASH supercomplex for their formation. Our RNAi experiments showed that the absence of either VPS35, a retromer core subunit, or WASH1, a

subunit of the WASH complex, reduced formation of Vx3 foci. ATG9A depletion also leads to the disappearance of Vx3 foci. Furthermore, ATG9A function is required to maintain general recycling of transmembrane proteins, such as TfR or CI-M6PR, a prototypical retromer cargo. These data suggest a functional relationship between ATG9A and the retromer, which has not been appreciated before. We propose a model in which the Vx3-mediated block of ESCRT function leads to the re-routing of the K63-polyubiquitinated cargo to a sorting pathway that is dependent on both the retromer and ATG9A. We hypothesize that ATG9A may function in concert with the retromer–WASH complex to concentrate K63-polyubiquitinated cargo within endosomal subdomains before being pinched-off into distinct vesicles. ATG9A itself has been implicated as a retromer cargo. Moreover, retromer dysfunction has been shown to impair autophagy. Therefore, it is tempting to speculate that K63-polyUb-decorated vesicles that pinch off of the maturing endosome then traffic toward an autophagy-related compartment before being delivered to the lysosome (**Fig 4**).

Whereas the ESCRT complex sorts ubiquitinated cargo into the MVB pathway for lysosomal degradation, the retromer–WASH supercomplex normally retrieves cargo for transport to the Golgi or plasma membrane. Although these two pathways have opposite functions, they occur along the limiting membrane of the same maturing endosome. Therefore, they must be highly regulated and coordinated. Unanticipated and emerging functions of K63-polyUb have been recently linked to transmembrane protein recycling [131,173]. USP8, a non-selective DUB, and AMSH, a K63-polyUb-specific DUB, have been implicated in promoting degradation of EGFR by removal of Ub chains before cargo is incorporated into late multivesicular endosomes as intraluminal vesicles [28]. However, the activities of these DUBs against other K63-polyUb-conjugates has not been broadly assessed. Besides its function in regulating EGFR degradation,

loss of USP8 has been shown to alter cellular distribution of the retromer cargo CI-M6PR, indicating a recycling defect [185]. USP8 deubiquitinates the ESCRT-0 protein Hrs, thereby controlling its stability. This function could provide a link with the retromer-dependent pathway. Hrs has been indeed shown to interact with the retromer component VPS35 and is required for retromer-dependent transport of the B subunit of Shiga Toxin [185]. Importantly, a recent study shows that Hrs regulates recruitment of WASH1 to facilitate the retrieval of endocytic cargo via an actin-dependent transport [186].

Our study places K63-polyUb and autophagic machinery as central regulators of cargo delivery at the sorting endosome. This pathway may potentially be important as part of an innate immunity response used for antimicrobial defense. After scission from the host cell membrane, the sequential fusion of a bacterium-containing phagosome with both sorting endosomes and late endosomes enables the gradual acquisition of membrane elements and the acidic pH necessary for the bacterial clearance by the host cell. In macrophages, invading pathogens such as *Mycobacterium tuberculosis* are capable of modifying phagosomes to resemble early/recycling endosomes, allowing the bacteria to escape destruction, continue their replication, and perpetuate the infection [188]. Thus, autophagy may promote remodeling of the phagosomal membrane and its proteins, thereby facilitating the progression into a lytic and bactericidal membrane compartments. Finally, understanding how autophagy regulates cargo sorting and recycling of phagosomal proteins in response to bacterial infection could be critical to design therapeutic interventions aimed at enhancing innate immunity in host cells.
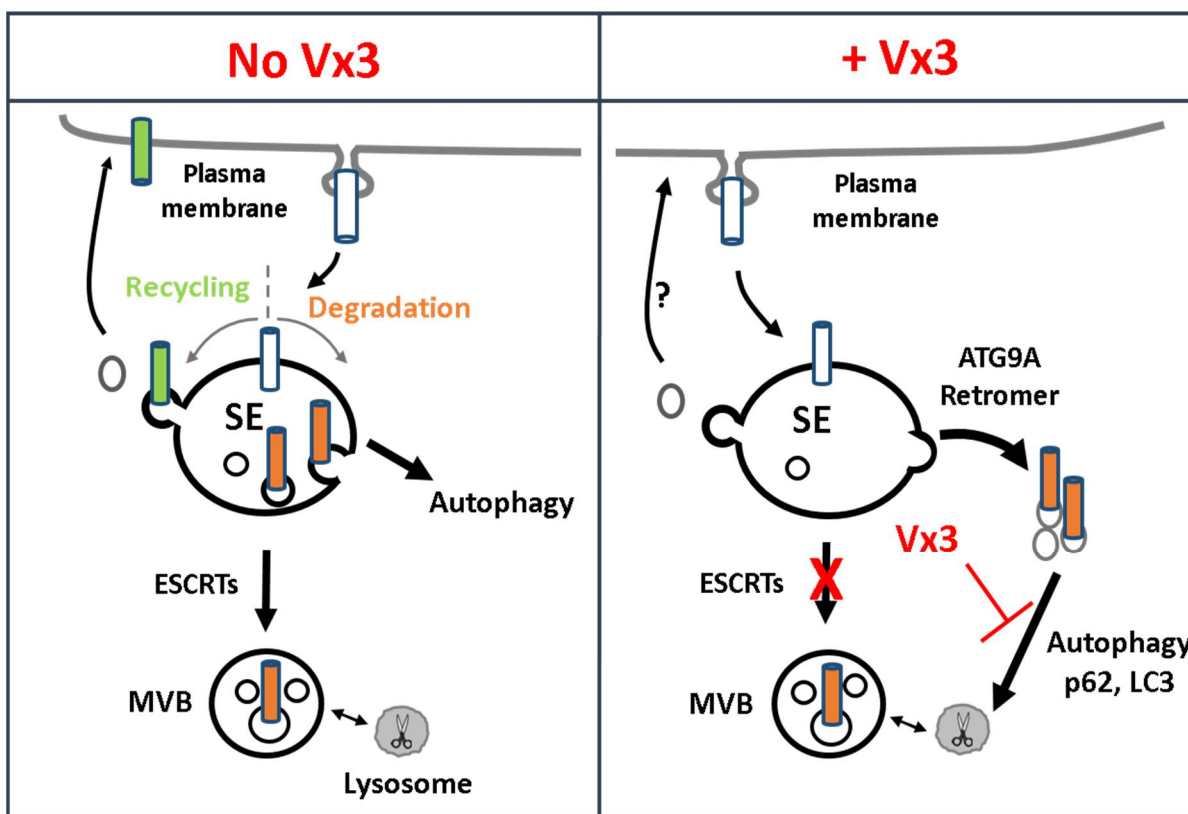
Figure 4: Model for Vx3-mediated re-routing of K63-polyubiquitinated cargo from the MVB pathway to an autophagic compartment. <u>Left panel:</u> In general, endocytosed plasma membrane proteins (*black*) are either K63-polyubiquitinated (Ub chain shown in *light blue*) to become degradative cargo destined for the ESCRTs–MVB pathway (MVB-cargo, *yellow*), or recognized by the retromer–WASH supercomplex (retromer-cargo, *green*) for their retrieval. <u>Right panel:</u> The presence of Vx3 accumulates cargo destined for degradation via the MVBs (MVB-cargo, *yellow*), most likely by directly competing with ESCRTs for binding to K63-polyUb (Ub chain shown in *light blue*). This block is likely to provoke the re-routing of K63-polyubiquitinated cargo (MVB-cargo, *yellow*) to an alternative lysosomal proteolysis that employs machinery from selective autophagy: ATG9A, p62 (also known as SQSTM1), and the autophagic membrane protein LC3. The retromer–WASH supercomplex may facilitate the pinching off of K63-polyubiquitinated cargo into discrete vesicles for their subsequent autophagic targeting. By tightly binding to K63-polyUb, we hypothesize that Vx3 interferes with both degradative systems: the MVB pathway and autophagy. SE= sorting endosome.

References:

1   Pickart, C. M. Mechanisms underlying ubiquitination. *Annual Review of Biochemistry* **70**, 503-533, doi:10.1146/annurev.biochem.70.1.503 (2001).

2   Komander, D. & Rape, M. The Ubiquitin Code. *Annual Review of Biochemistry, Vol 81* **81**, 203-229, doi:10.1146/annurev-biochem-060310-170328 (2012).

3   Peng, J. M. *et al.* A proteomics approach to understanding protein ubiquitination. *Nature Biotechnology* **21**, 921-926, doi:10.1038/nbt849 (2003).

4   Xu, P. *et al.* Quantitative Proteomics Reveals the Function of Unconventional Ubiquitin Chains in Proteasomal Degradation. *Cell* **137**, 133-145, doi:10.1016/j.cell.2009.01.041 (2009).

5   Pickart, C. M. & Fushman, D. Polyubiquitin chains: polymeric protein signals. *Current Opinion in Chemical Biology* **8**, 610-616, doi:10.1016/j.cbpa.2004.09.009 (2004).

6   Metzger, M. B., Hristova, V. A. & Weissman, A. M. HECT and RING finger families of E3 ubiquitin ligases at a glance. *Journal of Cell Science* **125**, 531-537, doi:10.1242/jcs.091777 (2012).

7   Ye, Y. H. & Rape, M. Building ubiquitin chains: E2 enzymes at work. *Nature Reviews Molecular Cell Biology* **10**, 755-764, doi:10.1038/nrm2780 (2009).

8   Zhang, X. F. *et al.* Fine-tuning BMP7 signalling in adipogenesis by UBE2O/E2-230K-mediated monoubiquitination of SMAD6. *Embo Journal* **32**, 996-1007, doi:10.1038/emboj.2013.38 (2013).

9   Hao, Y. H. *et al.* Regulation of WASH-Dependent Actin Polymerization and Protein Trafficking by Ubiquitination. *Cell* **152**, 1051-1064, doi:10.1016/j.cell.2013.01.051 (2013).

10   Clague, M. J., Urbe, S. & Komander, D. Breaking the chains: deubiquitylating enzyme specificity begets function. *Nature Reviews Molecular Cell Biology* **20**, 338-352, doi:10.1038/s41580-019-0099-1 (2019).

11   Pickart, C. M. Back to the future with ubiquitin. *Cell* **116**, 181-190, doi:10.1016/s0092-8674(03)01074-2 (2004).

12   Husnjak, K. & Dikic, I. Ubiquitin-Binding Proteins: Decoders of Ubiquitin-Mediated Cellular Functions. *Annual Review of Biochemistry, Vol 81* **81**, 291-322, doi:10.1146/annurev-biochem-051810-094654 (2012).

13   Sims, J. J. & Cohen, R. E. Linkage-Specific Avidity Defines the Lysine 63-Linked Polyubiquitin-Binding Preference of Rap80. *Molecular Cell* **33**, 775-783, doi:10.1016/j.molcel.2009.02.011 (2009).

14   Levine, B. & Kroemer, G. Biological Functions of Autophagy Genes: A Disease Perspective. *Cell* **176**, 11-42, doi:10.1016/j.cell.2018.09.048 (2019).

15 Grumati, P. & Dikic, I. Ubiquitin signaling and autophagy. *Journal of Biological Chemistry* **293**, 5404-5413, doi:10.1074/jbc.TM117.000117 (2018).

16 Clague, M. J. & Urbe, S. Ubiquitin: Same Molecule, Different Degradation Pathways. *Cell* **143**, 682-685, doi:10.1016/j.cell.2010.11.012 (2010).

17 Haglund, K. *et al.* Multiple monoubiquitination of RTKs is sufficient for their endocytosis and degradation. *Nature Cell Biology* **5**, 461-466, doi:10.1038/ncb983 (2003).

18 Huang, F., Goh, L. K. & Sorkin, A. EGF receptor ubiquitination is not necessary for its internalization. *Proceedings of the National Academy of Sciences of the United States of America* **104**, 16904-16909, doi:10.1073/pnas.0707416104 (2007).

19 Sigismund, S. *et al.* Clathrin-independent endocytosis of ubiquitinated cargos. *Proceedings of the National Academy of Sciences of the United States of America* **102**, 2760-2765, doi:10.1073/pnas.0409817102 (2005).

20 Hawryluk, M. J. *et al.* Epsin 1 is a polyubiquitin-selective clathrin-associated sorting protein. *Traffic* **7**, 262-281, doi:10.1111/j.1600-0854.2006.00383.x (2006).

21 Lauwers, E., Jacob, C. & Andre, B. K63-linked ubiquitin chains as a specific signal for protein sorting into the multivesicular body pathway. *Journal of Cell Biology* **185**, 493-502, doi:10.1083/jcb.200810114 (2009).

22   Huang, F. T., Kirkpatrick, D., Jiang, X. J., Gygi, S. & Sorkin, A. Differential regulation of EGF receptor internalization and degradation by multiubiquitination within the kinase domain. *Molecular Cell* **21**, 737-748, doi:10.1016/j.molcel.2006.02.018 (2006).

23   Tsuchiya, H. *et al.* Ub-ProT reveals global length and composition of protein ubiquitylation in cells. *Nature Communications* **9**, doi:10.1038/s41467-018-02869-x (2018).

24   Huang, F. T. *et al.* Lysine 63-linked polyubiquitination is required for EGF receptor degradation. *Proceedings of the National Academy of Sciences of the United States of America* **110**, 15722-15727, doi:10.1073/pnas.1308014110 (2013).

25   Sigismund, S. *et al.* Threshold-controlled ubiquitination of the EGFR directs receptor fate. *Embo Journal* **32**, 2140-2157, doi:10.1038/emboj.2013.149 (2013).

26   Duncan, L. M. *et al.* Lysine-63-linked ubiquitination is required for endolysosomal degradation of class I molecules. *Embo Journal* **25**, 1635-1645, doi:10.1038/sj.emboj.7601056 (2006).

27   Levkowitz, G. *et al.* Ubiquitin ligase activity and tyrosine phosphorylation underlie suppression of growth factor signaling by c-Cbl/Sli-1. *Molecular Cell* **4**, 1029-1040, doi:10.1016/s1097-2765(00)80231-2 (1999).

28   Piper, R. C., Dikic, I. & Lukacs, G. L. Ubiquitin-Dependent Sorting in Endocytosis. *Cold Spring Harbor Perspectives in Biology* **6**, doi:10.1101/cshperspect.a016808 (2014).

29   Polo, S. *et al.* A single motif responsible for ubiquitin recognition and monoubiquitination in endocytic proteins. *Nature* **416**, 451-455, doi:10.1038/416451a (2002).

30   Katz, M. *et al.* Ligand-independent degradation of epidermal growth factor receptor involves receptor ubiquitylation and hgs, an adaptor whose ubiquitin-interacting motif targets ubiquitylation by Nedd4. *Traffic* **3**, 740-751, doi:10.1034/j.1600-0854.2002.31006.x (2002).

31   Rotin, D. & Kumar, S. Physiological functions of the HECT family of ubiquitin ligases. *Nature Reviews Molecular Cell Biology* **10**, 398-409, doi:10.1038/nrm2690 (2009).

32   Belgareh-Touze, N. *et al.* Versatile role of the yeast ubiquitin ligase Rsp5p in intracellular trafficking. *Biochemical Society Transactions* **36**, 791-796, doi:10.1042/bst0360791 (2008).

33   Boase, N. A. & Kumar, S. NEDD4: The founding member of a family of ubiquitin-protein ligases. *Gene* **557**, 113-122, doi:10.1016/j.gene.2014.12.020 (2015).

34   Goel, P., Manning, J. A. & Kumar, S. NEDD4-2 (NEDD4L): The ubiquitin ligase for multiple membrane proteins. *Gene* **557**, 1-10, doi:10.1016/j.gene.2014.11.051 (2015).

35   Pizzirusso, M. & Chang, A. Ubiquitin-mediated targeting of a mutant plasma membrane ATPase, Pma1-7, to the endosomal/vacuolar system in yeast. *Molecular Biology of the Cell* **15**, 2401-2409, doi:10.1091/mbc.E03-10-0727 (2004).

36   Wang, S. Y., Thibault, G. & Ng, D. T. W. Routing Misfolded Proteins through the

        Multivesicular Body (MVB) Pathway Protects against Proteotoxicity. *Journal of*

        Biological Chemistry **286**, 29376-29387, doi:10.1074/jbc.M111.233346 (2011).

37   Zhao, Y. Y., MacGurn, J. A., Liu, M. & Emr, S. The ART-Rsp5 ubiquitin ligase network

        comprises a plasma membrane quality control system that protects yeast cells from

        proteotoxic stress. *Elife* **2**, doi:10.7554/eLife.00459 (2013).

38   MacGurn, J. A., Hsu, P. C. & Emr, S. D. Ubiquitin and Membrane Protein Turnover:

        From Cradle to Grave. *Annual Review of Biochemistry, Vol 81* **81**, 231-259,

        doi:10.1146/annurev-biochem-060210-093619 (2012).

39   Okiyoneda, T., Apaja, P. M. & Lukacs, G. L. Protein quality control at the plasma

        membrane. *Current Opinion in Cell Biology* **23**, 483-491, doi:10.1016/j.ceb.2011.04.012

        (2011).

40   Okiyoneda, T. *et al.* Peripheral Protein Quality Control Removes Unfolded CFTR from

        the Plasma Membrane. *Science* **329**, 805-810, doi:10.1126/science.1191542 (2010).

41   Okiyoneda, T. *et al.* Chaperone-Independent Peripheral Quality Control of CFTR by

        RFFL E3 Ligase. *Developmental Cell* **44**, 694-+, doi:10.1016/j.devcel.2018.02.001

        (2018).

42   Caohuy, H., Jozwik, C. & Pollard, H. B. Rescue of Delta F508-CFTR by the

        SGK1/Nedd4-2 Signaling Pathway. *Journal of Biological Chemistry* **284**, 25241-25253,

        doi:10.1074/jbc.M109.035345 (2009).

43 Hurley, J. H. ESCRTs are everywhere. *Embo Journal* **34**, 2398-2407, doi:10.15252/embj.201592484 (2015).

44 Kutateladze, T. G. *et al.* Phosphatidylinositol 3-phosphate recognition by the FYVE domain. *Molecular Cell* **3**, 805-811, doi:10.1016/s1097-2765(01)80013-7 (1999).

45 Bilodeau, P. S., Winistorfer, S. C., Kearney, W. R., Robertson, A. D. & Piper, R. C. Vps27-Hse1 and ESCRT-I complexes cooperate to increase efficiency of sorting ubiquitinated proteins at the endosome. *Journal of Cell Biology* **163**, 237-243, doi:10.1083/jcb.200305007 (2003).

46 Mizuno, E., Kawahata, K., Kato, M., Kitamura, N. & Komada, M. STAM proteins bind ubiquitinated proteins on the early endosome via the VHS domain and ubiquitin-interacting motif. *Molecular Biology of the Cell* **14**, 3675-3689, doi:10.1091/mbc.E02-12-0823 (2003).

47 Shields, S. B. & Piper, R. C. How Ubiquitin Functions with ESCRTs. *Traffic* **12**, 1306-1317, doi:10.1111/j.1600-0854.2011.01242.x (2011).

48 Raiborg, C., Bache, K. G., Mehlum, A., Stang, E. & Stenmark, H. Hrs recruits clathrin to early endosomes. *Embo Journal* **20**, 5008-5021, doi:10.1093/emboj/20.17.5008 (2001).

49 Raiborg, C. *et al.* Hrs sorts ubiquitinated proteins into clathrin-coated microdomains of early endosomes. *Nature Cell Biology* **4**, 394-398, doi:10.1038/ncb791 (2002).

50 Lu, Q., Hope, L. W. Q., Brasch, M., Reinhard, C. & Cohen, S. N. TSG101 interaction with HRS mediates endosomal trafficking and receptor down-regulation. *Proceedings of*

the National Academy of Sciences of the United States of America **100**, 7626-7631, doi:10.1073/pnas.0932599100 (2003).

51   Niendorf, S. *et al.* Essential role of ubiquitin-specific protease 8 for receptor tyrosine kinase stability and endocytic trafficking in vivo. *Molecular and Cellular Biology* **27**, 5029-5039, doi:10.1128/mcb.01566-06 (2007).

52   Wright, M. H., Berlin, I. & Nash, P. D. Regulation of Endocytic Sorting by ESCRT-DUB-Mediated Deubiquitination. *Cell Biochemistry and Biophysics* **60**, 39-46, doi:10.1007/s12013-011-9181-9 (2011).

53   Crespo-Yanez, X. *et al.* CHMP1B is a target of USP8/UBPY regulated by ubiquitin during endocytosis. *Plos Genetics* **14**, doi:10.1371/journal.pgen.1007456 (2018).

54   van Ijzendoorn, S. C. D. Recycling endosomes. *Journal of Cell Science* **119**, 1679-1681, doi:10.1242/jcs.02948 (2006).

55   Peschard, P. & Park, M. Escape from Cbl-mediated downregulation: A recurrent theme for oncogenic deregulation of receptor tyrosine kinases. *Cancer Cell* **3**, 519-523, doi:10.1016/s1535-6108(03)00136-3 (2003).

56   Cullen, P. J. & Steinberg, F. To degrade or not to degrade: mechanisms and significance of endocytic recycling. *Nature Reviews Molecular Cell Biology* **19**, 679-696, doi:10.1038/s41580-018-0053-7 (2018).

57   Burd, C. & Cullen, P. J. Retromer: A Master Conductor of Endosome Sorting. *Cold Spring Harbor Perspectives in Biology* **6**, doi:10.1101/cshperspect.a016774 (2014).

122

58   Gallon, M. & Cullen, P. J. Retromer and sorting nexins in endosomal sorting. *Biochemical Society Transactions* **43**, 33-47, doi:10.1042/bst20140290 (2015).

59   Rojas, R. *et al.* Regulation of retromer recruitment to endosomes by sequential action of Rab5 and Rab7. *Journal of Cell Biology* **183**, 513-526, doi:10.1083/jcb.200804048 (2008).

60   Seaman, M. N. J., Harbour, M. E., Tattersall, D., Read, E. & Bright, N. Membrane recruitment of the cargo-selective retromer subcomplex is catalysed by the small GTPase Rab7 and inhibited by the Rab-GAP TBC1D5. *Journal of Cell Science* **122**, 2371-2382, doi:10.1242/jcs.048686 (2009).

61   Harrison, M. S. *et al.* A mechanism for retromer endosomal coat complex assembly with cargo. *Proceedings of the National Academy of Sciences of the United States of America* **111**, 267-272, doi:10.1073/pnas.1316482111 (2014).

62   Seaman, M. N. J., Mukadam, A. S. & Breusegem, S. Y. Inhibition of TBC1D5 activates Rab7a and can enhance the function of the retromer cargo-selective complex. *Journal of Cell Science* **131**, doi:10.1242/jcs.217398 (2018).

63   Harbour, M. E. *et al.* The cargo-selective retromer complex is a recruiting hub for protein complexes that regulate endosomal tubule dynamics. *Journal of Cell Science* **123**, 3703-3717, doi:10.1242/jcs.071472 (2010).

64   Harbour, M. E., Breusegem, S. Y. & Seaman, M. N. J. Recruitment of the endosomal WASH complex is mediated by the extended 'tail' of Fam21 binding to the retromer protein Vps35. *Biochemical Journal* **442**, 209-220, doi:10.1042/bj20111761 (2012).

65   Jia, D., Gomez, T. S., Billadeau, D. D. & Rosen, M. K. Multiple repeat elements within the FAM21 tail link the WASH actin regulatory complex to the retromer. *Molecular Biology of the Cell* **23**, 2352-2361, doi:10.1091/mbc.E11-12-1059 (2012).

66   Derivery, E. *et al.* The Arp2/3 Activator WASH Controls the Fission of Endosomes through a Large Multiprotein Complex. *Developmental Cell* **17**, 712-723, doi:10.1016/j.devcel.2009.09.010 (2009).

67   Puthenveedu, M. A. *et al.* Sequence-Dependent Sorting of Recycling Proteins by Actin-Stabilized Endosomal Microdomains. *Cell* **143**, 761-773, doi:10.1016/j.cell.2010.10.003 (2010).

68   Zech, T. *et al.* The Arp2/3 activator WASH regulates alpha 5 beta 1-integrin-mediated invasive migration. *Journal of Cell Science* **124**, 3753-3759, doi:10.1242/jcs.080986 (2011).

69   Harterink, M. *et al.* A SNX3-dependent retromer pathway mediates retrograde transport of the Wnt sorting receptor Wntless and is required for Wnt secretion. *Nature Cell Biology* **13**, 914-U358, doi:10.1038/ncb2281 (2011).

70   Zhang, P., Wu, Y. H., Belenkaya, T. Y. & Lin, X. H. SNX3 controls Wingless/Wnt secretion through regulating retromer-dependent recycling of Wntless. *Cell Research* **21**, 1677-1690, doi:10.1038/cr.2011.167 (2011).

71   Chen, C. Y. *et al.* SNX3 REGULATES RECYCLING OF THE TRANSFERRIN RECEPTOR AND IRON ASSIMILATION. *American Journal of Hematology* **88**, E27-E28 (2013).

72   Zavodszky, E. *et al.* Mutation in VPS35 associated with Parkinson's disease impairs WASH complex association and inhibits autophagy. *Nature Communications* **5**, doi:10.1038/ncomms4828 (2014).

73   Jimenez-Orgaz, A. *et al.* Control of RAB7 activity and localization through the retromer-TBC1D5 complex enables RAB7-dependent mitophagy. *Embo Journal* **37**, 235-254, doi:10.15252/embj.201797128 (2018).

74   He, C. C. & Klionsky, D. J. Regulation Mechanisms and Signaling Pathways of Autophagy. *Annual Review of Genetics* **43**, 67-93, doi:10.1146/annurev-genet-102808-114910 (2009).

75   Cadwell, K. Crosstalk between autophagy and inflammatory signalling pathways: balancing defence and homeostasis. *Nature Reviews Immunology* **16**, 661-675, doi:10.1038/nri.2016.100 (2016).

76   Yang, Z. F. & Klionsky, D. J. Mammalian autophagy: core molecular machinery and signaling regulation. *Current Opinion in Cell Biology* **22**, 124-131, doi:10.1016/j.ceb.2009.11.014 (2010).

77   Jewell, J. L., Russell, R. C. & Guan, K. L. Amino acid signalling upstream of mTOR. *Nature Reviews Molecular Cell Biology* **14**, 133-139, doi:10.1038/nrm3522 (2013).

78   Noda, T. & Ohsumi, Y. Tor, a phosphatidylinositol kinase homologue, controls autophagy in yeast. *Journal of Biological Chemistry* **273**, 3963-3966, doi:10.1074/jbc.273.7.3963 (1998).

79   Lamb, C. A., Yoshimori, T. & Tooze, S. A. The autophagosome: origins unknown, biogenesis complex. *Nature Reviews Molecular Cell Biology* **14**, 759-774, doi:10.1038/nrm3696 (2013).

80   Russell, R. C. *et al.* ULK1 induces autophagy by phosphorylating Beclin-1 and activating VPS34 lipid kinase. *Nature Cell Biology* **15**, 741-+, doi:10.1038/ncb2757 (2013).

81   Kang, R., Zeh, H. J., Lotze, M. T. & Tang, D. The Beclin 1 network regulates autophagy and apoptosis. *Cell Death and Differentiation* **18**, 571-580, doi:10.1038/cdd.2010.191 (2011).

82   Dooley, H. C. *et al.* WIPI2 Links LC3 Conjugation with PI3P, Autophagosome Formation, and Pathogen Clearance by Recruiting Atg12-5-16L1. *Molecular Cell* **55**, 238-252, doi:10.1016/j.molcel.2014.05.021 (2014).

83   Proikas-Cezanne, T., Takacs, Z., Donnes, P. & Kohlbacher, O. WIPI proteins: essential PtdIns3P effectors at the nascent autophagosome. *Journal of Cell Science* **128**, 207-217, doi:10.1242/jcs.146258 (2015).

84   Ichimura, Y. *et al.* A ubiquitin-like system mediates protein lipidation. *Nature* **408**, 488-492, doi:10.1038/35044114 (2000).

85   Mizushima, N. *et al.* A protein conjugation system essential for autophagy. *Nature* **395**, 395-398, doi:10.1038/26506 (1998).

86   Kabeya, Y. *et al.* LC3, a mammalian homologue of yeast Apg8p, is localized in autophagosome membranes after processing. *Embo Journal* **19**, 5720-5728, doi:10.1093/emboj/19.21.5720 (2000).

87   Saitoh, T. *et al.* Atg9a controls dsDNA-driven dynamic translocation of STING and the innate immune response. *Proceedings of the National Academy of Sciences of the United States of America* **106**, 20842-20846, doi:10.1073/pnas.0911267106 (2009).

88   Kageyama, S. *et al.* The LC3 recruitment mechanism is separate from Atg9L1-dependent membrane formation in the autophagic response against Salmonella. *Molecular Biology of the Cell* **22**, 2290-2300, doi:10.1091/mbc.E10-11-0893 (2011).

89   Orsi, A. *et al.* Dynamic and transient interactions of Atg9 with autophagosomes, but not membrane integration, are required for autophagy. *Molecular Biology of the Cell* **23**, 1860-1873, doi:10.1091/mbc.E11-09-0746 (2012).

90   Young, A. R. J. *et al.* Starvation and ULK1-dependent cycling of mammalian Atg9 between the TGN and endosomes. *Journal of Cell Science* **119**, 3888-3900, doi:10.1242/jcs.03172 (2006).

91   Kotani, T., Kirisako, H., Koizumi, M., Ohsumi, Y. & Nakatogawa, H. The Atg2-Atg18 complex tethers pre-autophagosomal membranes to the endoplasmic reticulum for autophagosome formation. *Proceedings of the National Academy of Sciences of the United States of America* **115**, 10363-10368, doi:10.1073/pnas.1806727115 (2018).

92   Gomez-Sanchez, R. *et al.* Atg9 establishes Atg2-dependent contact sites between the endoplasmic reticulum and phagophores. *Journal of Cell Biology* **217**, 2743-2763, doi:10.1083/jcb.201710116 (2018).

93   Molejon, M. I. *et al.* The VMP1-Beclin 1 Interaction Regulates Autophagy Induction. *Faseb Journal* **27** (2013).

94   Tabora, L. C. & Escalante, R. VMP1 Establishes ER-Microdomains that Regulate Membrane Contact Sites and Autophagy. *Plos One* **11**, doi:10.1371/journal.pone.0166499 (2016).

95   Nascimbeni, A. C. *et al.* ER-plasma membrane contact sites contribute to autophagosome biogenesis by regulation of local PI3P synthesis. *Embo Journal* **36**, 2018-2033, doi:10.15252/embj.201797006 (2017).

96   Zhao, Y. G. *et al.* The ER-Localized Transmembrane Protein EPG-3/VMP1 Regulates

        SERCA Activity to Control ER-Isolation Membrane Contacts for Autophagosome

        Formation. *Molecular Cell* **67**, 974-+, doi:10.1016/j.molcel.2017.08.005 (2017).

97   Reggiori, F. & Ungermann, C. Autophagosome Maturation and Fusion. *Journal of*

        Molecular Biology **429**, 486-496, doi:10.1016/j.jmb.2017.01.002 (2017).

98   Itakura, E., Kishi-Itakura, C. & Mizushima, N. The Hairpin-type Tail-Anchored SNARE

        Syntaxin 17 Targets to Autophagosomes for Fusion with Endosomes/Lysosomes. *Cell*

        151, 1256-1269, doi:10.1016/j.cell.2012.11.001 (2012).

99   Takats, S. *et al.* Interaction of the HOPS complex with Syntaxin 17 mediates

        autophagosome clearance in Drosophila. *Molecular Biology of the Cell* **25**, 1338-1354,

        doi:10.1091/mbc.E13-08-0449 (2014).

100   Hara, T. *et al.* Suppression of basal autophagy in neural cells causes neurodegenerative

        disease in mice. *Nature* **441**, 885-889, doi:10.1038/nature04724 (2006).

101   Komatsu, M. *et al.* Loss of autophagy in the central nervous system causes

        neurodegeneration in mice. *Nature* **441**, 880-884, doi:10.1038/nature04723 (2006).

102   Fujita, N. *et al.* Recruitment of the autophagic machinery to endosomes during infection

        is mediated by ubiquitin. *Journal of Cell Biology* **203**, 115-128,

        doi:10.1083/jcb.201304188 (2013).

103   Shaid, S., Brandts, C. H., Serve, H. & Dikic, I. Ubiquitination and selective autophagy.

        Cell Death and Differentiation **20**, 21-30, doi:10.1038/cdd.2012.72 (2013).

104   Pankiv, S. *et al.* p62/SQSTM1 binds directly to Atg8/LC3 to facilitate degradation of ubiquitinated protein aggregates by autophagy. *Journal of Biological Chemistry* **282**, 24131-24145, doi:10.1074/jbc.M702824200 (2007).

105   Stolz, A., Ernst, A. & Dikic, I. Cargo recognition and trafficking in selective autophagy. *Nature Cell Biology* **16**, 495-501, doi:10.1038/ncb2979 (2014).

106   Lazarou, M. *et al.* The ubiquitin kinase PINK1 recruits autophagy receptors to induce mitophagy. *Nature* **524**, 309-+, doi:10.1038/nature14893 (2015).

107   Seibenhener, M. L. *et al.* Sequestosome 1/p62 is a polyubiquitin chain binding protein involved in ubiquitin proteasome degradation. *Molecular and Cellular Biology* **24**, 8055-8068, doi:10.1128/mcb.24.18.8055-8068.2004 (2004).

108   Long, J. *et al.* Ubiquitin recognition by the ubiquitin-associated domain of p62 involves a novel conformational switch. *Journal of Biological Chemistry* **283**, 5427-5440, doi:10.1074/jbc.M704973200 (2008).

109   Wild, P. *et al.* Phosphorylation of the Autophagy Receptor Optineurin Restricts Salmonella Growth. *Science* **333**, 228-233, doi:10.1126/science.1205405 (2011).

110   Thurston, T. L. M., Wandel, M. P., von Muhlinen, N., Foeglein, A. & Randow, F. Galectin 8 targets damaged vesicles for autophagy to defend cells against bacterial invasion. *Nature* **482**, 414-U1515, doi:10.1038/nature10744 (2012).

111   Falk, M. M. *et al.* Degradation of Endocytosed Gap Junctions by Autophagosomal and Endo-/lysosomal Pathways: A Perspective. *Journal of Membrane Biology* **245**, 465-476, doi:10.1007/s00232-012-9464-0 (2012).

112   Leithe, E. *et al.* Ubiquitylation of the gap junction protein connexin-43 signals its trafficking from early endosomes to lysosomes in a process mediated by Hrs and Tsg101. *Journal of Cell Science* **122**, 3883-3893, doi:10.1242/jcs.053801 (2009).

113   Bejarano, E. *et al.* Autophagy modulates dynamics of connexins at the plasma membrane in a ubiquitin-dependent manner. *Molecular Biology of the Cell* **23**, 2156-2169, doi:10.1091/mbc.E11-10-0844 (2012).

114   Bejarano, E. *et al.* Connexins modulate autophagosome biogenesis. *Nature Cell Biology* **16**, 401-U455, doi:10.1038/ncb2934 (2014).

115   Kells, R. M., Gumpert, A. M., Fong, J. T. & Falk, M. M. Internalized Gap Junctions are Degraded by Autophagy. *Molecular Biology of the Cell* **22** (2011).

116   Kells-Andrews, R. M., Margraf, R. A., Fisher, C. G. & Falk, M. M. Connexin 43 K63-polyubiquitylation on lysines 264 and 303 regulates gap junction internalization. *Journal of Cell Science* **131**, doi:10.1242/jcs.204321 (2018).

117   Tooze, S. A., Abada, A. & Elazar, Z. Endocytosis and Autophagy: Exploitation or Cooperation? *Cold Spring Harbor Perspectives in Biology* **6**, doi:10.1101/cshperspect.a018358 (2014).

118   Longatti, A. *et al.* TBC1D14 regulates autophagosome formation via Rab11-and ULK1-
        positive recycling endosomes. *Journal of Cell Biology* **197**, 659-675,
        doi:10.1083/jcb.201111079 (2012).

119   Puri, C., Renna, M., Bento, C. F., Moreau, K. & Rubinsztein, D. C. Diverse
        Autophagosome Membrane Sources Coalesce in Recycling Endosomes. *Cell* **154**, 1285-
        1299, doi:10.1016/j.cell.2013.08.044 (2013).

120   Puri, C. *et al.* The RAB11A-Positive Compartment Is a Primary Platform for
        Autophagosome Assembly Mediated by WIPI2 Recognition of PI3P-RAB11A.
        Developmental Cell **45**, 114-+, doi:10.1016/j.devcel.2018.03.008 (2018).

121   Rusten, T. E. & Stenmark, H. How do ESCRT proteins control autophagy? *Journal of
        Cell Science* **122**, 2179-2183, doi:10.1242/jcs.050021 (2009).

122   Lee, J. A., Beigneux, A., Ahmad, S. T., Young, S. G. & Gao, F. B. ESCRT-III
        dysfunction causes autophagosome accumulation and neurodegeneration. *Current
        Biology* **17**, 1561-1567, doi:10.1016/j.cub.2007.07.029 (2007).

123   Tamai, K. *et al.* Role of Hrs in maturation of autophagosomes in mammalian cells.
        Biochemical and Biophysical Research Communications **360**, 721-727,
        doi:10.1016/j.bbrc.2007.06.105 (2007).

124   Filimonenko, M. *et al.* Functional multivesicular bodies are required for autophagic
        clearance of protein aggregates associated with neurodegenerative disease. *Journal of Cell
        Biology* **179**, 485-500, doi:10.1083/jcb.200702115 (2007).

125   Fader, C. M. & Colombo, M. I. Autophagy and multivesicular bodies: two closely related partners. *Cell Death and Differentiation* **16**, 70-78, doi:10.1038/cdd.2008.168 (2009).

126   Fader, C. M., Sanchez, D. G., Mestre, M. B. & Colombo, M. I. TI-VAMP/VAMP7 and VAMP3/cellubrevin: two v-SNARE proteins involved in specific steps of the autophagy/multivesicular body pathways. *Biochimica Et Biophysica Acta-Molecular Cell Research* **1793**, 1901-1916, doi:10.1016/j.bbamcr.2009.09.011 (2009).

127   Sahu, R. *et al.* Microautophagy of Cytosolic Proteins by Late Endosomes. *Developmental Cell* **20**, 131-139, doi:10.1016/j.devcel.2010.12.003 (2011).

128   Colombo, M. *et al.* Analysis of ESCRT functions in exosome biogenesis, composition and secretion highlights the heterogeneity of extracellular vesicles. *Journal of Cell Science* **126**, 5553-5565, doi:10.1242/jcs.128868 (2013).

129   Noh, S. H. *et al.* Specific autophagy and ESCRT components participate in the unconventional secretion of CFTR. *Autophagy* **14**, 1761-1778, doi:10.1080/15548627.2018.1489479 (2018).

130   Curwin, A. J. *et al.* ESCRT-III drives the final stages of CUPS maturation for unconventional protein secretion. *Elife* **5**, doi:10.7554/eLife.16299 (2016).

131   Erpapazoglou, Z., Walker, O. & Haguenauer-Tsapis, R. Versatile roles of k63-linked ubiquitin chains in trafficking. *Cells* **3**, 1027-1088, doi:10.3390/cells3041027 (2014).

132   Levine, B. & Kroemer, G. Autophagy in the pathogenesis of disease. *Cell* **132**, 27-42, doi:10.1016/j.cell.2007.12.018 (2008).

133   Sims, J. J. *et al.* Polyubiquitin-sensor proteins reveal localization and linkage-type dependence of cellular ubiquitin signaling. *Nature Methods* **9**, 303-U122, doi:10.1038/nmeth.1888 (2012).

134   Zheng, Y. T. *et al.* The Adaptor Protein p62/SQSTM1 Targets Invading Bacteria to the Autophagy Pathway. *Journal of Immunology* **183**, 5909-5916, doi:10.4049/jimmunol.0900441 (2009).

135   Kimura, S., Noda, T. & Yoshimori, T. Dissection of the autophagosome maturation process by a novel reporter protein, tandem fluorescent-tagged LC3. *Autophagy* **3**, 452-460, doi:10.4161/auto.4451 (2007).

136   Snapp, E. Design and use of fluorescent fusion proteins in cell biology. *Current protocols in cell biology* **Chapter 21**, 21.24.21-21.24.13, doi:10.1002/0471143030.cb2104s27 (2005).

137   McCullough, J., Clague, M. J. & Urbe, S. AMSH is an endosome-associated ubiquitin isopeptidase. *Journal of Cell Biology* **166**, 487-492, doi:10.1083/jcb.200401141 (2004).

138   Ryu, K.-Y., Baker, R. T. & Kopito, R. R. Ubiquitin-specific protease 2 as a tool for quantification of total ubiquitin levels in biological specimens. *Analytical Biochemistry* **353**, 153-155, doi:10.1016/j.ab.2006.03.038 (2006).

139   Edelmann, M. J. *et al.* Structural basis and specificity of human otubain 1-mediated deubiquitination. *Biochemical Journal* **418**, 379-390, doi:10.1042/bj20081318 (2009).

140   Busija, A. R., Patel, H. H. & Insel, P. A. Caveolins and cavins in the trafficking, maturation, and degradation of caveolae: implications for cell physiology. *American Journal of Physiology-Cell Physiology* **312**, C459-C477, doi:10.1152/ajpcell.00355.2016 (2017).

141   Burana, D. *et al.* The Ankrd13 Family of Ubiquitin-interacting Motif-bearing Proteins Regulates Valosin-containing Protein/p97 Protein-mediated Lysosomal Trafficking of Caveolin 1. *Journal of Biological Chemistry* **291**, 6218-6231, doi:10.1074/jbc.M115.710707 (2016).

142   Ritz, D. *et al.* Endolysosomal sorting of ubiquitylated caveolin-1 is regulated by VCP and UBXD1 and impaired by VCP disease mutations. *Nature Cell Biology* **13**, 1116-U1148, doi:10.1038/ncb2301 (2011).

143   Ravikumar, B., Moreau, K., Jahreiss, L., Puri, C. & Rubinsztein, D. C. Plasma membrane contributes to the formation of pre-autophagosomal structures. *Nature Cell Biology* **12**, 747-U715, doi:10.1038/ncb2078 (2010).

144   Olson, A. L., Knight, J. B. & Pessin, J. E. Syntaxin 4, VAMP2, and/or VAMP3/cellubrevin are functional target membrane and vesicle SNAP receptors for insulin-stimulated GLUT4 translocation in adipocytes. *Molecular and Cellular Biology* **17**, 2425-2435, doi:10.1128/mcb.17.5.2425 (1997).

145   Xu, P. *et al.* COPI mediates recycling of an exocytic SNARE by recognition of a ubiquitin sorting signal. *Elife* **6**, doi:10.7554/elife.28342.001 (2017).

146   Simonsen, A. *et al.* EEA1 links PI(3)K function to Rab5 regulation of endosome fusion. *Nature* **394**, 494-498 (1998).

147   Banaszynski, L. A., Chen, L.-c., Maynard-Smith, L. A., Ooi, A. G. L. & Wandless, T. J. A rapid, reversible, and tunable method to regulate protein function in living cells using synthetic small molecules. *Cell* **126**, 995-1004, doi:10.1016/j.cell.2006.07.025 (2006).

148   Macia, E. *et al.* Dynasore, a cell-permeable inhibitor of dynamin. *Developmental Cell* **10**, 839-850, doi:10.1016/j.devcel.2006.04.002 (2006).

149   Bright, N. A., Lindsay, M. R., Stewart, A. & Luzio, J. P. The relationship between lumenal and limiting membranes in swollen late endocytic compartments formed after wortmannin treatment or sucrose accumulation. *Traffic* **2**, 631-642, doi:10.1034/j.1600-0854.2001.20906.x (2001).

150   Spiro, D. J., Boll, W., Kirchhausen, T. & WesslingResnick, M. Wortmannin alters the transferrin receptor endocytic pathway in vivo and in vitro. *Molecular Biology of the Cell* **7**, 355-367 (1996).

151   Pasquier, B. SAR405, a PIK3C3/Vps34 inhibitor that prevents autophagy and synergizes with MTOR inhibition in tumor cells. *Autophagy* **11**, 725-726, doi:10.1080/15548627.2015.1033601 (2015).

152   Gillooly, D. J. *et al.* Localization of phosphatidylinositol 3-phosphate in yeast and mammalian cells. *Embo Journal* **19**, 4577-4588, doi:10.1093/emboj/19.17.4577 (2000).

153   Huotari, J. & Helenius, A. Endosome maturation. *Embo Journal* **30**, 3481-3500, doi:10.1038/emboj.2011.286 (2011).

154   Shen, Y., Rosendale, M., Campbell, R. E. & Perrais, D. pHuji, a pH-sensitive red fluorescent protein for imaging of exo- and endocytosis. *Journal of Cell Biology* **207**, 419-432, doi:10.1083/jcb.201404107 (2014).

155   Tachiyama, R. *et al.* Proteome of ubiquitin/MVB pathway: possible involvement of iron-induced ubiquitylation of transferrin receptor in lysosomal degradation. *Genes to Cells* **16**, 448-466, doi:10.1111/j.1365-2443.2011.01499.x (2011).

156   Iyyathurai, J., Decuypere, J.-P., Leybaert, L., D'Hondt, C. & Bultynck, G. Connexins: substrates and regulators of autophagy. *Bmc Cell Biology* **17**, doi:10.1186/s12860-016-0093-9 (2016).

157   Langlois, S., Cowan, K. N., Shao, Q., Cowan, B. J. & Laird, D. W. Caveolin-1 and-2 interact with connexin43 and regulate gap junctional intercellular communication in keratinocytes. *Molecular Biology of the Cell* **19**, 912-928, doi:10.1091/mbc.E07-06-0596 (2008).

158   Goodwin, J. M. *et al.* Autophagy-Independent Lysosomal Targeting Regulated by ULK1/2-FIP200 and ATG9. *Cell Reports* **20**, 2341-2356, doi:10.1016/j.celrep.2017.08.034 (2017).

159   Bader, C. A., Shandala, T., Ng, Y. S., Johnson, I. R. D. & Brooks, D. A. Atg9 is required for intraluminal vesicles in amphisomes and autolysosomes. *Biology Open* **4**, 1345-1355, doi:10.1242/bio.013979 (2015).

160   Takahashi, Y. *et al.* An autophagy assay reveals the ESCRT-III component CHMP2A as a regulator of phagophore closure. *Nature Communications* **9**, doi:10.1038/s41467-018-05254-w (2018).

161   Zhen, Y. *et al.* ESCRT-mediated phagophore sealing during mitophagy. *Autophagy*, doi:10.1080/15548627.2019.1639301 (2019).

162   Zhou, F. *et al.* Rab5-dependent autophagosome closure by ESCRT. *Journal of Cell Biology* **218**, 1908-1927, doi:10.1083/jcb.201811173 (2019).

163   Bultema, J. J. *et al.* Myosin Vc Interacts with Rab32 and Rab38 Proteins and Works in the Biogenesis and Secretion of Melanosomes. *Journal of Biological Chemistry* **289**, 33513-33528, doi:10.1074/jbc.M114.578948 (2014).

164   Gudmundsson, S., Kahlhofer, J., Baylac, N., Kallio, K. & Eskelinen, E.-L. Correlative Light and Electron Microscopy of Autophagosomes. *Methods in molecular biology (Clifton, N.J.)* **1880**, 199-209, doi:10.1007/978-1-4939-8873-0_12 (2019).

165   Meehl, J. B., Giddings, T. H., Jr. & Winey, M. High Pressure Freezing, Electron Microscopy, and Immuno-Electron Microscopy of Tetrahymena thermophila Basal Bodies. *Cytoskeleton Methods and Protocols* **586**, 227-241, doi:10.1007/978-1-60761-376-3_12 (2009).

166   Imai, K. *et al.* Atg9A trafficking through the recycling endosomes is required for autophagosome formation. *Journal of Cell Science* **129**, 3781-3791, doi:10.1242/jcs.196196 (2016).

167   Popovic, D. & Dikic, I. TBC1D5 and the AP2 complex regulate ATG9 trafficking and initiation of autophagy. *Embo Reports* **15**, 392-401, doi:10.1002/embr.201337995 (2014).

168   Soreng, K. *et al.* SNX18 regulates ATG9A trafficking from recycling endosomes by recruiting Dynamin-2. *Embo Reports* **19**, doi:10.15252/embr.201744837 (2018).

169   Lamb, C. A. *et al.* TBC1D14 regulates autophagy via the TRAPP complex and ATG9 traffic. *Embo Journal* **35**, 281-301, doi:10.15252/embj.201592695 (2016).

170   McGough, I. J. *et al.* Retromer Binding to FAM21 and the WASH Complex Is Perturbed by the Parkinson Disease-Linked VPS35(D620N) Mutation. *Current Biology* **24**, 1670-1676, doi:10.1016/j.cub.2014.06.024 (2014).

171   Kakuta, S. *et al.* Atg9 Vesicles Recruit Vesicle-tethering Proteins Trs85 and Ypt1 to the Autophagosome Formation Site. *Journal of Biological Chemistry* **287**, 44261-44269, doi:10.1074/jbc.M112.411454 (2012).

172   Shirahama-Noda, K., Kira, S., Yoshimori, T. & Noda, T. TRAPPIII is responsible for vesicular transport from early endosomes to Golgi, facilitating Atg9 cycling in autophagy. *Journal of Cell Science* **126**, 4963-4973, doi:10.1242/jcs.131318 (2013).

173   Zhang, J., Liu, J., Norris, A., Grant, B. D. & Wang, X. A novel requirement for ubiquitin-conjugating enzyme UBC-13 in retrograde recycling of MIG-14/Wntless and Wnt

signaling. *Molecular Biology of the Cell* **29**, 2098-2112, doi:10.1091/mbc.E17-11-0639 (2018).

174   Hao, Y.-H. *et al.* USP7 Acts as a Molecular Rheostat to Promote WASH-Dependent Endosomal Protein Recycling and Is Mutated in a Human Neurodevelopmental Disorder. *Molecular Cell* **59**, 956-969, doi:10.1016/j.molcel.2015.07.033 (2015).

175   Grasso, D. *et al.* Zymophagy, a Novel Selective Autophagy Pathway Mediated by VMP1-USP9x-p62, Prevents Pancreatic Cell Death. *Journal of Biological Chemistry* **286**, 8308-8324, doi:10.1074/jbc.M110.197301 (2011).

176   Nielsen, C. P., Jemigan, K. K., Diggins, N. L., Webb, D. J. & MacGurn, J. A. USP9X Deubiquitylates DVL2 to Regulate WNT Pathway Specification. *Cell Reports* **28**, 1074-+, doi:10.1016/j.celrep.2019.06.083 (2019).

177   Kim, W. *et al.* Systematic and Quantitative Assessment of the Ubiquitin-Modified Proteome. *Molecular Cell* **44**, 325-340, doi:10.1016/j.molcel.2011.08.025 (2011).

178   Emanuele, M. J. *et al.* Global Identification of Modular Cullin-RING Ligase Substrates. *Cell* **147**, 459-474, doi:10.1016/j.cell.2011.09.019 (2011).

179   Judith, D. *et al.* ATG9A shapes the forming autophagosome through Arfaptin 2 and phosphatidylinositol 4-kinase III beta. *Journal of Cell Biology* **218**, 1634-1652, doi:10.1083/jcb.201901115 (2019).

180   Nazio, F. *et al.* Fine-tuning of ULK1 mRNA and protein levels is required for autophagy oscillation. *Journal of Cell Biology* **215**, 841-856, doi:10.1083/jcb.201605089 (2016).

181   Silva, G. M., Finley, D. & Vogel, C. K63 polyubiquitination is a new modulator of the oxidative stress response. *Nature Structural & Molecular Biology* **22**, 116-123, doi:10.1038/nsmb.2955 (2015).

182   Thorslund, T. *et al.* Histone H1 couples initiation and amplification of ubiquitin signalling after DNA damage. *Nature* **527**, 389-+, doi:10.1038/nature15401 (2015).

183   Polo, S. Signaling-mediated control of ubiquitin ligases in endocytosis. *Bmc Biology* **10**, doi:10.1186/1741-7007-10-25 (2012).

184   Komada, M. & Soriano, P. Hrs, a FYVE finger protein localized to early endosomes, is implicated in vesicular traffic and required for ventral folding morphogenesis. *Genes & Development* **13**, 1475-1485, doi:10.1101/gad.13.11.1475 (1999).

185   MacDonald, E., Urbe, S. & Clague, M. J. USP8 Controls the Trafficking and Sorting of Lysosomal Enzymes. *Traffic* **15**, 879-888, doi:10.1111/tra.12180 (2014).

186   MacDonald, E. *et al.* HRS-WASH axis governs actin-mediated endosomal recycling and cell invasion. *Journal of Cell Biology* **217**, 2549-2564, doi:10.1083/jcb.201710051 (2018).

187   Pike, J. A. *et al.* Quantifying receptor trafficking and colocalization with confocal microscopy. *Methods* **115**, 42-54, doi:10.1016/j.ymeth.2017.01.005 (2017).

188   Uribe-Querol E. and Rosales C. Control of phagocytosis by microbial pathogens. Front. Immunol., 24 October 2017 | https://doi.org/10.3389/fimmu.2017.01368 (2017)